ISBN 978-82-471-2156-6 (printed ver.)
ISBN 978-82-471-2157-3 (electronic ver.)
ISSN 1503-8181




Doctoral theses at NTNU, 2010-97

Anders Rødningsby

# Multitarget Multisensor Tracking in the Presence of Wakes

**NTNU**
Norwegian University of
Science and Technology
Thesis for the degree of
philosophiae doctor
Faculty of Information Technology, Mathematics and
Electrical Engineering
Department of Engineering Cybernetics

NTNU
Norwegian University of
Science and Technology

Doctoral theses at NTNU, 2010-97

NTNU

NTNU
Norwegian University of
Science and Technology

Anders Rødningsby

# Multitarget Multisensor Tracking in the Presence of Wakes

Thesis for the degree of philosophiae doctor

Trondheim, May 2010

Norwegian University of
Science and Technology
Faculty of Information Technology, Mathematics and Electrical Engineering
Department of Engineering Cybernetics

**NTNU**
Norwegian University of Science and Technology

Thesis for the degree of philosophiae doctor

Faculty of Information Technology, Mathematics and Electrical Engineering
Department of Engineering Cybernetics



ISBN 978-82-471-2156-6 (printed ver.)
ISBN 978-82-471-2157-3 (electronic ver.)
ISSN 1503-8181

ITK-report 2010-10-W

Doctoral Theses at NTNU, 2010-97

Printed by Tapir Uttrykk

*I give thanks to you,*
*O Lord my God,*
*with my whole heart,*
*and I will glorify your name*
*forever.*

*Psalm 86, 12 (ESV)*

# Preface

This thesis is submitted in fulfillment of the requirements for the degree *Philosophiae Doctor* (PhD) at the Norwegian University of Science and Technology (NTNU). The work has mostly been carried out at University Graduate Center, Kjeller, and partly at the University of Connecticut, USA. I have been part of the Sea, Air and Land Surveillance (SEALS) project which is funded by the Norwegian Research Council (NFR), Kongsberg Maritime (KM), Kongsberg Defence & Aerospace (KDA), Norcontrol IT, Park Air Systems and University Graduate Center.

## Acknowledgements

I would first of all like to express my gratitude to all those who gave me the possibility, motivation and strength to complete this thesis. Without you, this thesis would not have existed.

My supervisor and advisor during this work have been Prof. Oddvar Hallingstad at University Graduate Center and Dr. John Glattetre at Kongsberg Maritime, respectively. I want to thank them for all their support and guidance, and for providing me with all the necessary equipment, especially real experimental sonar data which has been indispensable during my work.

I am also deeply indebted to Prof. Yaakov Bar-Shalom who not only was my advisor during my stay at the University of Connecticut, but also gave me support and wise advice via email messages after I returned to Norway. His help, stimulating suggestions and encouragement have been of great influence to my work. I also truly want to thank all the people at the International Christian Fellowship (ICF) for your warm-heartedness and help with practical problems during my stay in the USA, with special thanks to June Miller who also proofread all my publications.

To all the students at University Graduate Center I want to express my gratitude for the time we have had together in the form of lunch conversations, table tennis tournaments, floor ball and other social activities. You have all contributed to giving me a friendly and pleasant time as a PhD candidate. Especially I want to thank my office-mate Edmund Brekke and colleagues Morten Topland, Øyvind Hegrenæs, Morten Stakkeland, Roar Tungland, Kjetil Ånonsen and Are Willumsen for all their good discussions, support and valuable hints. To Kjell Magne Fauske, without you my life with LaTeX would have been much harder.

Last, but not least, I would like to give my special thanks to my nearest family and friends whose patient support enabled and encouraged me to complete this work. To my parents Bitten Karin and Håkon, my sister Kari Solveig with her family, and my grandmothers Solveig and Kari, I owe it all to you!

# Summary

TARGET tracking is an essential requirement for surveillance and control systems to interpret the environment. This environment may contain multiple targets, and the environmental information may be obtained by multiple sensors in a multitarget multisensor tracking system. In this thesis we focus on targets which, in addition to reflecting signals themselves, also have a trailing path behind them, called a wake. This wake causes additional measurements to those originating from the target. When the measurements are processed, the estimated track can be misled and sometimes lose the real target because of the wake. This problem becomes even more severe in multitarget environments where targets are operating close to each other in the presence of wakes.

In this thesis a probabilistic model is developed which reflects the probability that a false measurement originates from the wake behind a target. This wake model is integrated in the probabilistic data association filter (PDAF) to improve the track continuity for tracking single targets. The modified PDAF is further extended to handle multiple targets in the presence of wakes by using a probabilistic wake model for each of the targets in the multitarget environment that has a wake behind it. These single wake models are combined to form a joint wake model which augments the joint probabilistic data association filter (JPDAF) for both coupled and decoupled filtering.

The wake-originated measurements may also cause confusion in the track initiation. To prevent this problem, a clustering method is proposed based on morphological operators which allows tracks to be initialized based on two-point differencing of the cluster centroids from succeeding scans.

The modified PDAF is tested on data of a real scuba diver with an open breathing system. In this case the air bubbles produced by the diver form a wake which extends far behind the diver. The experiment showed that the above modifications of the PDAF improved the track continuity significantly.

Finally, a relatively extensive simulation, based on real scuba diver data, is presented. Four different multitarget multisensor tracking scenarios are simulated, considering two targets with wakes that are:

1. Crossing each other.
2. Moving in parallel to each other.
3. One following after another.
4. Meeting and then passing each other.

The results of these simulation scenarios show that the presented modifications improve the tracking performance, and the probability of lost tracks is significantly reduced. The targets are observed by two sensors, and it is shown that tracks estimated in a centralized fusion configuration are better than the local tracks estimated using data from individual sensors only. It is also shown that applying the wake model to targets that do not generate a wake, yields almost no deterioration of the tracking performance.

# Nomenclature

## Notations

| | |
|---|---|
| $A$ | amplitude squared (energy) |
| $A_i$ | amplitude squared (energy) in cell number $i$ |
| $A_{(i)}$ | amplitude squared number $i$ in an ordered sequence (increasing values) |
| $A_{av}$ | average amplitude squared |
| $B$ | structuring element [paper A, Section 2.2] |
| $\beta_k(i)$ | conditional probability of association event $\theta_k(i)$ |
| $\beta^{k,l}$ | conditional probability of association event $\theta^{k,l}$ |
| $c$ | center of the joint validation region |
| $c_{ij}$ | cost of choosing hypothesis $i$ when $j$ is true |
| cov | covariance |
| $d$ | distance |
| $d_{max}$ | maximum distance |
| $D_k$ | eigenvalue matrix [paper A, Appendix B] |
| $\delta_\Theta^t$ | target detection indicator (indicates if a measurement is associated to target $t$ in event $\Theta$) |
| $\delta_\Theta$ | vector of target detection indicators (corresponding to event $\Theta$) |
| $\delta_B(X)$ | dilation of image $X$ by structuring element $B$ [paper A, Section 2.2] |
| $\Delta t$ | time delay |
| $E\{\cdot\}$ | expectation |
| $\epsilon_B(X)$ | erosion of image $X$ by structuring element $B$ [paper A, Section 2.2] |

| | |
|---|---|
| $f(x,k)$ | non-linear plant equation of $x$ at time $k$ |
| $f_{\mathbf{H}}(y)$ | likelihood function under hypothesis $\mathbf{H}$ |
| $F$ | transition matrix |
| $\gamma$ | validation gate threshold |
| $\gamma$ [deg] | trajectory crossing angle |
| $\Gamma(\cdot)$ | gamma function |
| $h(x,k)$ | non-linear measurement equation of $x$ at time $k$ |
| $H$ | measurement matrix |
| $\mathbf{H}$ | hypothesis that only noise is present (null hypothesis) |
| $I$ | identity matrix |
| $I_{n_x}$ | $n_x \times n_x$ identity matrix |
| $I^x_\Theta$ | block identity matrix [see Equation (45) in paper C] |
| $j_t(\Theta_k)$ | index of the measurement associated with target $t$ in event $\Theta_k$ |
| $k$ | time index |
| $\mathbf{K}$ | hypothesis that a target and noise are present |
| $(l,w)$ | measurement ($l$-behind and $w$-sideways to the predicted target position) [paper B, Appendix A and paper C, Appendix A] |
| $L_k$ | number of measurement histories at time $k$ [Part I, Section 4.1] |
| $L_{(\cdot)}$ | limit of the variable $(\cdot)$ (for bubble and wake models) |
| $L(y)$ | likelihood ratio of $y$, $L(y) = \frac{f_{\mathbf{K}}(y)}{f_{\mathbf{H}}(y)}$ |
| $\lambda$ | spatial density of the number of false measurements |
| $\lambda_w$ | wake generation parameter (exponential distribution) [paper B, Section 4] |
| $m_k$ | number of validated measurements at time $k$ |
| $m^k$ | vector containing all $m_k$ up to and including time $k$ |
| $M$ | measurement generation area [paper C, Section 5.3] |
| $M_k$ | eigenvector matrix [paper A, Appendix B] |
| $\mu$ | mean |
| $\mu_F(\cdot)$ | pmf of the number of false measurements |
| $n$ | number of samples |
| $n_x$ | dimension of vector $x$ |
| $\mathcal{N}(\mu,\sigma^2)$ | normal (Gaussian) distribution with mean $\mu$ and variance $\sigma^2$ |
| $\mathcal{N}(x;\mu,\sigma^2)$ | pdf of a normal (Gaussian) random vector $x$ with mean $\mu$ and variance $\sigma^2$ |
| $N_{(\cdot)}$ | number of elements of the type $(\cdot)$ |
| $\nu_k$ | combined innovation [see Equation (4.62)] |
| $\nu_k(i)$ | innovation of measurement number $i$ |
| $\nu^S_k(\Theta)$ | stacked innovation associated to event $\Theta_k$ [paper C, Section 3.4] |
| $\Omega$ | validation matrix |
| $\Omega_\Theta$ | matrix representation of the event $\Theta$ |

| | |
|---|---|
| $\omega(j,t)$ | indicating whether measurement $j$ lies in the validation gate of target $t$ |
| $\omega_\Theta(j,t)$ | binary element indicating whether the event $\theta(j,t)$ is part of $\Theta$ |
| $p(\cdot)$ | pdf |
| $p[\cdot]$ | pdf [paper B and paper C] |
| $p_B(\cdot)$ | bubble pdf [paper A] |
| $p_W(\cdot)$ | wake pdf [paper B and paper C] |
| $P\{\cdot\}$ | probability of an event |
| $P(\cdot)$ | probability of an event [paper A] |
| $P_{k\|j}$ | conditional covariance matrix of the state at time $k$ given measurements through time $j$ |
| $\tilde{P}$ | spread of the means term |
| $P_{k\|k}(i)$ | estimated covariance matrix of the state at time $k$ given that measurement $i$ originates from the target |
| $P_B$ | bubble probability [paper A] |
| $P_D$ | detection probability |
| $P_{FA}$ | false alarm rate (false alarm probability in a given resolution cell) |
| $P_{FT}$ | false track probability [paper A] |
| $P_G$ | gate probability |
| $P_{GB}$ | bubble gate probability [paper A] |
| $P_{GW}$ | wake gate probability [paper B and paper C] |
| $P_W$ | wake probability [paper B and paper C] |
| $P_{\mathbf{H}}$ | probability of being in hypothesis $\mathbf{H}$ |
| ${}_nP_r$ | permutations (without repetition) of $r$ elements out of total $n$ elements |
| $\phi_\Theta$ | number of false (unassociated) measurements in event $\Theta$ |
| $\phi_B(X)$ | closing of image $X$ by structuring element $B$ [paper A, Section 2.2] |
| $\varphi$ | signal direction |
| $\xi$ | phase (of a signal) |
| $Q$ | process noise covariance matrix |
| $r$ | radius of the joint validation region [paper B, App. A and paper C, App. A] |
| $r(t)$ | received signal at time $t$ |
| $(r,\psi)$ | position measurements (range and bearing) in polar coordinates |
| $\mathcal{R}$ | amplitude |
| $R$ | measurement noise covariance matrix |
| $R_c$ | measurement noise covariance matrix in Cartesian coordinates |
| $R_p$ | measurement noise covariance matrix in polar coordinates |
| $(\rho,\alpha)$ | measurement ($\rho$-behind and $\alpha$-sideways to the predicted target position) [paper A, Appendix B] |
| $(\rho,\alpha,\beta)$ | wake model parameters [paper B, Appendix A and paper C, Appendix A] |
| $s(t)$ | signal at time $t$ |
| $\mathcal{S}$ | number of sensors in a multisensor configuration |
| $S$ | surveillance area covering the full trajectories of the targets |
| $S_k$ | innovation covariance matrix at time $k$ |
| $S_{\text{fix}}$ | fixed innovation covariance matrix [see Equation (52) in paper C] |

| | |
|---|---|
| $\sigma_\theta$ | standard deviation of $\theta$ |
| $\sigma_\theta^2$ | variance of $\theta$ |
| $\sigma_p(s)$ | standard deviation of the process noise in the simulation model |
| $\sigma_p(f)$ | standard deviation of the process noise in the filter model |
| $t$ | target number |
| $t_j$ | index of the target to which measurement $j$ is associated |
| $T$ | time between each scan |
| $\tau$ | constant scale factor (included in the detection threshold) |
| $\mathcal{T}$ | detection threshold |
| $\tau_\Theta(j)$ | measurement association indicator (indicates if measurement $j$ is associated to a target or not in event $\Theta$) |
| $\theta_k(i)$ | association event that measurement $z_k(i)$ originates from the target |
| $\theta(j,t)$ | event that measurement $j$ originates from target $t$ |
| $\theta^{k,l}$ | event that the $l^{\text{th}}$ sequence of measurements is correct at time $k$ |
| $\Theta$ | joint association event [see Equation (5.3)] |
| $\vartheta$ | speed |
| $(u_i, u_q)$ | in-phase and quadrature components |
| $v$ | process noise |
| $v[m/s]$ | target velocity [paper A, App. B, paper B, App. A, and paper C, App. A] |
| var | variance |
| $\mathcal{V}_k(\gamma)$ | measurement validation region at time $k$ with gate threshold $\gamma$ |
| $V_k$ | volume of the validation region at time $k$ |
| $V_{(\cdot)}$ | volume of $(\cdot)$ |
| $w$ | measurement noise |
| $W$ | wake area |
| $W_k$ | Kalman gain (filter gain) at time $k$ |
| $x$ | target state |
| $\hat{x}_{k\|k}(i)$ | target state estimate at time $k$ given measurements through time $k$ and that measurement $i$ originates from the target |
| $\hat{x}^S_{k\|k}(\Theta)$ | stacked state estimate of the targets at time $k$ given measurements through time $k$ and that the joint association event $\Theta$ is true |
| $(x, y)$ | position measurement in Cartesian coordinates |
| $X$ | image |
| $y$ | sample of the received signal |
| $Y$ | amplitude squared of the cell to be tested for detection |
| $z$ | measurement |
| $\bar{z}$ | predicted position measurement |
| $z(i)$ | measurement number $i$ |
| $\hat{z}^{t_j}_{k\|k-1}$ | predicted measurement of target $t_j$ at time $k$, given measurements through time $k-1$ |
| $Z_k$ | set of measurements at time $k$ |
| $Z^k$ | set of all measurements up to and including time $k$ |
| $Z^{k,l}$ | $l^{\text{th}}$ sequence of measurements (measurement histories) at time $k$ |

| | |
|---|---|
| $\hat{(\cdot)}$ | estimate |
| $\tilde{(\cdot)}$ | error corresponding to $(\cdot)$ |
| $(\cdot)^{-1}$ | inverse of matrix |
| $(\cdot)^T$ | transposition (of a matrix or a vector) |
| $\bar{(\cdot)}$ | complement of set (or event) |
| $(\cdot)_{\text{true}}$ | true state of $(\cdot)$ |
| $(\cdot)^t$ | probability, pdf, vector or matrix associated to target $t$ |
| $(\cdot)^S$ | stacked vector or matrix |
| $(\cdot)^l$ | vector or matrix conditioned on the $l^{\text{th}}$ sequence of measurements, out of all combinations of measurement sequences, being true |
| $(\cdot)_k$ | $(\cdot)$ at time $k$ |
| $(\cdot)_{(k\|j)}$ | conditional estimate or covariance at time $k$ given measurements up to and including time $j$ |
| $(\cdot\|\cdot)$ | conditioning (for probabilities, estimates or covariances) |
| $\|\cdot\|$ | magnitude (of a scalar) or determinant (of a matrix) |
| $\|\|\cdot\|\|$ | norm (of a vector or matrix) |
| $[\omega(j,t)]$ | a matrix whose components at $j$-row $t$-column is $\omega(j,t)$ |
| $[a,b]$ | closed interval between points $a$ and $b$ (includes the endpoints) |
| $f(x)\|_{x=\hat{x}_{k\|k}}$ | function evaluated at $x = \hat{x}_{k\|k}$ |
| $\infty$ | infinity |
| $m \to \infty$ | as $m$ approaches infinity |
| $\sim$ | distributed as |
| $\approx$ | approximately equal |
| $\triangleq$ | equal by definition |
| $\neq$ | not equal |
| $\leq$ | less than or equal to |
| $a \underset{\mathbf{H}}{\overset{\mathbf{K}}{\gtrless}} b$ | choose $\mathbf{K}$ if $a$ is greater than $b$, otherwise choose $\mathbf{H}$ |
| ! | factorial |
| $\cap$ | logical "AND" operation (set intersection) |
| $\cup$ | logical "OR" operation (set union) |
| $\oplus$ | dilation [paper A, Section 2.2] |
| $\ominus$ | erosion [paper A, Section 2.2] |
| $\emptyset$ | empty set (impossible event) |
| $\subseteq$ | subset of (included in) |
| $\in$ | element of |
| $^\circ$ | degrees (of arc) |

## Acronyms

| | |
|---|---|
| AWGN | additive white Gaussian noise |
| CA-CFAR | cell averaging - constant false alarm rate |
| CDF | cumulative distribution function |
| CFAR | constant false alarm rate |
| CLT | central limit theorem |
| CMKF | converted measurement Kalman filter |
| CPDA | coupled data association filter |
| dB | decibel |
| EKF | extended Kalman filter |
| GO-CFAR | greatest of - constant false alarm rate |
| GPS | Global Positioning System |
| i.i.d. | independent identically distributed |
| IMMPDAF | interacting multiple model probabilistic data association filter |
| IPDAF | integrated probabilistic data association filter |
| ISODATA | iterative self-organizing data analysis techniques |
| JIPDAF | joint integrated probabilistic data association filter |
| JPDACF | joint probabilistic data association coupled filter |
| JPDAF | joint probabilistic data association filter |
| KF | Kalman filter |
| MCA-CFAR | morphological cell averaging - constant false alarm rate |
| MDA | multidimensional assignment |
| MHT | multiple hypothesis tracking |
| MMSE | minimum mean square error |
| MSE | mean square error |
| MSJPDACF | multisensor joint probabilistic data association coupled filter |
| MSJPDAF | multisensor joint probabilistic data association filter |
| MSPDAF | multisensor probabilistic data association filter |
| NP | Neyman-Pearson |
| OBA | optimal Bayesian approach |
| OS-CFAR | ordered statistics - constant false alarm rate |
| PDAF | probabilistic data association filter |
| pdf | probability density function |
| pmf | point mass function |
| psf | point spread function |
| RMS | root mean square |
| ROC | receiver operating characteristic |
| SNR | signal-to-noise ratio |
| SO-CFAR | smallest of - constant false alarm rate |
| TBD | track-before-detect |
| VTC | vessel traffic control |

# Table of Contents

# Part I

# Topics in Multitarget Multisensor Tracking

# 1

# Introduction

This thesis consists of two parts, Part I (Topics in Multitarget Multisensor Tracking) and Part II (Publications). The purpose of Part I is to present a framework for the research reported in the included papers in Part II, and to explain how these papers relate to each other and to the existing theory.

This chapter gives a brief introduction of the main elements considered in this thesis. These elements are described more thoroughly in the following chapters and in the included papers in Part II. First, the problem description is given. Then the tracking system is presented in Section 1.2, starting with the surveillance area containing the target, the sensor system observing the target, the signal processing that generates measurements of the target, and finally the information processing which processes the measurements to obtain the target state estimate and the corresponding uncertainty. Section 1.3 shows an example where multiple sensors are used to track multiple targets in a multitarget multisensor tracking system. The included papers in this thesis are presented in Section 1.4, and the main contributions of the thesis are listed in Section 1.5.

## 1.1 Problem Description

This thesis is concerned with the problem of tracking targets which, in addition to reflecting signals themselves, also have a trailing path behind them, called a wake. Ideally, only the target itself would be detected in the tracking process. This is unfortunately not true, and more or less random measurements will always appear due to a noisy background, unknown objects and noise in the sensor itself. It is therefore an important factor in a tracking system to correctly associate each measurement to its origin. False measurements may not be a problem as long as they are well separated from the target of interest since this implies that the measurements are unlikely to originate from the tar-

get. More problematic are the measurements caused by the wake since they are closer to the target. When these wake measurements are processed, the tracking system may be misled to follow the wake instead of the target. In the worst case, these measurements will cause a lost track. In this thesis we have developed methods to prevent this problem.

### 1.1.1 The Wake Phenomenon

This thesis considers target tracking in the presence of wakes, which is a phenomenon that appears behind certain targets. This phenomenon could be air bubbles from a diver, the wake behind a ship, or the wake from ballistic vehicles in the re-entry stage. One possible approach to this problem is to handle both the target and the wake behind it as an extended target. A problem with this approach is the varying and unknown size of the wake which may reach far behind the target yielding a large bias. In this thesis the wake is not considered as part of the target, but rather as a special kind of clutter.

When wake-originated measurements are fed to the tracking system, it becomes important to associate them correctly to prevent a lost track. If these wake-originated measurements are taken as target-originated, it is likely that the track estimate will start to follow the wake rather than the target, and in the worst case this will end up with a lost track.

### 1.1.2 Diver Tracking

In recent years the surveillance of divers near marine infrastructures such as bridges, power plants, port and harbor facilities has received renewed interest [3], [20], [24], [39], [47], [48]. The detection of divers is considered a challenging problem in underwater acoustics, and the target strength is the main unknown in assessing the feasibility of using a sonar to detect them. The target strength of a diver is a complicated function of aspect angle and frequency, where the human lungs and the oxygen tank are thought to be the largest contributors [58]. Especially for re-breathers with a fully closed breathing system, the target strength is particularly low. In addition, the surrounding environment could be noisy and non-stationary especially in ports and shallow water [62].

Divers with open breathing systems have received a special focus in this thesis since the air bubbles they produce create wakes behind them. This is illustrated in both Figure 1.1 and Figure 1.2. The bubbles behind a diver with an open breathing system was the original motivation for the development of the tracking methods presented in this thesis. In **paper A**, a tracking method that accounts for the bubbles is tested on a real diver, and the multisensor multitarget tracking simulations in **paper C** are also based on divers with open breathing systems.

## 1.2 The Tracking System

Tracking is the estimation of the state of a moving object based on remote measurements obtained by one or more sensors. An example of a traditional tracking system where a single sensor is tracking a single target is outlined in Figure 1.1. Traditional tracking systems may be built by using several serial processes, such as the signal processor and information processor in Figure 1.1, where each process has the purpose of extracting the desired information and pass it to the next process.

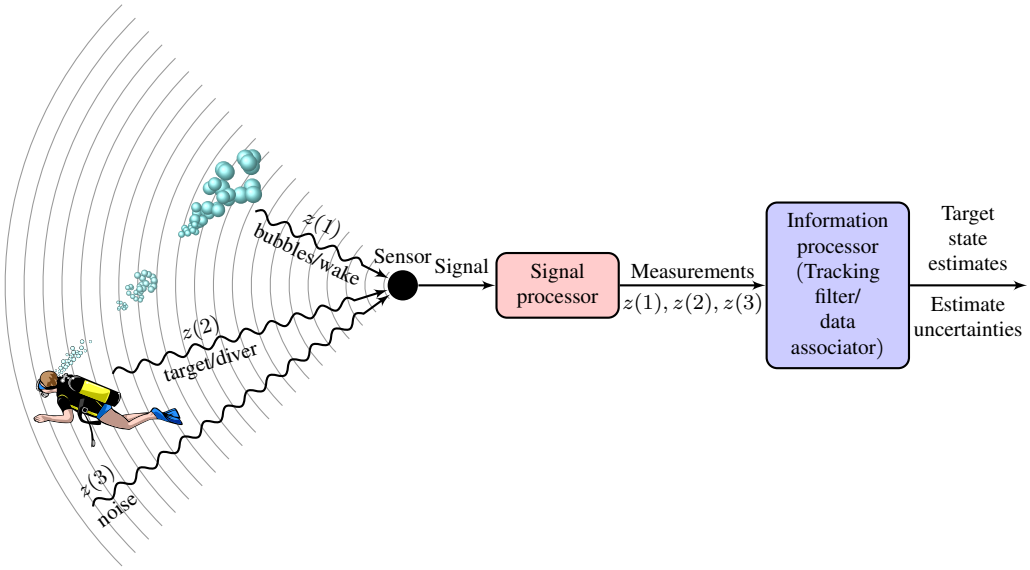


***Figure 1.1:*** *Overview of the tracking system.*

Another approach, which is not considered in this thesis, is the track-before-detect (TBD) approach [34], [57] where the signal processing and information processing are combined such that detection and track confirmation occur simultaneously. The thresholding process, in which detected measurements are produced, is avoided to preserve weak signal information in the raw sensor data.

### 1.2.1 Surveillance Area

The first element in a tracking system is the area in which a target can be observed, often called the scene or the surveillance area. This area could be outer space for tracking missiles or spacecraft, airspace for controlling air traffic, the surface of the ocean for vessel traffic control (VTC), the ocean for underwater surveillance, or outside and inside buildings for tracking vehicles or people of special interest. The example in Figure 1.1 illustrates an underwater tracking system where the target of interest is a diver with an open breathing system. This is the setting of the problem discussed in **paper A**.

### 1.2.2 Sensors

Information of the surveillance area is obtained by the use of different types of sensors. These sensors are analogous to our use of eyes, ears and nose to collect information about our surroundings. Remote sensors are divided into two classes, active and passive sensors. The active sensors transmit a signal (energy) into the scene, and then search for signals that are reflected (or emitted) from the objects in the scene. Passive sensors do not actively transmit any signals themselves, but are searching for signals that are emitted from the objects (or reflected if there is another source present, such as the sun). Examples of active sensors are radar [13] and active sonar [62], while passive sensors can be passive sonar [62] and most optical sensors [17], [61]. The real data presented in this thesis (**paper A** and **paper C**) is recorded by active sonar sensors.

In addition to signals reflected or emitted from the targets of interest, the sensor will also receive energy from other objects in the scene in addition to noise from the background and the sensor itself, resulting in false measurements. In Figure 1.1, these false measurements are due to the background noise (measurement $z(3)$) and the bubbles/wake (measurement $z(1)$). Only measurement $z(2)$ originates from the diver, the target of interest. Note that all measurements in this thesis are defined as position measurements.

### 1.2.3 Signal Processing

The information obtained by a sensor, often called the raw data, is transmitted to the signal processor. The main goal for the signal processor is to extract target-originated measurements from the raw data. In both radar and active sonar systems, the information is divided into different cells, where each cell represents a specific location in the surveillance area. This is done by beamforming (presented in Chapter 2) where the different cells are specified by polar coordinates, range and bearing (angle). Each of those cells has to be tested, and only those with signal energy above a certain threshold are defined as detected. The detected cells (in polar coordinates) are then transformed to position measurements in Cartesian coordinates (described in Chapter 3). It is also possible to define measurements that contain more information than the position of the detected cells, e.g. amplitude information [18]. However, this thesis considers position measurements only, and the two terms "measurement" and "detection" may therefore be used interchangeably. The position measurements are either processed further, as in the clustering method presented in **paper A**, or directly fed to the next element in the tracking system, namely the information processor. In the example in Figure 1.1, only three measurements are obtained in the signal processor, and only one of them originates from the target of interest.

### 1.2.4 Information Processing

The information processing consists of data association and filtering. The data associator decides which measurement (or weighted combination of measurements) is to be used in the filter, while the tracking filter is used to estimate the state and corresponding uncertainty of the target.

#### Data Association

An important part in a tracking system is to associate the data to its origin. Let a track be defined as a state trajectory estimated from a set of measurements (the data) that have been associated with the same target. By this definition, the data association problem may be categorized in three different groups, according to "what is associated with what":

1. *measurement to measurement association*
   In the track formation procedure, measurements from different time steps are associated to each other to initialize or form a new track.

2. *track to track association*
   In a multisensor system, one single target can be tracked by several sensors simultaneously, resulting in several local tracks of the same target. To fuse these local tracks into one global track, an association method is needed to decide which tracks are to be fused.

3. *measurement to track association*
   This type of data association is used to maintain or update already established tracks, and answers the question: Which measurement originates from which track or target?

There are two fundamentally different approaches one can take in associating the data. In non-Bayesian data association a hard decision is carried out for how to associate the data, and the fact that this decision is not necessarily correct is ignored. In the probabilistic (Bayesian) data association, probabilities are evaluated for each association hypothesis.

All the above categories of data association are presented in this thesis, but the main focus is put on the *measurement to track association* in a probabilistic (Bayesian) approach, which is thoroughly discussed in the included papers and in Chapter 4 and Chapter 5.

#### Filtering

Filtering is the estimation of the (current) state of a dynamic system, and the term "filter" is used since the process of obtaining the best estimate from noisy data amounts to

filtering out the noise. That is, the filter tries to find the best weighted mean between the associated measurements (or weighted combination of measurements) and the predicted state at each time step. This process is based on a model of the target's dynamics, a model of the measuring process, and a model of the noise that corrupts the measurements. Some of the traditional tracking filters, with and without data association, are presented in this thesis.

## 1.3 Multitarget Multisensor Tracking

When multiple targets are tracked simultaneously in a tracking system including multiple sensors, we have a multisensor multitarget tracking system. An example of such a system is illustrated in Figure 1.2. In this example there are two radars and two active sonars observing several types of targets. Tracking of multiple targets is discussed in Chapter 5, and the multisensor systems are briefly described in Chapter 5.4.

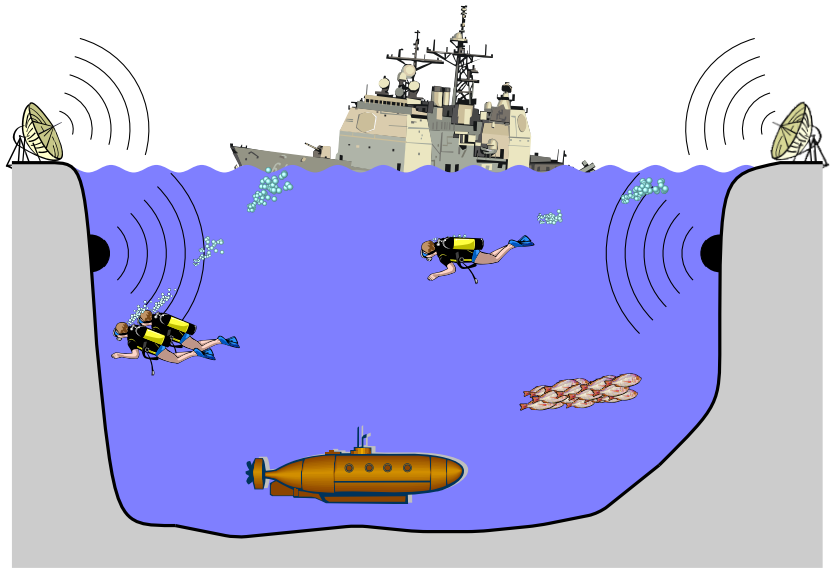

***Figure 1.2:*** *Multitarget multisensor tracking system.*

## 1.4 Publications

This thesis is based on the following publications:

### Paper A: Tracking of Divers Using a Probabilistic Data Association Filter with a Bubble Model

A. Rødningsby and Y. Bar-Shalom, "Tracking of divers using a probabilistic data association filter with a bubble model," *IEEE Transactions on Aerospace and Electronic Systems*, pp. 1181-1193, vol. 45, no. 3, July 2009. A preliminary version of this paper was presented in [55]

**Summary:** Detection and tracking of divers have become an important factor in port protection against underwater intruders. A problem arises from divers with open breathing systems because detections of the air bubbles they produce can mislead the tracking filter and sometimes result in a lost track. In this paper a probabilistic model is developed which reflects the probability that a false measurement originates from the bubbles. The novel contribution of this paper is the integration of this model in the probabilistic data association filter (PDAF) to improve the track continuity. The bubble detections may also cause confusion in the track initiation. To prevent this problem, a clustering method is proposed based on morphological operators which allows tracks to be initialized based on two-point differencing of the cluster centroids from succeeding scans. This morphological clustering method is included in a cell averaging constant false alarm rate (CA-CFAR) detector in such a way that both the point detections and their corresponding clusters can be fed to the tracking filter. These techniques are implemented and applied to real data of two divers, one with an open breathing system and the other with a closed breathing system, operating simultaneously in a coastal area. The real data were recorded from an active 90 kHz narrowband multibeam imaging sonar.

### Paper B: Multitarget Tracking in the Presence of Wakes

A. Rødningsby, Y. Bar-Shalom, O. Hallingstad, and J. Glattetre, "Multitarget tracking in the presence of wakes," in *Proceedings of the 11th International Conference on Information Fusion*, pp. 1536-1543, Cologne, Germany, July 2008. This paper was nominated for Best Student Paper Award, Fusion 2008.

**Summary:** In this paper we focus on targets which, in addition to reflecting signals themselves, also have a trailing path behind them, called a wake. When the detections are fed to a tracking system like the Probabilistic Data Association Filter, the estimated track can be misled and sometimes lose the real target because of the wake. This problem becomes even more severe in multitarget environments where targets are operating close to each other in the presence of wakes. To prevent this, we have developed a probabilistic model of the wakes in a multitarget environment. This model is used to augment the Joint Probabilistic Data Association Filter (JPDAF). Simulations of two crossing targets with wakes show that this modification gives good results and the number of lost tracks is significantly reduced.

#### Paper C: Multitarget Multisensor Tracking in the Presence of Wakes

A. Rødningsby, Y. Bar-Shalom, O. Hallingstad, and J. Glattetre, "Multitarget multisensor tracking in the presence of wakes," *Journal of Advances in Information Fusion*, pp. 117-145, vol. 4, no. 2, December 2009.

**Summary:** In this paper we focus on targets which, in addition to reflecting signals themselves, also have a trailing path behind them, called a wake, which causes additional detections. When the detections are fed to a tracking system like the probabilistic data association filter (PDAF), the estimated track can be misled and sometimes lose the real target because of the wake. This problem becomes even more severe in multitarget environments where targets are operating close to each other in the presence of wakes. To prevent this, we have developed a probabilistic model of the wakes in a multitarget environment. This model is used to augment the joint probabilistic data association filter (JPDAF) for both coupled and decoupled filtering.

This paper provides a systematic comparison of the standard data association filters (PDAF and JPDAF) and their modified versions presented here in a multitarget multisensor environment. Simulations of two targets with wakes in four different scenarios show that this modification gives good results and the probability of lost tracks is significantly reduced. The targets are observed by two sensors and it is shown that tracks estimated in a centralized fusion configuration are better than those from the local sensors. It is also shown that applying the wake model to targets that do not generate a wake, yields almost no deterioration of the tracking performance.

## 1.5 The scientific contribution of the thesis

The main contributions in this thesis are briefly presented below.

- The development of a probabilistic model which reflects the probability that a false measurement originated from the bubbles behind a diver with an open breathing system. This model is incorporated in the PDAF algorithm in **paper A**. The PDAF is presented in Chapter 4.

- The use of mathematical morphology to form clusters used in the track initialization. Measurements that are likely to originate from the same target are grouped together in one single cluster by the use of mathematical morphology. This allows tracks to be initialized based on two-point differencing of the cluster centroids from succeeding scans. Mathematical morphology and two-point differencing are described in Chapter 2 and Chapter 3, respectively, and the use of these techniques is presented in **paper A**.

- The development of a multitarget joint probabilistic model which reflects the probability that a false measurement originated from the wakes behind one or more

targets. This model is incorporated in the JPDAF algorithm in **paper B** and **paper C**. The JPDAF is presented in Chapter 5.

- The modified version of the coupled filter (JPDACF) algorithm that accounts for partial target detections and targets in the presence of wakes, derived in **paper C**.
- The demonstration of four different multitarget multisensor tracking simulation scenarios of two open breathing system divers in **paper C**. These simulations give a solid background for the analysis of tracking in the presence of wakes.

# 2

# Measurement Extraction

THE information in the scene or surveillance area in a tracking system is embedded in a form of energy depending on the surrounding transmission media. The form of energy is typically electromagnetic in a radar system or acoustic in an underwater system such as shown in Figure 1.1. This chapter focuses on active sensors since these are the types of sensors considered in the included papers. In active sensors an electrical signal is transformed into an appropriate type of energy, like acoustic for an active sonar or electromagnetic for a radar. This energy is transmitted into the scene to impose reflections from possible targets, and the reflected energy is transformed back into an electrical signal in the sensor. Then the electrical signal is processed to extract the desired information, which in our case are point position measurements and clusters of closely spaced point position measurements. Ideally, these measurements should all be originating from the true targets under consideration, but due to noise and clutter, some of them are false alarms. The measurements are then fed to the tracker where the data association and filtering are carried out.

This chapter briefly describes some of the main issues in signal processing, starting with the principles for how to obtain a signal in a given distance (range) and "look" direction (beamforming). Then a short introduction to detection theory with focus on hypothesis testing is given. The detection method in this thesis is based on a Rayleigh distributed background model. This model is presented and some familiar target models are considered leading to the receiver operating characteristics (ROC) curves and the constant false alarm rate (CFAR) processor. The final section in this chapter gives a short introduction to clustering where detections originating from the same source are combined in a single group or cluster.

## 2.1 Resolution Cells and Beamforming

Instead of dealing with the total amount of information in the whole scene in one operation, the scene is divided into smaller parts, called resolution cells, covering a certain area in the surveillance region. An example of resolution cells in a two-dimensional sensor system is shown in Figure 2.4(a) where each cell represents a specific range (distance from the sensor) and bearing (direction) interval. A detector can now "look" for a target in each of these resolution cells.

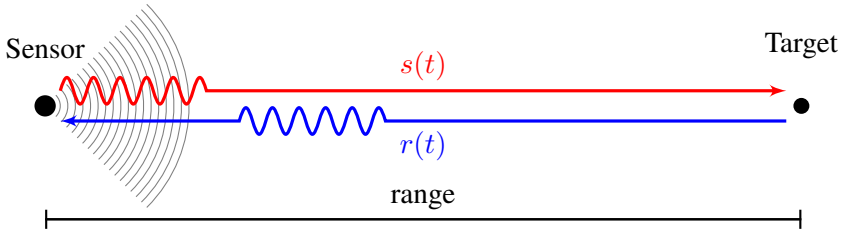


***Figure 2.1:*** *Signal transmission between the sensor and a point target model. The transmitted and reflected signals are denoted $s(t)$ and $r(t)$, respectively.*

The time between transmission of the signal $s(t)$ and reception of $r(t)$ in Figure 2.1 is given by the distance to the target (range) and the speed $\vartheta$ of the signal. This delay gives us therefore information about the target range, assuming the speed $\vartheta$ is known, but it gives no directional information. The principles for how to obtain information about what direction the signal is coming from, called beamforming, is illustrated in Figure 2.2. Here, an array of $N_r$ receivers are located with a given distance $d$ between them. Assuming the incoming signal has a plane wavefront with angle $\varphi$ to the row of receivers, as shown in Figure 2.2, this wavefront will reach the different receivers at different times depending on the signal direction $\varphi$. In beamforming, these receivers delay their inputs to observe a signal at a given "look" direction. In Figure 2.2, let Receiver 1 have no delay ($\Delta t_1 = 0$). The wavefront arrives at Receiver 2 $\Delta t_2$ time units before it arrives at Receiver 1, where $\Delta t_2 = \frac{d\sin(\varphi)}{\vartheta}$. In general, Receiver $n$ receives the wavefront $\Delta t_n$ time units before Receiver 1, where

$$\Delta t_n = \frac{(n-1)d\sin(\varphi)}{\vartheta} \tag{2.1}$$

Therefore, by delaying the signal with $\Delta t_n$ at Receiver $n$, each receiver samples the wave from this given direction at the same phase. Since the beamformed signal is the sum of all these samples from the individual delayed receivers, the resulting signal is enhanced and the noise is suppressed. For further information about beamforming and array signal processing, see [38].

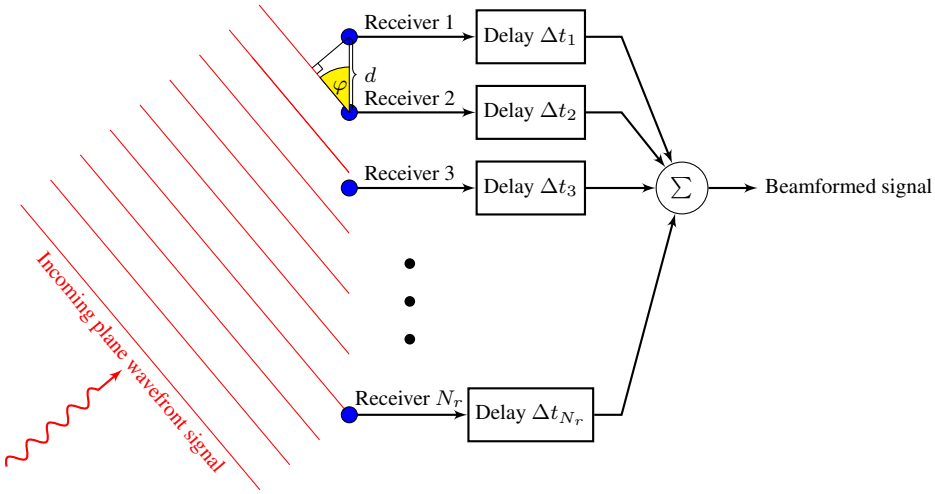


***Figure 2.2:*** *Illustration of beamforming to observe some signal at a given direction by using an array of sensors that delay their inputs.*

## 2.2 Detection Theory

The main problem in detection theory is deciding between two or more possible hypotheses. Because of this, detection theory is often associated with other names like hypothesis testing and decision theory. For the purpose of detecting a target in a tracking system, let the two hypotheses $\mathbf{K}$ and $\mathbf{H}$ be defined as follows:

$$\mathbf{K} : \text{A target and noise are present}$$
$$\mathbf{H} : \text{Only noise is present}$$

The purpose of detection theory is to use the received data from any kind of sensor as efficiently as possible in making the decision between these two hypotheses, with the goal of being correct most of the time. The error of declaring a detection (choosing hypothesis $\mathbf{K}$) when a target is absent is called a type I error or false alarm, and has a probability $P_{FA}$, also called the false alarm rate. The probability of correctly choosing hypothesis $\mathbf{K}$ when a target is present is denoted $P_D$ or the power of the test. The main goal for a detector is to maximize the probability of detection $P_D$ and at the same time keep the false alarm rate as low as possible. Unfortunately, these two probabilities are interconnected such that increasing one of them also increases the other. A practical way to analyze the relationship between $P_D$ and $P_{FA}$ is by using receiver operating characteristic (ROC) curves, presented in Section 2.5, and an example of ROC-curves is shown in Figure 2.3.

Let $y$ be a sample of the received signal, and define its pdf $p(y)$ under the two

hypotheses as:

$$\mathbf{K} : y \sim p(y|\mathbf{K}) \triangleq f_{\mathbf{K}}(y) \tag{2.2}$$

$$\mathbf{H} : y \sim p(y|\mathbf{H}) \triangleq f_{\mathbf{H}}(y) \tag{2.3}$$

where $f_{\mathbf{K}}(y)$ is the likelihood function under the hypothesis $\mathbf{K}$ that both noise and a target are present, and $f_{\mathbf{H}}(y)$ is the likelihood function under the hypothesis $\mathbf{H}$ that there is no target present, only noise. From this the detection probability $P_D$ and false alarm rate $P_{FA}$ are calculated as

$$P_D = \int_{\mathcal{T}}^{\infty} f_{\mathbf{K}}(y)\mathrm{d}y \tag{2.4}$$

$$P_{FA} = \int_{\mathcal{T}}^{\infty} f_{\mathbf{H}}(y)\mathrm{d}y \tag{2.5}$$

where $\mathcal{T}$ is the detection threshold.

One of the most well-known detection methods is the Neyman-Pearson (NP) approach to hypothesis testing [42]. This test aims to maximize $P_D$ subject to a false alarm rate constraint, where the desired false alarm rate $P_{FA}$ is chosen a priori. The NP detector is then as follows:

$$L(y) = \frac{f_{\mathbf{K}}(y)}{f_{\mathbf{H}}(y)} \underset{\mathbf{H}}{\overset{\mathbf{K}}{\gtrless}} \mathcal{T} \tag{2.6}$$

where the threshold $\mathcal{T}$ is given by the false alarm constraint (2.5). If the likelihood ratio $L(y)$ exceeds the threshold $\mathcal{T}$ a detection is declared (hypothesis $\mathbf{K}$ is chosen). Otherwise we assume the target is absent (hypothesis $\mathbf{H}$ is chosen).

Another detection method is Bayes' test [42]. This test is similar to the NP detector, but differs in the way the threshold is computed

$$L(y) = \frac{f_{\mathbf{K}}(y)}{f_{\mathbf{H}}(y)} \underset{\mathbf{H}}{\overset{\mathbf{K}}{\gtrless}} \frac{P_{\mathbf{H}}(c_{\mathbf{KH}} - c_{\mathbf{HH}})}{P_{\mathbf{K}}(c_{\mathbf{HK}} - c_{\mathbf{KK}})} = \mathcal{T} \tag{2.7}$$

In (2.7) $P_{\mathbf{K}}$ and $P_{\mathbf{H}}$ are a priori probabilities for being in hypothesis $\mathbf{K}$ and $\mathbf{H}$ respectively. The $c_{ij}$ is the cost of choosing hypothesis $i$ when $j$ is true. For further information about fundamental detection theory the reader is referred to [42], and for detection in non-Gaussian noise, see [41].

## 2.3 Rayleigh Background Model

This section describes the statistical model of the received signal under the $\mathbf{H}$ hypothesis (when there is no target present) used in this thesis. Let the sampled signal in one

resolution cell (after complex demodulation, beamforming and matched filtering) be represented by the in-phase $u_i$ and quadrature $u_q$ components [42]. From the central limit theorem (CLT) [27], a sum of many independent random variables each with finite variance tends to behave like a normal random variable. By assuming that there are enough independent scatters in any given resolution cell contributing to the received signal so that the CLT holds, the $u_i$ and $u_q$ components are assumed to be i.i.d. Gaussian random variables with zero mean and variance $\sigma^2$

$$\mathbf{H}: \begin{cases} u_i = w_i & w_i \sim \mathcal{N}\left(0, \sigma^2\right) \\ u_q = w_q & w_q \sim \mathcal{N}\left(0, \sigma^2\right) \end{cases} \tag{2.8}$$

From (2.8) the likelihood function under the $\mathbf{H}$ hypothesis is

$$f_{\mathbf{H}}(u_i, u_q) = \frac{1}{2\pi\sigma^2} e^{-\frac{1}{2\sigma^2}\left(u_i^2 + u_q^2\right)} \tag{2.9}$$

The Gaussian signal in (2.9) can be represented as an amplitude $\mathcal{R}$ and a phase $\xi$, defined as

$$\mathcal{R} = \sqrt{u_i^2 + u_q^2} \qquad \xi = \tan^{-1}\left(\frac{u_q}{u_i}\right) \tag{2.10}$$

Then, from [52], the amplitude and phase of the received signal in one resolution cell are distributed as

$$f_{\mathbf{H}}(\mathcal{R}) = \frac{\mathcal{R}}{\sigma^2} e^{-\frac{\mathcal{R}^2}{2\sigma^2}} \qquad f_{\mathbf{H}}(\xi) = \frac{1}{2\pi} \tag{2.11}$$

The amplitude in (2.11) is Rayleigh distributed, and by defining $A = \mathcal{R}^2$ as the energy (amplitude squared) in one resolution cell, the resulting distribution is exponential with mean $\mu = 2\sigma^2$

$$f_{\mathbf{H}}(A) = \frac{1}{2\sigma^2} e^{-\frac{A}{2\sigma^2}} = \frac{1}{\mu} e^{-\frac{A}{\mu}} \tag{2.12}$$

In reality the number of scatters in a resolution cell may not be high enough for the CLT to hold. It is therefore often observed that the background is more heavy-tailed than the Rayleigh distribution. Because of this, several non-Rayleigh distributions have been proposed in the literature. Popular models are the K-distribution, the Rayleigh mixture, the Weibull and the log-normal distributions [2], [33], [37], [45]. A comparison of various heavy-tailed distributions can be found in [1]. These models are more complex than the Rayleigh distribution, and it is important to be aware that more samples are required in order to obtain an accurate estimate of the distribution parameters. On the other hand the possibility of nonstationarity and interfering targets makes it advisable to use few cells in the process of estimating these parameters (in Figure 2.4 these cells are denoted "cells in the averaging process"). The potential damage from interfering targets is actually more serious when a heavy-tailed background is assumed, since the outliers due to a neighboring target can be misinterpreted as evidence of a much higher degree of heavy-tailedness than what is actually the case. It should also be noted that the tracking filters and data association algorithms discussed in the included papers are

mainly applied to targets where the signal-to-noise ratio (SNR) is of a moderate nature. In these situations, where the target is most likely to stand out from the background, the demand for an accurate background model is less critical. The accuracy of the background model becomes more important when tracking very low observable targets, but in these situations one should consider other tracking methods, like track-before-detect (TBD) or multiple hypothesis tracking (MHT). In this thesis, however, the main focus has been on information processing rather than signal processing, and the measurements are therefore obtained by considering only the Rayleigh background model.

## 2.4 Swerling Target Models

In this section the Swerling target models [60], modeling the fluctuations of the energy in one resolution cell under the $\mathbf{K}$ hypothesis, are presented. These target models are all special cases of the following gamma distribution

$$f_{\mathbf{K}}(A) = \frac{A^{m-1}}{\Gamma(m)} \left( \frac{m}{A_{av}} \right)^m e^{-\frac{mA}{A_{av}}} \tag{2.13}$$

where $m$ is often called the "shape parameter" and $A_{av}$ is the average energy in one resolution cell. Let the average energy $A_{av}$ in (2.13) be described as $A_{av} = \mu + \mu_{\text{target}}$ where $\mu$ is the average energy in a resolution cell under the $\mathbf{H}$ hypothesis, defined in (2.11), and $\mu_{\text{target}}$ is the part of the average energy due to the target. By defining the SNR as $\text{SNR} = \frac{\mu_{\text{target}}}{\mu}$, the average energy can be written as

$$A_{av} = \mu(1 + \text{SNR}) \tag{2.14}$$

The Swerling I target model is obtained by setting $m = 1$ in (2.13)

$$f_{\mathbf{K}}(A) = \frac{1}{\mu(1 + \text{SNR})} e^{-\frac{A}{\mu(1+\text{SNR})}} \tag{2.15}$$

This model applies to a target consisting of many independent reflectors, none of which is dominant. Similar to the reasoning for the Rayleigh background model, assuming the CLT to hold, this results in Gaussian distributed $u_i$ and $u_q$ components. The energy $A$ in one resolution cell (under the $\mathbf{K}$ hypothesis) is therefore still exponentially distributed as under the $\mathbf{H}$ hypothesis in (2.12), but the mean is now scaled by the SNR. The received energy on any scan is assumed to be constant throughout the entire scan but is independent (uncorrelated) from scan to scan.

The pdf of a Swerling II target model is the same as for Swerling I, but the fluctuations are more rapid and are assumed to be independent from pulse to pulse instead of scan to scan. This is the case for radars that transmit several pulses within one scan, but are not common in sonar applications where usually only one pulse is transmitted each scan.

In the Swerling III target model, the target can be approximated by one dominant reflector together with several smaller reflectors. The target fluctuations are here, as in Swerling I, independent from scan to scan with pdf obtained by setting $m = 2$ in (2.13)

$$f_{\mathbf{K}}(A) = \frac{4A}{\mu^2(1+\text{SNR})^2} e^{-\frac{2A}{\mu(1+\text{SNR})}} \tag{2.16}$$

This model is suitable for targets such as ballistic missiles [6].

The Swerling IV target model has the same pdf as Swerling III, but the energy is independent from pulse to pulse instead of scan to scan.

Finally, the Swerling V (or Swerling 0) target model is obtained from (2.13) in the limit as $m \to \infty$, and results in a non-fluctuating target model.

## 2.5 Receiver Operating Characteristics

The ROC curves give the relation between $P_D$ and $P_{FA}$ for a detector. By using the background model given in (2.12) in (2.5), the false alarm probability is

$$P_{FA} = P\{A > \mathcal{T}|\mathbf{H}\} = \int_{\mathcal{T}}^{\infty} \frac{1}{\mu} e^{-\frac{A}{\mu}} \mathrm{d}A = e^{-\frac{\mathcal{T}}{\mu}} \tag{2.17}$$

where $\mathcal{T}$ is the detection threshold. The sensors considered in the included papers are active sonars, where only a single pulse is transmitted each scan. In this case the Swerling I and III are the most appropriate fluctuating target models. The detection probabilities, calculated from (2.4), and the corresponding relations to $P_{FA}$ are for these two models:

- Swerling I

$$P_D = P\{A > \mathcal{T}|\mathbf{K}\} = \int_{\mathcal{T}}^{\infty} \frac{1}{\mu(1+\text{SNR})} e^{-\frac{A}{\mu(1+\text{SNR})}} \mathrm{d}A = e^{-\frac{\mathcal{T}}{\mu(1+\text{SNR})}} \tag{2.18}$$

$$P_D = P_{FA}^{\left(\frac{1}{1+\text{SNR}}\right)} \tag{2.19}$$

- Swerlling III

$$\begin{aligned} P_D = P\{A > \mathcal{T}|\mathbf{K}\} &= \int_{\mathcal{T}}^{\infty} \frac{4A}{\mu^2(1+\text{SNR})^2} e^{-\frac{2A}{\mu(1+\text{SNR})}} \mathrm{d}A \\ &= \left(1 + \frac{2\mathcal{T}}{\mu(1+\text{SNR})}\right) e^{-\frac{2\mathcal{T}}{\mu(1+\text{SNR})}} \end{aligned} \tag{2.20}$$

$$P_D = \left(1 - \frac{2\ln P_{FA}}{1+\text{SNR}}\right) P_{FA}^{\left(\frac{2}{1+\text{SNR}}\right)} \tag{2.21}$$

The ROC curves for the Swerling I and Swerling III target models, obtained from (2.19) and (2.21) respectively, are shown for different SNRs in Figure 2.3. These ROC curves are in fact valid only when the noise parameter $\mu$ is known (perfectly estimated). As shown in the next section, the local $\mu$ is estimated using a given number $n$ of samples of the surrounding cells. In practice, by using say $n > 20$, the resulting ROC curves would not be far from Figure 2.3. In the included papers, the chosen $P_D$ and $P_{FA}$ are in the intervals $[0.6, 0.7]$ and $\left[5 \cdot 10^{-4}, 5 \cdot 10^{-3}\right]$ respectively. Assuming the targets to be somewhere between a Swerling I and a Swerling III target, the above values of $P_D$ and $P_{FA}$ correspond to targets with SNR about 8-13 dB. This corresponds to the results in [19], where the SNR of human divers was estimated to 10-12 dB.

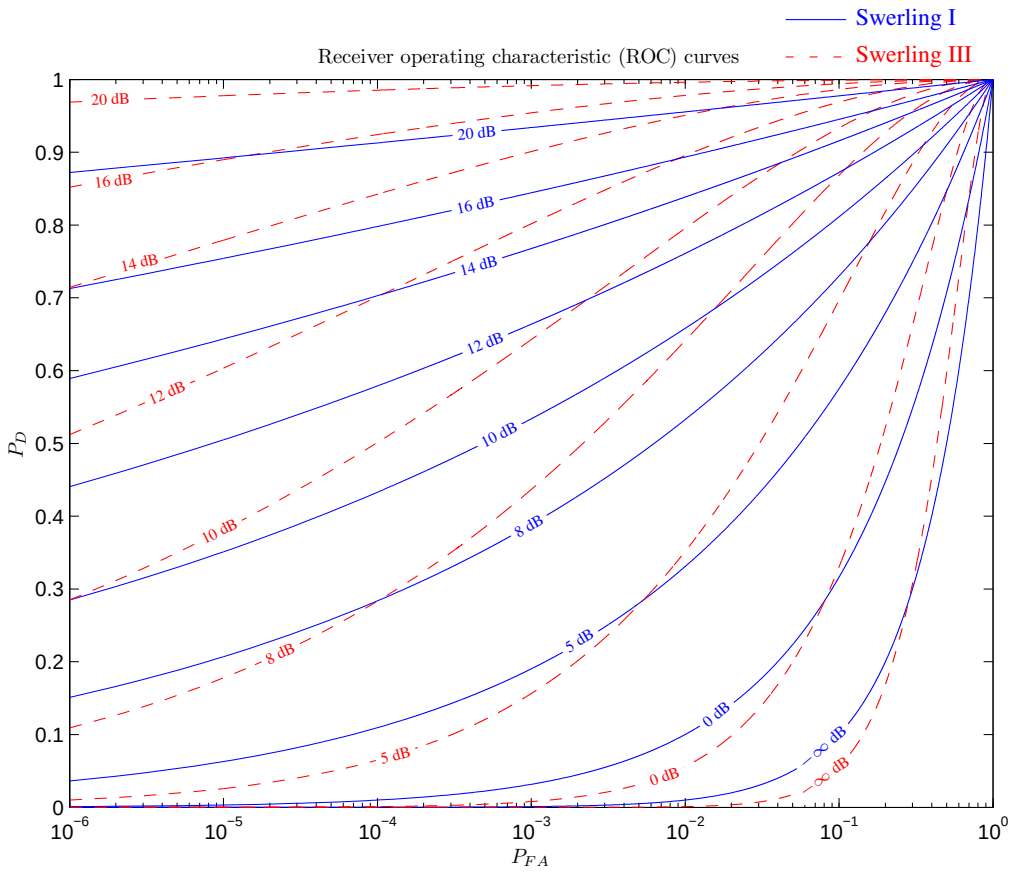


***Figure 2.3:*** *ROC curves for different SNR assuming a Swerling I target model (blue solid line) and Swerling III target model (red dashed line).*

## 2.6 Cell Averaging - Constant False Alarm Rate Detection

In a CFAR detector, the main issue is to keep the false alarm rate $P_{FA}$ constant. Because the false alarm rate is based only on the background model, assumed to be Rayleigh distributed as in Section 2.3, the CFAR detector does not need any knowledge about the target model. In an environment with spatially varying noise parameter $\mu$, the false alarm probability stays constant by keeping the exponent $\frac{\mathcal{T}}{\mu}$ in (2.17) constant. This is achieved by letting the threshold $\mathcal{T}$ be proportional to $\mu$, which yields the test

$$Y \underset{\mathbf{H}}{\overset{\mathbf{K}}{\gtrless}} \mathcal{T} = \tau\mu \tag{2.22}$$

where $Y$ is the amplitude squared (energy) of the cell to be tested for detection and $\tau$ is a constant scale factor to be deduced next. Since the noise parameter $\mu$ is not assumed to be known a priori, it has to be estimated for each resolution cell.

In a cell averaging CFAR (CA-CFAR), $\mu$ is estimated by averaging over $n$ cells with the squared amplitudes $A_i$, $i = 1, \ldots, n$, in a local neighborhood around the cell under test $Y$

$$\hat{\mu} = \frac{1}{n}\sum_{i=1}^{n} A_i \tag{2.23}$$

The CA-CFAR is according to [31], assuming the Rayleigh distributed background and a Swerling I target, optimal in the NP sense (maximize $P_D$ subject to $P_{FA}$). By assuming the neighboring cells $A_i$ to be independent and exponentially distributed variables, the sum in (2.23) forms a gamma distribution

$$n\hat{\mu} = \sum_{i=1}^{n} A_i = x \sim \frac{x^{n-1}}{\mu^n (n-1)!} e^{-\frac{x}{\mu}} \tag{2.24}$$

The probability that the test cell $Y$ exceeds the threshold is

$$\begin{aligned} P_{FA} &= P\left\{Y > \tau\hat{\mu}\right\} = P\left\{Y > \frac{\tau x}{n}\right\} \\ &= \int_0^\infty P\left\{Y > \frac{\tau x}{n}\middle| x\right\} p(x)\mathrm{d}x = \int_0^\infty e^{-\frac{\tau x}{n\mu}} \frac{x^{n-1}}{\mu^n (n-1)!} e^{-\frac{x}{\mu}}\mathrm{d}x \\ &= \frac{1}{\mu^n\left(\frac{1}{\mu}+\frac{\tau}{n\mu}\right)^n} \underbrace{\int_0^\infty \frac{x^{n-1}}{(n-1)!\left(\frac{1}{\mu}+\frac{\tau}{n\mu}\right)^{-n}} e^{-x\left(\frac{1}{\mu}+\frac{\tau}{n\mu}\right)}\mathrm{d}x}_{1} \\ &= \frac{1}{\mu^n\left(\frac{1}{\mu}+\frac{\tau}{n\mu}\right)^n} = \frac{1}{\left(1+\frac{\tau}{n}\right)^n} \end{aligned} \tag{2.25}$$

where the unity in the fourth line of (2.25) results from the cumulative distribution function (CDF) of a gamma distribution. It is clear that $P_{FA}$ is independent of $\mu$, and from (2.25) the constant scale factor $\tau$ in (2.22) can for a desired $P_{FA}$ be calculated as

$$\tau = nP_{FA}^{-\frac{1}{n}} - n \tag{2.26}$$

In the CA-CFAR detector it is assumed that the resolution cells used to estimate the noise parameter $\mu$ are free of targets. This may not be true for extended targets or when there are several adjacent targets. Therefore, in practical implementations of the CA-CFAR, the cells nearest to the one under test are often defined as a guard band, see Figure 2.4. These cells are not included in the cells used to estimate the noise parameter $\mu$.

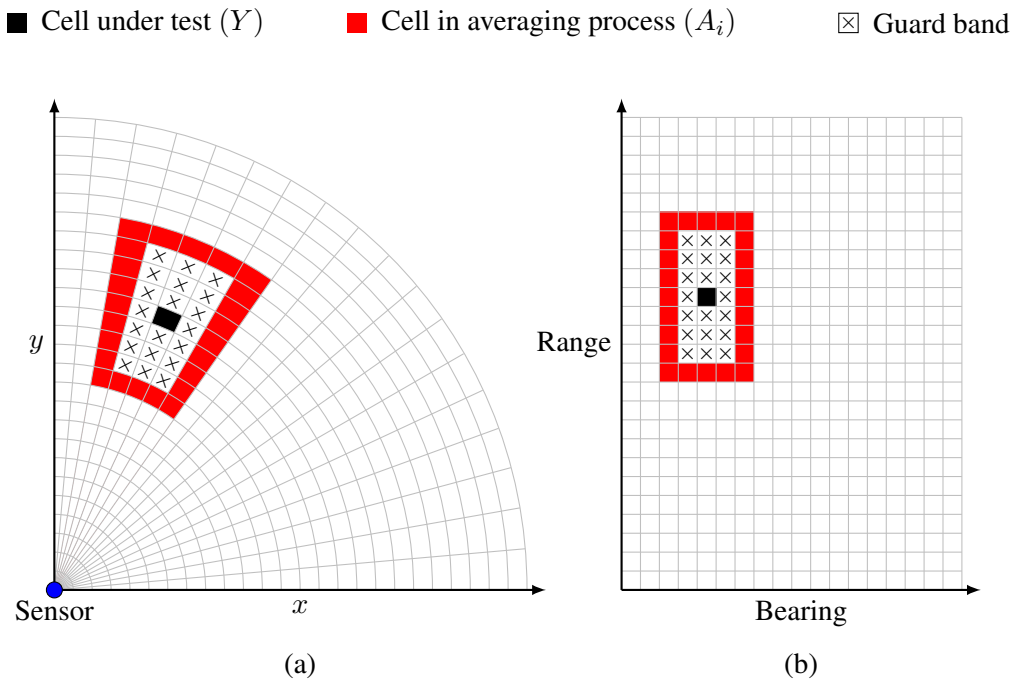


***Figure 2.4:*** *Resolution cells used to estimate the noise parameter $\mu$ in the CA-CFAR detector. The resolution cells are shown in a Cartesian coordinate system (a), and in the corresponding range-bearing coordinate system (b). In this example one cell in bearing and three cells in range are used as guard band.*

An alternative is using order statistics in the CFAR process, called OS$(l)$-CFAR [30], where the cells $(A_1, A_2, \ldots, A_n)$ are first ordered $(A_{(1)}, A_{(2)}, \ldots, A_{(n)})$, and then cell

number $l$ in the ordered sequence is used in the test

$$Y \underset{\mathbf{H}}{\overset{\mathbf{K}}{\gtrless}} \tau A_{(l)} \tag{2.27}$$

This specific cell $A_{(l)}$ is usually one of those with largest amplitudes to reduce the false alarms, but to avoid using cells that are target-originated, $l$ is set lower than $n$.

Two other CFAR alternatives are obtained by first ordering the cells as in the OS-CFAR, and then divide them into two groups (e.g., of the same size). After choosing either the greatest of them (GO-CFAR), or the smallest of them (SO-CFAR), the estimate is calculated as the average of the chosen cells such as in the CA-CFAR [30]. The GO-CFAR processor is specifically designed to control the false alarm rate during clutter power transition, but fails to detect closely spaced targets. On the other hand, the SO-CFAR processor proposed to resolve multiple targets is unable to prevent excessive false alarms in the presence of clutter edges.

## 2.7 Clustering

The point detections resulting from a CFAR detector may be directly fed into a tracking algorithm, but for targets that yield several point detections, it is sometimes desirable to gather these detections in a single cluster. In that way the assumption that each target yields only one single measurement, which is a common assumption in many tracking algorithms, becomes more appropriate. Many possible algorithms for clustering are available, such as ISODATA and the K-means [26]. However, most of these suffer from the problem of requiring knowledge of the number of clusters a priori. A technique from image analysis that does not require this is called mathematical morphology [59]. This approach has been mainly concerned with image analysis to extract shape information from digital images [36]. Additional applications include low signal amplitude detection and pattern recognition [49], [54]. More interesting is the application of group tracking [46], where the morphological operators are used to cluster measurements into groups with a common activity. In **paper A** this method is used to create clusters of the detections from an open breathing system diver and the bubbles he produces. The clusters are used in the track initiation to avoid confusion of the many possibilities of two-point differencing [11] that could have been set up among the point detections. Instead, two-point differencing is used for the cluster centroids from succeeding scans.

# 3

# Tracking Filters

THIS chapter starts with the tracking model before some of the basic tracking filters are presented. These filters include the Kalman filter (KF), the extended Kalman filter (EKF) and the converted measurement Kalman filter (CMKF). Target tracking is often divided into three successive operations:

1. Track formation (initialization of new tracks)
2. Track maintenance or continuation (update an already established track with new measurements at the current time)
3. Track termination (delete the track)

where the presented filters consider only the track maintenance. A short description of how tracks are initially formed and finally terminated is given at the end of this chapter.

## 3.1 Tracking Model

In the process of developing a tracking filter, a mathematical model of the physical system to which the state is being estimated is needed. This model is called the truth model[1]. The purpose of the truth model is to represent the physical system from the evolution of the state to the generation of measurements, and to evaluate the tracking filter performance by means of simulations. The truth model may be linear or nonlinear, but since most physical systems are nonlinear in nature, the truth model is also generally nonlinear. In the tracking filters, however, it is often desirable, for practical reasons and due to computational limitations, to have a simpler model than the truth model. The model

[1] In simulations, the truth model is often called simulation model.

which the implemented equations in the tracking filter are based on, called the filter model, is therefore typically a simplified version of the truth model (often to a linear form). The performance of the tracking filter is usually evaluated by implementing the truth model and the filter equations in Monte Carlo simulations[2]. This makes it possible to evaluate several different filter models without testing them in real tracking systems. To summarize, the term tracking model is actually representing two different systems:

1. The truth model, representing the physical system in real tracking scenarios, or the truth in simulations (called simulation model in **paper C**).

2. The filter model, which the implemented equations in the tracking filter are based on.

When certain filters are said to be optimal, it is with an underlying assumption that the filter model is equal to the truth model. It is therefore important to have that separation in mind whenever the term tracking model is used.

The standard linear discrete-time dynamic model in tracking is

$$x_{k+1} = Fx_k + v_k \qquad z_k = Hx_k + w_k \tag{3.1}$$

where

| | | | |
|---|---|---|---|
| $x:$ | target state | $F:$ | transition matrix |
| $z:$ | measurement | $H:$ | measurement matrix |
| $v:$ | process noise | $w:$ | measurement noise |
| $k:$ | time index | | |

The plant equation in (3.1)

$$x_{k+1} = Fx_k + v_k \tag{3.2}$$

represents the target and its dynamics, and uncertainties about the target's dynamics are included in the process noise $v_k$. The measurement equation in (3.1)

$$z_k = Hx_k + w_k \tag{3.3}$$

describes the sensor and the way measurements are obtained. The uncertainties in the sensor and the disturbances in the medium between the sensor and the target are included in the measurement noise $w_k$. The process and measurement noises are assumed additive, independent, white and Gaussian with covariance matrices

$$E\{v_k v_k^T\} = Q \qquad E\{w_k w_k^T\} = R \tag{3.4}$$

In the linear system above, a Kalman filter (KF) is optimal as long as there is no measurement association uncertainty. Unfortunately, in real data this is not true due to false measurements originating from the background noise. Instead, a set of measurements is available at time $k$, which after validation is reduced to a set of $m_k$ validated

[2]If the truth model is linear, covariance analysis is sufficient to evaluate the performance.

measurements $Z_k = \{z_k(1), z_k(2), \ldots, z_k(m_k)\}$. This set, $Z_k$, are measurements that have fallen inside a validation gate around the predicted target position. Because of this uncertainty of the origin of the measurements, a form of data association is needed. Filters that include data association are presented in the following chapters, and are based on the filters presented in this chapter.

## 3.2 Kalman Filter

The Kalman filter (KF), first introduced by [40], is probably the most common filtering technique for state estimation in linear systems.

### 3.2.1 Assumptions

The fundamental assumptions of the KF are:

(a) The state evolves according to a known linear plant equation with additive process noise. The process noise is zero-mean and white, with known covariance $Q$.

(b) Measurements are obtained from a known linear function of the state, with additive measurement noise. The measurement noise is zero-mean and white, with known covariance $R$.

(c) The initial state is assumed to be a random variable with known mean and covariance.

(d) The initial errors and noises are mutually uncorrelated.

With the above assumptions, the KF is the best linear minimum mean square error (MMSE) state estimator (best within the class of linear estimators). If in addition the initial state and all the noises are Gaussian distributed, the KF is the MMSE state estimator.

### 3.2.2 KF Algorithm

Define the state estimate at the current time $k$ as

$$\hat{x}_{k|k} \triangleq E\left\{x_k | Z^k\right\} \tag{3.5}$$

which is the conditional mean of the state at time $k$ given the measurements up to and including time $k$, $Z^k$. The associated covariance matrix at time $k$ is

$$P_{k|k} = E\left\{\left(x_k - \hat{x}_{k|k}\right)\left(x_k - \hat{x}_{k|k}\right)^T | Z^k\right\} \tag{3.6}$$

One cycle of the KF algorithm consists of mapping the estimates at time $k-1$, $\hat{x}_{k-1|k-1}$ and $P_{k-1|k-1}$, into the corresponding estimates at time $k$, $\hat{x}_{k|k}$ and $P_{k|k}$, using the following equations:

$$\hat{x}_{k|k} = \hat{x}_{k|k-1} + W_k \left( z_k - \hat{z}_{k|k-1} \right) \tag{3.7}$$

$$P_{k|k} = P_{k|k-1} - W_k S_k W_k^T \tag{3.8}$$

where the predicted state $\hat{x}_{k|k-1}$, covariance $P_{k|k-1}$ and measurement $\hat{z}_{k|k-1}$ are

$$\hat{x}_{k|k-1} = F\hat{x}_{k-1|k-1} \tag{3.9}$$

$$P_{k|k-1} = FP_{k-1|k-1}F^T + Q \tag{3.10}$$

$$\hat{z}_{k|k-1} = H\hat{x}_{k|k-1} \tag{3.11}$$

and the Kalman gain $W_k$ and the predicted measurement covariance $S_k$ are

$$W_k = P_{k|k-1}H^T S_k^{-1} \tag{3.12}$$

$$S_k = HP_{k|k-1}H^T + R \tag{3.13}$$

The initial values assumed to be available are $\hat{x}_{0|0}$ and $P_{0|0}$.

The KF is often divided into two steps:

1. Time update (prediction).
2. Measurement update.

The first step is to predict the future, given by (3.9) - (3.11), based on our knowledge at the current time. In the measurement update, the predicted state is adjusted by incorporating the new information given by the measurement $z_k$ according to (3.7), and the uncertainty in (3.8) is reduced as a direct consequence of the fact that new information has been added.

The key factor in the KF is the Kalman gain, $W_k$ in (3.12), which is (in the scalar case) proportional to the state variance and inversely proportional to the predicted measurement variance. Using (3.11) in (3.7), the updated state can be written as

$$\hat{x}_{k|k} = (I - W_k H)\, \hat{x}_{k|k-1} + W_k z_k \tag{3.14}$$

where the updated state is clearly a weighted sum of the predicted state and the measurement. From this, the Kalman gain is:

- large if the state prediction is inaccurate (large $P_{k|k-1}$) and the measurement accurate (small $S_k$).
- small if the state prediction is accurate (small $P_{k|k-1}$) and the measurement inaccurate (large $S_k$).

The Kalman filter is thoroughly discussed in the literature, and can be found in several text books, such as [10], [11] and [32].

## 3.3 Extended Kalman Filter

Many of the problems encountered in practice are nonlinear in nature. A suboptimal state estimation algorithm for nonlinear systems is the extended Kalman filter (EKF) [11]. The EKF is similar to the KF in form, and is obtained by linearization. The assumptions are the same as for the KF except that the plant equation and/or the measurement equation are nonlinear functions (still assuming additive noise)

$$x_k = f(x_{k-1}, k-1) + v_{k-1} \qquad z_k = h(x_k, k) + w_k \tag{3.15}$$

One cycle of the EKF algorithm consists of mapping the estimates at time $k-1$, $\hat{x}_{k-1|k-1}$ and $P_{k-1|k-1}$, into the corresponding estimates at time $k$, $\hat{x}_{k|k}$ and $P_{k|k}$, using the following equations:

$$\hat{x}_{k|k} = \hat{x}_{k|k-1} + W_k \left(z_k - \hat{z}_{k|k-1}\right) \tag{3.16}$$
$$P_{k|k} = P_{k|k-1} - W_k S_k W_k^T \tag{3.17}$$

where the predicted state, covariance and measurement are

$$\hat{x}_{k|k-1} = f\left(\hat{x}_{k-1|k-1}, k-1\right) \tag{3.18}$$
$$P_{k|k-1} = F_{k-1} P_{k-1|k-1} F_{k-1}^T + Q \tag{3.19}$$
$$\hat{z}_{k|k-1} = h(\hat{x}_{k|k-1}, k) \tag{3.20}$$

and the Kalman gain and the predicted measurement covariance are

$$W_k = P_{k|k-1} H_k^T S_k^{-1} \tag{3.21}$$
$$S_k = H_k P_{k|k-1} H_k^T + R \tag{3.22}$$

The Jacobians $F_k$ and $H_k$ are obtained by

$$F_k = \left.\frac{\partial f(x,k)}{\partial x}\right|_{x=\hat{x}_{k|k}} \qquad H_k = \left.\frac{\partial h(x,k)}{\partial x}\right|_{x=\hat{x}_{k|k-1}} \tag{3.23}$$

where the linearization (evaluation of the Jacobians) are done at the latest state estimate. The main difference from the KF is this evaluation of the Jacobians such that $F_k$ and $H_k$ take the role of the transition matrix $F$ and measurement matrix $H$ in the KF.

The use of linearization, where the Jacobians are evaluated at the estimated states rather than the true states, and higher order terms are neglected, has the potential of introducing unmodeled errors. The EKF is also very sensitive to the accuracy of the initial conditions. However, if the initial errors and the noises are not too large, the EKF performs well in practice [10].

## 3.4 Converted Measurement Kalman Filter

The target motion in target tracking is best modeled in Cartesian coordinates. In some practical tracking scenarios, the plant equation is linear but the measurement equation is nonlinear because the measurements are obtained in polar coordinates (range and bearing) by an active sonar or radar system. An alternative to the EKF, when only the measurement equation is nonlinear, is the converted measurement Kalman filter (CMKF). By using a proper polar to Cartesian conversion, the linearization of the nonlinear measurement equation in the EKF is omitted, and a standard KF can be used. In [10] the CMKF with debiasing is shown to be consistent (the estimation error is unbiased and the estimated covariance matrix is compatible with the actual mean square error (MSE) covariance matrix). This is unlike the EKF which is consistent only for small errors. Since the CMKF has the correct covariance, it processes the measurements with a gain that is (nearly) optimal, and yields smaller errors than the EKF, even in the case of moderately accurate sensors.

Define the measured range $r$ and measured bearing $\psi$ based on the true range $r_{\text{true}}$ and bearing $\psi_{\text{true}}$ as

$$r = r_{\text{true}} + \tilde{r} \qquad \psi = \psi_{\text{true}} + \tilde{\psi}$$

where $\tilde{r}$ and $\tilde{\psi}$ are the true errors. The true errors are assumed to be independent and zero-mean with standard deviation $\sigma_r$ and $\sigma_\psi$ in range and bearing respectively, yielding the polar covariance matrix

$$R_p = \begin{bmatrix} \sigma_r^2 & 0 \\ 0 & \sigma_\psi^2 \end{bmatrix} \tag{3.24}$$

These polar measurements are converted to Cartesian by the standard coordinate conversion

$$x = r\cos\psi \qquad y = r\sin\psi \tag{3.25}$$

The true Cartesian coordinates $(x_{\text{true}}, y_{\text{true}})$ can be approximated by taking the first order terms of the Taylor series expansion of (3.25) at $(r, \psi)$

$$x_{\text{true}} = r_{\text{true}}\cos\psi_{\text{true}} \approx r\cos\psi + \cos\psi(r_{\text{true}} - r) - r\sin\psi(\psi_{\text{true}} - \psi) \tag{3.26}$$

$$y_{\text{true}} = r_{\text{true}}\sin\psi_{\text{true}} \approx r\sin\psi + \sin\psi(r_{\text{true}} - r) + r\cos\psi(\psi_{\text{true}} - \psi) \tag{3.27}$$

By using this, the linearized Cartesian coordinate errors $(\tilde{x}_L, \tilde{y}_L)$ are defined as

$$x - x_{\text{true}} \approx \tilde{r}\cos\psi - \tilde{\psi}r\sin\psi \triangleq \tilde{x}_L \tag{3.28}$$

$$y - y_{\text{true}} \approx \tilde{r}\sin\psi + \tilde{\psi}r\cos\psi \triangleq \tilde{y}_L \tag{3.29}$$

From the assumption above, the linearized Cartesian coordinate errors $(\tilde{x}_L, \tilde{y}_L)$ in (3.28) and (3.29) are zero-mean with the corresponding covariance matrix in Cartesian coordinates

$$R_c = \begin{bmatrix} R_c^{11} & R_c^{12} \\ R_c^{21} & R_c^{22} \end{bmatrix} \tag{3.30}$$

where

$$R_c^{11} \triangleq \text{var}(\tilde{x}_L) = r^2\sigma_\psi^2 \sin^2\psi + \sigma_r^2 \cos^2\psi \tag{3.31}$$

$$R_c^{22} \triangleq \text{var}(\tilde{y}_L) = r^2\sigma_\psi^2 \cos^2\psi + \sigma_r^2 \sin^2\psi \tag{3.32}$$

$$R_c^{12} = R_c^{21} \triangleq \text{cov}(\tilde{x}_L, \tilde{y}_L) = (\sigma_r^2 - r^2\sigma_\psi^2)\cos\psi \sin\psi \tag{3.33}$$

Due to the linearization in the CMKF using the standard coordinate conversion, the converted measurements will be biased and the corresponding covariance matrices will be optimistic. A slightly more complicated method than the standard conversion is the debiased conversion where the bias and covariance are obtained without linearization. This leads to the CMKF with debiasing, presented in [10]. According to [10], the debiased conversion is recommended whenever the limit of the validity of the standard conversion is exceeded. The limit for when the standard conversion is valid is given as

$$\frac{r\sigma_\psi^2}{\sigma_r} < 0.4 \qquad \sigma_\psi < 0.4\text{rad} \approx 23^\circ \tag{3.34}$$

In the real tracking scenarios in this thesis (**paper A** and **paper C**) the above limit is not exceeded, hence the standard conversion is used.

## 3.5 Track Formation and Termination

The tracking filters discussed above assume that the track is already initialized (initial values are available), and when a track is initialized, there are no included rules for how to terminate the track. This is also true for some of the tracking filters presented in the following chapters, such as the probabilistic data association filter (PDAF) and the joint probabilistic data association filter (JPDAF). Hence, procedures for formation and termination of tracks are necessary. A simple and common method to initialize tracks is the two-point differencing method [11]. Any successive pair of detections within a maximum distance based on target maximum motion parameters and measurement noise variances initiates a preliminary track. This preliminary track, containing the initial state and the corresponding covariance, can now initialize the filter. To reduce the amount of false tracks, a "$p/q$" logic-based track formation procedure can be used. In this procedure a preliminary track has to receive measurements for a minimum of $p$ time steps during the first $q$ scans to become valid.

To terminate a track a logic suitable for the application is needed, and a set of rules has to be made. As an example, some simple rules on how to terminate tracks are listed below:

- The estimated speed exceeds a minimum or maximum threshold.
- The measurement is already associated with another target.
- There are no validated measurements during a given period of time.

- The position moves more than a threshold between two successive scans.
- The estimation error variance exceeds a threshold.
- The estimated position has not changed during several time steps.

It should also be noted that in some filters, such as the integrated probabilistic data association filter (IPDAF) [50], the version of the interacting multiple model probabilistic data association filter (IMMPDAF) presented in [10], and the multiple hypothesis tracking (MHT) presented in Chapter 5, the track formation and termination are included.

# 4

# Single-Target Single-Sensor Tracking

THIS chapter considers tracking of single targets, or more precisely, targets that are well separated in space. For well spatially separated targets, each of them can be tracked by running several single target filters in parallel. This simple approach for multitarget tracking is possible for all the presented algorithms in this chapter. The optimal Bayesian approach (OBA), considering all possible combinations of measurement sequences, is presented first. Then the probabilistic data association filter (PDAF), where only the latest set of measurements is considered, is derived. Finally, an approach of tracking targets in the presence of a wake is presented.

## 4.1 Optimal Bayesian Approach

In the optimal Bayesian approach (OBA) the decomposition of the state estimate is based on all combinations of measurements from the initial to the present time. This optimal method is presented next, with the following assumptions:

(a) There is only one target, modeled by (3.1) and (3.4), whose track is already initialized.

(b) A validation region or gate is set up for each time step to select the candidate measurements for association (called validated measurements).

(c) At time $k$ there are $m_k$ validated measurements but at most one of them can be target-originated. The remaining measurements are assumed due to i.i.d. uniformly spatially distributed false alarms, independent across time.

(d) Detections of the real target occur independently over time with known detection probability $P_D$.

Denote the measurements up to and including time $k$ as $Z^k = \{Z_0, Z_1, \ldots, Z_k\}$, where $Z_k = \{z_k(1), z_k(2), \ldots, z_k(m_k)\}$ are the validated measurements at time $k$. From $Z^k$, let $Z^{k,l}$ be the $l^{\text{th}}$ sequence of measurements out of all combinations of measurement sequences up to time $k$. The sequence $Z^{k,l}$, also called the measurement history, is composed of the current measurement $z_k(i)$ at time $k$ and the history $Z^{k-1,s}$, which is the prior part of the history $Z^{k,l}$ up to time $k$

$$Z^{k,l} = \left\{ Z^{k-1,s}, z_k(i) \right\} \tag{4.1}$$

The total number of measurement histories at time $k$ is

$$L_k = \prod_{j=1}^{k} (1 + m_j) \tag{4.2}$$

where $m_j$ is the number of measurements at time $j$. The possibility that none of the measurements are correct is also accounted for in (4.2).

The event that the $l^{\text{th}}$ history at time $k$ is the correct sequence of measurements is denoted as $\theta^{k,l}$, and its probability, conditioned on all the measurements up to time $k$, as

$$\beta^{k,l} = P\left\{ \theta^{k,l} | Z^k \right\} \tag{4.3}$$

### 4.1.1 State and Covariance Update

The conditional mean of the state estimate at time $k$ can, using the total probability theorem, be written as

$$\hat{x}_{k|k} = E\left\{ x_k | Z^k \right\} = \sum_{l=1}^{L_k} E\left\{ x_k | \theta^{k,l}, Z^k \right\} P\left\{ \theta^{k,l} | Z^k \right\} = \sum_{l=1}^{L_k} \hat{x}^l_{k|k} \beta^{k,l} \tag{4.4}$$

since the events $\theta^{k,l}$, for $l = 1, \ldots, L_k$, are mutually exclusive and exhaustive. Each history-conditioned estimate is provided by a standard filter

$$\hat{x}^l_{k|k} = \hat{x}^s_{k|k-1} + W^l_k \left( z_k(i) - \hat{z}^s_{k|k-1} \right) \tag{4.5}$$

where $z_k(i)$ is the latest measurement of sequence $l$ and $\hat{z}^s_{k|k-1}$ is the predicted measurement corresponding to its ancestor $\theta^{k-1,s}$, with covariance

$$S^s_k = H P^s_{k|k-1} H^T + R \tag{4.6}$$

The predicted state $\hat{x}^s_{k|k-1}$, measurement $\hat{z}^s_{k|k-1}$, and state covariance $P^s_{k|k-1}$, corresponding to event $\theta^{k-1,s}$, are obtained using the standard prediction equations presented for the KF in the previous chapter. The Kalman gain in (4.5) is

$$W^l_k = P^s_{k|k-1} H S^{sT}_k \tag{4.7}$$

The covariance of the history-conditioned updated state is given by the standard equation

$$P_{k|k}^{l} = E\left\{\left(x_k - \hat{x}_{k|k}^{l}\right)\left(x_k - \hat{x}_{k|k}^{l}\right)^T |\theta^{k,l}, Z^k\right\} = P_{k|k-1}^{s} - W_k^l S_k^s {W_k^l}^T \tag{4.8}$$

Finally, according to [9], the covariance associated with the combined estimate is

$$P_{k|k} = \sum_{l=1}^{L_k} \beta^{k,l} P_{k|k}^{l} + \sum_{l=1}^{L_k} \beta^{k,l} \hat{x}_{k|k}^{l} \left[\hat{x}_{k|k}^{l}\right]^T - \hat{x}_{k|k}\hat{x}_{k|k}^T \tag{4.9}$$

The combined estimates in (4.4) and (4.9) are used for output (display) and measurement validation only. The measurement validation is described next.

### 4.1.2 Measurement Validation

At time $k$, prior to obtaining the latest set of measurements, $Z_k$, the predicted state $\hat{x}_{k|k-1}$, the associated covariance $P_{k|k-1}$, and the predicted measurement $\hat{z}_{k|k-1}$, are calculated as in the KF. Then a set of measurements is obtained in the detection process, but to reduce the computational load, only those measurements that fall in the validation region set up around the predicted measurement will be used in the filter. This measurement validation region, also called the validation gate, is the elliptical region

$$\mathcal{V}_k(\gamma) = \left\{z : [z - \hat{z}_{k|k-1}]^T S_k^{-1} [z - \hat{z}_{k|k-1}] \leq \gamma\right\} \tag{4.10}$$

where $\gamma$ is the gate threshold determined by the chosen gate probability $P_G$, and

$$S_k = H P_{k|k-1} H^T + R \tag{4.11}$$

is the covariance of the innovation corresponding to the true target-originated measurement, calculated as in the KF. The volume of the gate is

$$V_k = c_{n_z} |\gamma S_k|^{1/2} = c_{n_z} \gamma^{\frac{n_z}{2}} |S_k|^{1/2} \tag{4.12}$$

where the coefficient $c_{n_z}$, given by

$$c_{n_z} = \frac{\pi^{n_z/2}}{\Gamma(n_z/2 + 1)} \tag{4.13}$$

is the volume of the $n_z$-dimensional unit hypersphere, and $n_z$ is the dimension of the measurement vector.

### 4.1.3 Probabilities of Measurement Histories

In this section the association probabilities of the measurement histories $\beta^{k,l}$ in (4.3) are derived. Define the association events of the latest set of measurements, $Z_k$, as

$$\theta_k(i) = \begin{cases} z_k(i) \text{ originates from the target} & i = 1, \ldots, m_k \\ \text{none of the measurements originate from the target} & i = 0 \end{cases} \tag{4.14}$$

where $\theta_k(i)$ is mutually exclusive and exhaustive for $m_k \geq 1$, and let $m^k$ be the vector containing the number of validated measurements at each time step up to time $k$, $m^k = [m_1, m_2, \ldots, m_k]$. Since $m^k$ follows from $Z^k$, the probability $\beta^{k,l}$ can be written as

$$\begin{aligned}\beta^{k,l} &= P\left\{\theta^{k,l}|Z^k, m^k\right\} = P\left\{\theta_k(i), \theta^{k-1,s}|Z_k, m_k, Z^{k-1}, m^{k-1}\right\} \\ &= \frac{1}{c} p\left(Z_k|\theta_k(i), \theta^{k-1,s}, m_k, Z^{k-1}, m^{k-1}\right) P\left\{\theta_k(i)|\theta^{k-1,s}, m_k, Z^{k-1}, m^{k-1}\right\} \beta^{k-1,s}\end{aligned} \tag{4.15}$$

where the last line is obtained using Bayes' formula, and $c$ is a normalization constant.

The target-originated measurement at time $k$ is assumed Gaussian distributed

$$\begin{aligned}p\left(z_k(i)|\theta_k(i), \theta^{k-1,s}, m_k, Z^{k-1}, m^{k-1}\right) &= \frac{1}{P_G}\mathcal{N}\left(z_k(i); \hat{z}^s_{k|k-1}, S^s_k\right) \\ &= \frac{1}{P_G}\mathcal{N}\left(\nu^s_k(i); 0, S^s_k\right)\end{aligned} \tag{4.16}$$

where $P_G$ is used to account for restricting the normal density to the validation gate, and $\nu^s_k(i) = z_k(i) - \hat{z}^s_{k|k-1}$ is the innovation of measurement $z_k(i)$ corresponding to event $\theta^{k-1,s}$ being true. The pdf of a false measurement is assumed uniform in the validation region whose volume $V_k$ is given in (4.12)

$$p(z_k(i)|\theta_k(j), j \neq i) = \frac{1}{V_k} \tag{4.17}$$

The conditional joint density of the validated measurements in (4.15) is the product of the pdf of each measurement, given by (4.16) and (4.17), assuming that the measurements are independent

$$p\left(Z_k|\theta_k(i), \theta^{k-1,s}, m_k, Z^{k-1}, m^{k-1}\right) = \begin{cases} \left(\frac{1}{V_k}\right)^{m_k - 1} \frac{\mathcal{N}\left(\nu^s_k(i); 0, S^s_k\right)}{P_G} & i = 1, \ldots, m_k \\ \left(\frac{1}{V_k}\right)^{m_k} & i = 0 \end{cases} \tag{4.18}$$

Next, consider the third term of (4.15)

$$P\left\{\theta_k(i)|\theta^{k-1,s}, m_k, Z^{k-1}, m^{k-1}\right\} = P\left\{\theta_k(i)|m_k\right\} \tag{4.19}$$

Here, the conditioning terms $Z^{k-1}$, $m^{k-1}$ and $\theta^{k-1,s}$ (the past measurements and association event) are omitted since the prior probability of the association event $\theta_k(i)$ does not depend on them. Denote the number of measurements $m_k$ as $\boldsymbol{m} = m$ where $m$ is the realization and $\boldsymbol{m}$ the random variable, and let $\phi$ be the number of false measurements.

Then (4.19) yields

$$
\begin{aligned}
P\{\theta_k(i)|m_k\} =& P\{\theta_k(i)|\boldsymbol{m}=m\} \\
=& P\{\theta_k(i)|\boldsymbol{m}=m,\phi=m-1\}\, P\{\phi=m-1|\boldsymbol{m}=m\} \\
&+ P\{\theta_k(i)|\boldsymbol{m}=m,\phi=m\}\, P\{\phi=m|\boldsymbol{m}=m\} \\
=& \begin{cases} \frac{1}{m} P\{\phi=m-1|\boldsymbol{m}=m\} + 0P\{\phi=m|\boldsymbol{m}=m\} & i=1,\ldots,m \\ 0P\{\phi=m-1|\boldsymbol{m}=m\} + 1P\{\phi=m|\boldsymbol{m}=m\} & i=0 \end{cases} \\
=& \begin{cases} \frac{1}{m} P\{\phi=m-1|\boldsymbol{m}=m\} & i=1,\ldots,m \\ P\{\phi=m|\boldsymbol{m}=m\} & i=0 \end{cases}
\end{aligned} \tag{4.20}
$$

Using Bayes' formula one has

$$
\begin{aligned}
P\{\phi=m-1|\boldsymbol{m}=m\} =& \frac{P\{\boldsymbol{m}=m|\phi=m-1\}\, P\{\phi=m-1\}}{P\{\boldsymbol{m}=m\}} \\
=& \frac{P_G P_D \mu_F(m-1)}{P\{\boldsymbol{m}=m\}}
\end{aligned} \tag{4.21}
$$

where $\mu_F$ is the point mass function (pmf) of the number of false measurements, and $P_D P_G$ is the probability that the target has been detected and its measurement is inside the validation region. Similarly,

$$
P\{\phi=m|\boldsymbol{m}=m\} = \frac{P\{\boldsymbol{m}=m|\phi=m\}\, P\{\phi=m\}}{P\{\boldsymbol{m}=m\}} = \frac{(1-P_G P_D)\mu_F(m)}{P\{\boldsymbol{m}=m\}} \tag{4.22}
$$

where the denominator is

$$
P\{\boldsymbol{m}=m\} = P_G P_D \mu_F(m-1) + (1-P_G P_D)\mu_F(m) \tag{4.23}
$$

Combining (4.21), (4.22) and (4.23) into (4.20) yields

$$
\begin{aligned}
P\{\theta_k(i)|m_k\} &= \begin{cases} \frac{1}{m_k} \frac{P_G P_D \mu_F(m_k-1)}{P_G P_D \mu_F(m_k-1)+(1-P_G P_D)\mu_F(m_k)} & i=1,\ldots,m_k \\ \frac{(1-P_G P_D)\mu_F(m_k)}{P_G P_D \mu_F(m_k-1)+(1-P_G P_D)\mu_F(m_k)} & i=0 \end{cases} \\
&= \begin{cases} \frac{\frac{1}{m_k} P_G P_D}{P_G P_D + (1-P_G P_D)\frac{\mu_F(m_k)}{\mu_F(m_k-1)}} & i=1,\ldots,m_k \\ \frac{(1-P_G P_D)\frac{\mu_F(m_k)}{\mu_F(m_k-1)}}{P_G P_D + (1-P_G P_D)\frac{\mu_F(m_k)}{\mu_F(m_k-1)}} & i=0 \end{cases}
\end{aligned} \tag{4.24}
$$

Two models can be used for the pmf $\mu_F(m)$ in a volume of interest $V$:

1. The Poisson model with a spatial density $\lambda$

$$\mu_F(m) = e^{\lambda V} \frac{(\lambda V)^m}{m!} \tag{4.25}$$

2. The diffuse prior model with a constant that is irrelevant since it cancels out

$$\mu_F(m) = \mu_F(m-1) = \epsilon \tag{4.26}$$

Inserting these models in (4.24) yields

1. The Poisson model approach

$$P\left\{\theta_k(i)|m_k\right\} = \begin{cases} \frac{P_G P_D}{P_G P_D m_k + (1-P_G P_D)\lambda V_k} & i = 1, \ldots, m_k \\ \frac{(1-P_G P_D)\lambda V_k}{P_G P_D m_k + (1-P_G P_D)\lambda V_k} & i = 0 \end{cases} \tag{4.27}$$

2. The diffuse prior model approach

$$P\left\{\theta_k(i)|m_k\right\} = \begin{cases} \frac{1}{m_k} P_G P_D & i = 1, \ldots, m_k \\ (1 - P_G P_D) & i = 0 \end{cases} \tag{4.28}$$

Notice that the nonparametric model (diffuse prior) can be obtained from the parametric model (Poisson) by setting

$$\lambda = \frac{m_k}{V_k} \tag{4.29}$$

The last step, assuming the nonparametric diffuse prior model approach, is to insert (4.18) and (4.27) into $\beta^{k,l}$ in (4.15)

$$\begin{aligned} \beta^{k,l} =& p\left(Z_k|\theta_k(i), \theta^{k-1,s}, m_k, Z^{k-1}, m^{k-1}\right) P\left\{\theta_k(i)|m_k\right\} \beta^{k-1,s} \\ =& \frac{1}{c} \begin{cases} \left(\frac{1}{V_k}\right)^{m_k - 1} \mathcal{N}\left(\nu_k^S(i); 0, S_k^s\right) \frac{P_D}{m_k} \beta^{k-1,s} & i = 1, \ldots, m_k \\ \left(\frac{1}{V_k}\right)^{m_k} (1 - P_G P_D) \beta^{k-1,s} & i = 0 \end{cases} \\ =& \frac{1}{c} \begin{cases} \frac{P_D}{m_k} \left(\frac{1}{V_k}\right)^{m_k - 1} \mathcal{N}\left(\nu_k^s(i); 0, S_k^s\right) \beta^{k-1,s} & i = 1, \ldots, m_k \\ \frac{P_D}{m_k} \left(\frac{1}{V_k}\right)^{m_k - 1} \frac{(1-P_G P_D) m_k}{P_D V_k} \beta^{k-1,s} & i = 0 \end{cases} \\ =& \frac{1}{c'} \begin{cases} \frac{1}{\left|2\pi S_k^s\right|^{\frac{1}{2}}} e^{-\frac{1}{2} \nu_k^s(i)^T (S_k^s)^{-1} \nu_k^s(i)} \beta^{k-1,s} & i = 1, \ldots, m_k \\ \frac{(1-P_G P_D) m_k}{P_D V_k} \beta^{k-1,s} & i = 0 \end{cases} \end{aligned} \tag{4.30}$$

In the last step of (4.30) the term

$$\frac{P_D}{m_k}\left(\frac{1}{V_k}\right)^{m_k-1} \tag{4.31}$$

is brought into the normalizing constant, and the Gaussian distribution $\mathcal{N}\left(\nu_k^s(i);0,S_k^s\right)$ is substituted by the explicit expression

$$\mathcal{N}\left(\nu_k^s(i);0,S_k^s\right)=\frac{1}{\left|2\pi S_k^s\right|^{\frac{1}{2}}}e^{-\frac{1}{2}\nu_k^s(i)^T(S_k^s)^{-1}\nu_k^s(i)} \tag{4.32}$$

The last term in (4.15), $\beta^{k-1,s}$, is the probability of the ancestor part of history under consideration, available from the previous sampling time.

To summarize: the association probabilities, assuming a nonparametric model, can be calculated as

$$\beta^{k,l}=\begin{cases} ce^{-\frac{1}{2}\nu_k^s(i)^T(S_k^s)^{-1}\nu_k^s(i)}\beta^{k-1,s} & i=1,\ldots,m_k \\ c\left|2\pi S_k^s\right|^{\frac{1}{2}}\frac{(1-P_GP_D)m_k}{P_DV_k}\beta^{k-1,s} & i=0 \end{cases} \tag{4.33}$$

and by using (4.29), the parametric model approach yields

$$\beta^{k,l}=\begin{cases} ce^{-\frac{1}{2}\nu_k^s(i)^T(S_k^s)^{-1}\nu_k^s(i)}\beta^{k-1,s} & i=1,\ldots,m_k \\ c\left|2\pi S_k^s\right|^{\frac{1}{2}}\frac{(1-P_GP_D)\lambda}{P_D}\beta^{k-1,s} & i=0 \end{cases} \tag{4.34}$$

where $c$ is a normalizing constant to ensure that $\sum_{l=1}^{L_k}\beta^{k,l}=1$.

### 4.1.4 Example of the OBA

An example of the first four time steps of the OBA is illustrated in Figure 4.1. Assume, for simplicity, that the track is perfectly initialized at time $k=1$. At time $k=2$ a validation gate is set up around the predicted measurement $\hat{z}_{2|1}$. At this time, two measurements (one true and one false) are validated. These two measurements, in addition to the predicted measurement (accounting for the possibility that none of the validated measurements are correct), yield three different measurement histories at $k=2$. These three history-conditioned estimates are combined to a single estimate $\hat{x}_{2|2}$, and the corresponding predicted measurement $\hat{z}_{3|2}$ determines the validation region at time $k=3$. This procedure repeats for the next time steps resulting in 12 measurement histories at time $k=4$. Notice that in the case of only a single measurement at a time step (as in $k=3$ and $k=4$), the number of measurement histories is doubled.

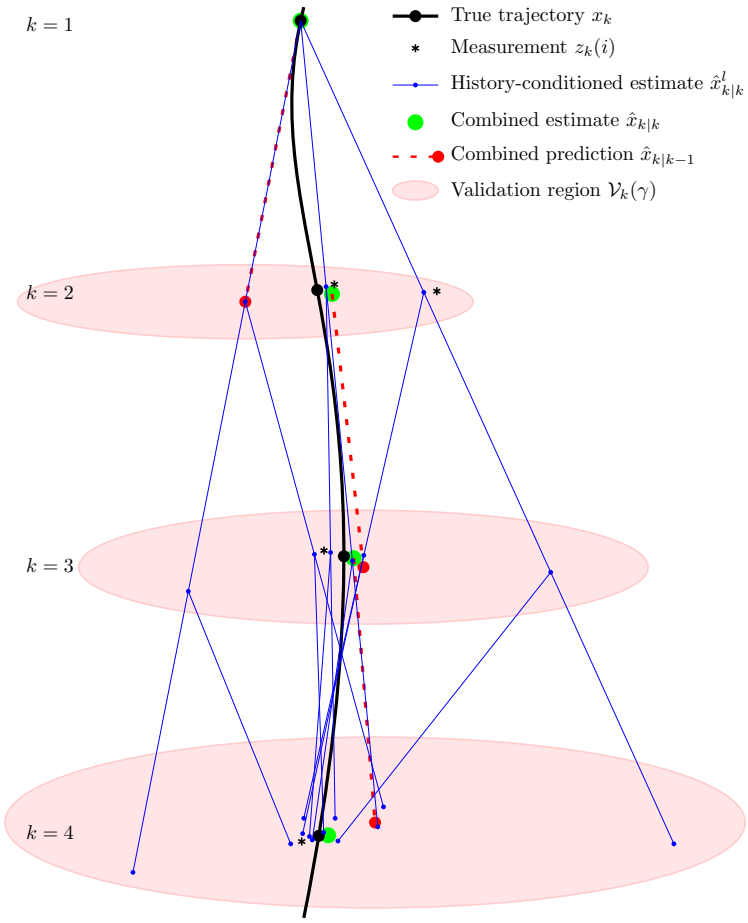


***Figure 4.1:*** *Overview of the OBA algorithm.*

### 4.1.5 Suboptimality

The price for optimality in the presented approach is increased memory and computational requirements. This is due to the exponentially increasing number of measurement histories, given in (4.2). At each time step $k$, every measurement history is propagated through its own tracking filter, e.g., a Kalman filter, and then these histories are saved to the consecutive time step $k + 1$. Since the increasing number of histories is unpractical, several suboptimal versions are developed to reduce the memory and computational requirements. One approach is to limit the histories within a sliding window that covers the current and the previous $N$ sampling times, also called the $N-$scan memory filter [43]. The well-known PDAF, where no measurement histories are carried along and the past is approximated by a single Gaussian distribution, corresponds to $N = 0$ and is described next.

## 4.2 Probabilistic Data Association Filter

The approach of the probabilistic data association filter (PDAF) is to calculate the association probabilities for each validated measurement at the current time to the target of interest. Since the target's state is assumed Gaussian distributed, each measurement, conditioned on originating from the true target, is also Gaussian distributed. The posterior track probability density is therefore a mixture of Gaussian probability density functions (pdf), but instead of propagating all the components in the Gaussian mixture to the next time step, as in the OBA, the Gaussian mixture is forced back to Gaussianity by moment matching for the succeeding scan. In other words, the decomposition of the state estimate in the PDAF is based only on the latest set of measurements, which makes the PDAF suboptimal. The PDAF was originally developed in [12], and is derived in this section.

### 4.2.1 Assumptions

At time $k-1$ the state of the target of interest is estimated as $\hat{x}_{k-1|k-1}$ with associated covariance $P_{k-1|k-1}$. The estimate is conditioned on the entire past up to time $k-1$, and the following assumptions are made:

(a) There is only one target, modeled by (3.1) and (3.4), whose track is already initialized.

(b) The past information about the target is summarized approximately by the Gaussian pdf

$$p\left(x_k|Z^{k-1}\right) \approx \mathcal{N}\left(x_k; \hat{x}_{k|k-1}, P_{k|k-1}\right) \tag{4.35}$$

where

$$Z^{k-1} = \{Z_0, Z_1, \dots Z_{k-1}\} \tag{4.36}$$

and $\hat{x}_{k|k-1}$ and $P_{k|k-1}$ is the predicted state and covariance, respectively.

(c) A validation region or gate is set up for each time step to select the candidate measurements for association.

(d) At time $k$ there are $m_k$ validated measurements, but at most one of them can be target-originated. The remaining measurements are assumed due to i.i.d. uniformly spatially distributed false alarms, independent across time.

(e) Detections of the real target occur independently over time with known detection probability $P_D$.

These assumptions make it possible to obtain a state estimation scheme that is almost as simple as the KF, but much more effective in the presence of false alarms. From assumption (b), the target-originated measurement is Gaussian distributed, and a false alarm is, according to assumption (d), uniformly distributed. This is illustrated in Figure 4.2.

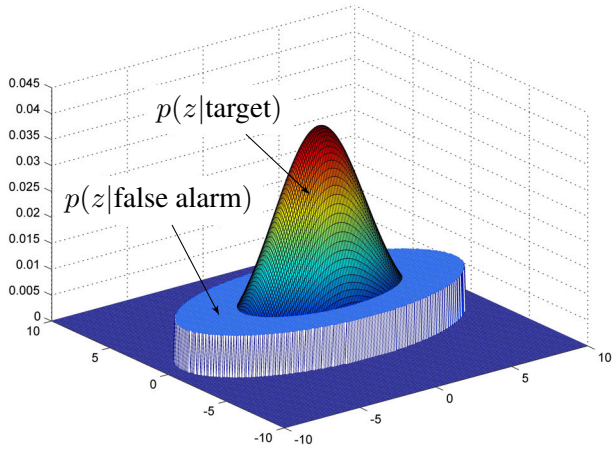


***Figure 4.2:*** *Illustration of the pdfs in the PDAF. The pdf of the target-originated measurement is assumed to be Gaussian, and false alarms are assumed uniformly distributed inside the elliptical validation region.*

The predictions of the target state $\hat{x}_{k|k-1}$, associated covariance $P_{k|k-1}$ and measurement $\hat{z}_{k|k-1}$ at time $k$, based on the estimates at $k-1$, are calculated as in the KF. The validated measurements are obtained by the same procedure as for the OBA, described in Section 4.1.2.

### 4.2.2 State and Covariance Update

Refresh the association events defined in Section 4.1.3:

$$\theta_k(i) = \begin{cases} z_k(i) \text{ originates from the target} & i = 1, \ldots, m_k \\ \text{none of the measurements originate from the target} & i = 0 \end{cases} \tag{4.37}$$

where $\theta_k(i)$ is mutually exclusive and exhaustive for $m_k \geq 1$. Using the total probability theorem [52], the conditional mean of the state at time $k$ is

$$\hat{x}_{k|k} = E\left\{x_k|Z^k\right\} = \sum_{i=0}^{m_k} E\left\{x_k|\theta_k(i), Z^k\right\} P\left\{\theta_k(i)|Z^k\right\} = \sum_{i=0}^{m_k} \hat{x}_{k|k}(i)\beta_k(i) \tag{4.38}$$

where $\hat{x}_{k|k}(i)$ is the updated state conditioned on the event $\theta_k(i)$ being correct, and

$$\beta_k(i) \triangleq P\left\{\theta_k(i)|Z^k\right\} \tag{4.39}$$

is the conditional probability (association probability) of this event. These association probabilities $\beta_k(i)$ are presented in Section 4.2.3.

The estimate conditioned on measurement $i$ being correct is

$$\hat{x}_{k|k}(i) = \hat{x}_{k|k-1} + W_k \nu_k(i) \quad i = 1, \ldots, m_k \tag{4.40}$$

where the corresponding innovation is

$$\nu_k(i) = z_k(i) - \hat{z}_{k|k-1} \tag{4.41}$$

The gain $W_k$ is the same as in the Kalman filter

$$W_k = P_{k|k-1} H^T S_k^{-1} \tag{4.42}$$

since conditioned on the event $\theta_k(i)$, $i \neq 0$, there is no measurement origin uncertainty. For the event $\theta_k(0)$ that all measurements are false, or there is no validated measurement ($m_k = 0$), one has by definition $\nu_k(0) = 0$. Using this in (4.40) yields

$$\hat{x}_{k|k}(0) = \hat{x}_{k|k-1} \tag{4.43}$$

The estimate can now be written as

$$\hat{x}_{k|k} = \sum_{i=0}^{m_k} \beta_k(i) \hat{x}_k(i) = \sum_{i=0}^{m_k} \beta_k(i) \left( \hat{x}_{k|k-1} + W_k \nu_k(i) \right) = \hat{x}_{k|k-1} + W_k \nu_k \tag{4.44}$$

In (4.44) the identity $\sum_{i=0}^{m_k} \beta_k(i) = 1$ is used together with the fact that

$$\sum_{i=0}^{m_k} \beta_k(i) \nu_k(i) = \sum_{i=1}^{m_k} \beta_k(i) \nu_k(i) = \nu_k \tag{4.45}$$

The covariance of the updated state is derived in the same way as the second order

moment of a Gaussian mixture [11]

$$\begin{aligned}
P_{k|k} =& E\left\{\left(x_k - \hat{x}_{k|k}\right)\left(x_k - \hat{x}_{k|k}\right)^T | Z^k\right\} \\
=& \sum_{i=0}^{m_k} E\left\{\left(x_k - \hat{x}_{k|k}\right)\left(x_k - \hat{x}_{k|k}\right)^T | \theta_k(i), Z^k\right\}\beta_k(i) \\
=& \sum_{i=0}^{m_k} E\Big\{\left(x_k - \hat{x}_{k|k}(i) + \hat{x}_{k|k}(i) - \hat{x}_{k|k}\right) \\
& \qquad \times \left(x_k - \hat{x}_{k|k}(i) + \hat{x}_{k|k}(i) - \hat{x}_{k|k}\right)^T | \theta_k(i), Z^k\Big\}\beta_k(i) \\
=& \sum_{i=0}^{m_k} \underbrace{E\left\{[x_k - \hat{x}_{k|k}(i)][x_k - \hat{x}_{k|k}(i)]^T | \theta_k(i), Z^k\right\}}_{P_{k|k}(i)}\beta_k(i) \\
& + \sum_{i=0}^{m_k}[\hat{x}_{k|k}(i) - \hat{x}_{k|k}][\hat{x}_{k|k}(i) - \hat{x}_{k|k}]^T\beta_k(i) \\
=& \underbrace{\sum_{i=0}^{m_k} P_{k|k}(i)\beta_k(i)}_{\bar{P}_{k|k}} + \underbrace{\sum_{i=0}^{m_k} \hat{x}_{k|k}(i)\hat{x}_{k|k}(i)^T\beta_k(i) - \hat{x}_{k|k}\hat{x}_{k|k}^T}_{\tilde{P}_k} \\
=& \bar{P}_{k|k} + \tilde{P}_k
\end{aligned} \tag{4.46}$$

For $i = 0$ in $P_{k|k}(i)$ one has the predicted covariance, while for $i \neq 0$ one has the updated covariance

$$P_{k|k}(0) = P_{k|k-1} \tag{4.47}$$

$$P_{k|k}(i) = P_{k|k-1} - W_k S_k W_k^T \qquad \text{for} \quad i = 1, \ldots, m_k \tag{4.48}$$

which are the same as in the KF. By using $\beta_k(0) = 1 - \sum_{i=1}^{m_k}\beta_k(i)$, $\bar{P}_{k|k}$ in (4.46) can be written as

$$\bar{P}_{k|k} = \sum_{i=0}^{m_k} P_{k|k}(i)\beta_k(i) = \beta_k(0)P_{k|k-1} + [1 - \beta_k(0)]\left(P_{k|k-1} - W_k S_k W_k^T\right) \tag{4.49}$$

The "spread of the means" term $\tilde{P}_k$ in (4.46) can, by using (4.40), (4.43) and (4.44), be rewritten as follows

$$\begin{aligned}
\tilde{P}_k =& \sum_{i=0}^{m_k} \hat{x}_{k|k}(i)\hat{x}_{k|k}(i)^T\beta_k(i) - \hat{x}_{k|k}\hat{x}_{k|k}^T \\
=& \sum_{i=0}^{m_k} \left[\hat{x}_{k|k-1} + W_k\nu_k(i)\right]\left[\hat{x}_{k|k-1} + W_k\nu_k(i)\right]^T\beta_k(i) \\
& - \left[\hat{x}_{k|k-1} + W_k\nu_k\right]\left[\hat{x}_{k|k-1} + W_k\nu_k\right]^T
\end{aligned} \tag{4.50}$$

This becomes, by using the identity $\sum_{i=0}^{m_k} \beta_k(i) = 1$ and (4.45)

$$\begin{aligned}\tilde{P}_k =& \hat{x}_{k|k-1}\hat{x}_{k|k-1}^T + \hat{x}_{k|k-1}\left[W_k\nu_k\right]^T + W_k\nu_k\hat{x}_{k|k-1}^T \\ &+ W_k\sum_{i=0}^{m_k}\left(\beta_k(i)\nu_k(i)\nu_k(i)^T\right)W_k^T - \hat{x}_{k|k-1}\hat{x}_{k|k-1}^T \\ &- \hat{x}_{k|k-1}\left[W_k\nu_k\right]^T - W_k\nu_k\hat{x}_{k|k-1}^T - W_k\nu_k\nu_k^T W_k^T \\ =& W_k\left[\sum_{i=0}^{m_k}\left(\beta_k(i)\nu_k(i)\nu_k(i)^T\right) - \nu_k\nu_k^T\right]W_k^T \end{aligned} \tag{4.51}$$

Inserting (4.49) and (4.51) in (4.46) yields

$$\begin{aligned}P_{k|k} =& \beta_k(0)P_{k|k-1} + \left[1-\beta_k(0)\right]\left(P_{k|k-1} - W_kS_kW_k^T\right) \\ &+ W_k\left[\sum_{i=0}^{m_k}\beta_k(i)\nu_k(i)\nu_k(i)^T - \nu_k\nu_k^T\right]W_k^T \end{aligned} \tag{4.52}$$

Note that the updated pdf of the state is a Gaussian mixture, but is forced back to Gaussianity by moment matching:

$$p\left(x_k|Z^k\right) = \sum_{i=0}^{m_k}\beta_k(i)\mathcal{N}\left(x;\hat{x}_{k|k}(i),P_{k|k}(i)\right) \approx \mathcal{N}\left(x;\hat{x}_{k|k},P_{k|k}\right) \tag{4.53}$$

### 4.2.3 Association Probabilities

In this section the association probabilities $\beta_k(i)$ in (4.39) are derived. By using Bayes' formula, these probabilities can be written as

$$\begin{aligned}\beta_k(i) &= P\left\{\theta_k(i)|Z^k\right\} = P\left\{\theta_k(i)|Z_k,m_k,Z^{k-1}\right\} \\ &= \frac{1}{c}p\left(Z_k|\theta_k(i),m_k,Z^{k-1}\right)P\left\{\theta_k(i)|m_k,Z^{k-1}\right\}\end{aligned} \tag{4.54}$$

The above equation is similar to (4.15) in the OBA, except for the term $\beta^{k-1,s}$, and can be deduced by following the same procedure as for the OBA. The association probabilities, assuming a nonparametric model (4.28), can be calculated as

$$\beta_k(i) = \begin{cases} ce^{-\frac{1}{2}\nu_k(i)^T S_k^{-1}\nu_k(i)} & i = 1,\ldots,m_k \\ c\left|2\pi S_k\right|^{\frac{1}{2}}\frac{(1-P_GP_D)m_k}{P_DV_k} & i = 0 \end{cases} \tag{4.55}$$

and by using (4.29), the parametric model approach (4.27) yields

$$\beta_k(i) = \begin{cases} ce^{-\frac{1}{2}\nu_k(i)^T S_k^{-1}\nu_k(i)} & i = 1,\ldots,m_k \\ c\left|2\pi S_k\right|^{\frac{1}{2}}\frac{(1-P_GP_D)\lambda}{P_D} & i = 0 \end{cases} \tag{4.56}$$

where $c$ is a normalizing constant to ensure that $\sum_{i=0}^{m_k}\beta_k(i) = 1$.

### 4.2.4 Summary of the PDAF

In this section a summary of the PDAF algorithm is given. The following steps in the algorithm are illustrated in Figure 4.3.

(a) The input values at time $k$ are the estimated target state and associated covariance from time $k-1$, denoted as $\hat{x}_{k-1|k-1}$ and $P_{k-1|k-1}$, respectively.

(b) Predict the target state, associated covariance and measurement at time $k$ based on the estimates at $k-1$:

$$\begin{aligned} \hat{x}_{k|k-1} &= F\hat{x}_{k-1|k-1} \\ P_{k|k-1} &= FP_{k-1|k-1}F^T + Q \\ \hat{z}_{k|k-1} &= H\hat{x}_{k|k-1} \end{aligned} \tag{4.57}$$

(c) Compute the innovation covariance for the true target-originated measurement

$$S_k = HP_{k|k-1}H^T + R \tag{4.58}$$

and use $S_k$ to form the measurement validation region.

(d) The validated measurements $Z_k = \{z_k(1), z_k(2), \ldots, z_k(m_k)\}$ result in $m_k$ innovations:

$$\nu_k(i) = z_k(i) - \hat{z}_{k|k-1} \qquad i = 1, \ldots, m_k \tag{4.59}$$

(e) Update the target state and covariance according to

$$\hat{x}_{k|k} = \hat{x}_{k|k-1} + W_k\nu_k \tag{4.60}$$

$$\begin{aligned} P_{k|k} =& \beta_k(0)P_{k|k-1} + [1-\beta_k(0)]\left(P_{k|k-1} - W_kS_kW_k^T\right) \\ &+ W_k\left[\sum_{i=0}^{m_k}\beta_k(i)\nu_k(i)\nu_k(i)^T - \nu_k\nu_k^T\right]W_k^T \end{aligned} \tag{4.61}$$

where the Kalman gain and the combined innovation is

$$W_k = P_{k|k-1}H^TS_k^{-1} \qquad \nu_k = \sum_{i=1}^{m_k}\beta_k(i)\nu_k(i) \tag{4.62}$$

The association probabilities $\beta_k(i)$ (for the nonparametric approach) are calculated as:

$$\beta_k(i) = \begin{cases} ce^{-\frac{1}{2}\nu_k(i)^TS_k^{-1}\nu_k(i)} & i = 1, \ldots, m_k \\ c\left|2\pi S_k\right|^{\frac{1}{2}} m_k\frac{1-P_GP_D}{V_kP_D} & i = 0 \end{cases} \tag{4.63}$$

(f) The track is updated, and by going back to point (a), the updated state and covariance at time $k$ can be used as input values at time $k+1$.

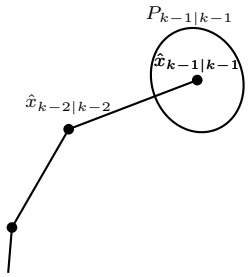


(a) The estimated state $\hat{x}_{k-1|k-1}$ and its covariance $P_{k-1|k-1}$ at time $k-1$.

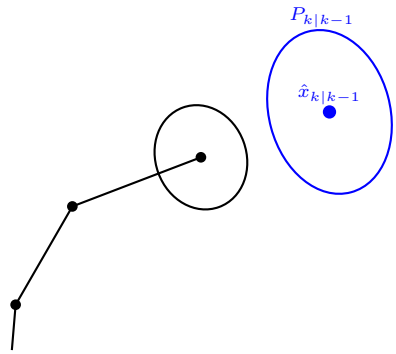


(b) The predicted state $\hat{x}_{k|k-1}$ and covariance $P_{k|k-1}$ at time $k$.

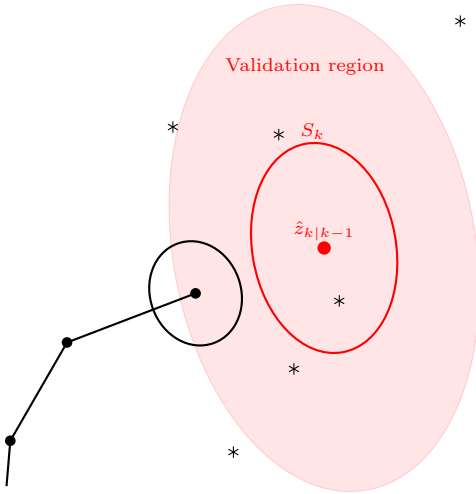


(c) The predicted measurement $\hat{z}_{k|k-1}$, innovation covariance $S_k$, measurements $(*)$ and the validation region at time $k$. Note that $\hat{z}_{k|k-1}$ is the position elements of $\hat{x}_{k|k-1}$.

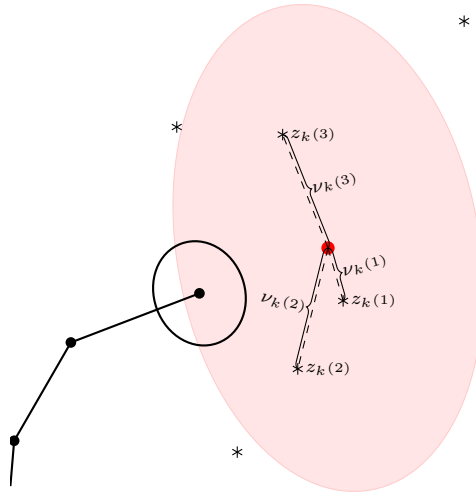


(d) The validated measurements $z_k(1)$, $z_k(2)$ and $z_k(3)$, and their innovations $\nu_k(1)$, $\nu_k(2)$ and $\nu_k(3)$ at time $k$.

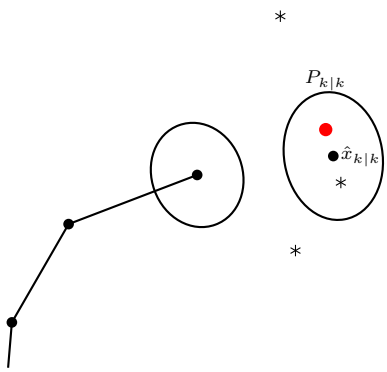


(e) The updated state $\hat{x}_{k|k}$ and covariance $P_{k|k}$ at time $k$.

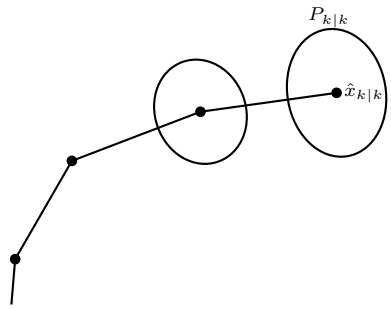


(f) The new track.

***Figure 4.3:*** *Overview of the PDAF algorithm.*

In **paper A** the PDAF is modified to handle false measurements originating from the bubbles behind a diver with an open breathing system. This is accomplished by incorporating a special probabilistic model of the bubbles, such that the false measurements can originate from either the bubbles or from the i.i.d. uniformly distributed noise. The motivation for using such a model was the method of tracking in the presence of a wake [4]. This method is presented next.

## 4.3 Target Tracking in the Presence of a Wake

In this section an algorithm similar to the PDAF in Section 4.2 for the tracking of targets in the presence of a wake is presented [4], [10]. This wake could be air bubbles from a diver, the wake behind a ship, or the wake from ballistic vehicles in the re-entry stage. It is assumed that a single measurement is extracted at each time step in the signal processing, and that this measurement originates from either the target or the wake. The corresponding events are denoted as

$$\theta_k(1) = \{z_k \text{ originates from the target}\} \tag{4.64}$$
$$\theta_k(0) = \{z_k \text{ is false}\} \tag{4.65}$$

with probabilities

$$\beta_k(1) = P\left\{\theta_k(1)|Z^k\right\} \tag{4.66}$$
$$\beta_k(0) = P\left\{\theta_k(0)|Z^k\right\} = 1 - \beta_k(1) \tag{4.67}$$

The estimation is done by evaluating at each time the probability of the latest measurement being correct and using this to update the state.

### 4.3.1 State and Covariance Update

The estimation equations are obtained directly from the PDAF algorithm

$$\hat{x}_{k|k} = \hat{x}_{k|k-1} + \beta_k(1)W_k\nu_k(1) \tag{4.68}$$

$$P_{k|k} = \beta_k(0)P_{k|k-1} + \beta_k(1)\left(P_{k|k-1} - W_kS_kW_k^T\right) + \beta_k(0)\beta_k(1)W_k\nu_k(1)\nu_k(1)^TW_k^T \tag{4.69}$$

by using the "simpler" combined innovation

$$\nu_k = \beta_k(1)\nu_k(1) = \beta_k(1)\left(z_k - \hat{z}_{k|k-1}\right) \tag{4.70}$$

The two association probabilities, $\beta_k(0)$ and $\beta_k(1)$, are presented in the next section.

### 4.3.2 Association Probabilities

The probability $\beta_k(1)$ is obtained as

$$\beta_k(1) = P\left\{\theta_k(1)|Z^k\right\} = P\left\{\theta_k(1)|z_k, Z^{k-1}\right\} \tag{4.71}$$

$$= \frac{p\left(z_k|\theta_k(1), Z^{k-1}\right) P\left\{\theta_k(1)\right\}}{p\left(z_k|\theta_k(0), Z^{k-1}\right) P\left\{\theta_k(0)\right\} + p\left(z_k|\theta_k(1), Z^{k-1}\right) P\left\{\theta_k(1)\right\}} \tag{4.72}$$

where $P\left\{\theta_k(1)\right\}$ and $P\left\{\theta_k(0)\right\}$ are the a priori probabilities of the measurement being correct and false, respectively. Similarly to (4.16), the pdf of a target-originated measurement is

$$p\left(z_k|\theta_k(1), Z^{k-1}\right) = \frac{1}{P_G}\mathcal{N}\left(\nu_k; 0, S_k\right) \tag{4.73}$$

Assuming that the target's wake points away from the sensor, which measures range and bearing, the range measurement $r_k$ can be assumed to have a linear pdf in the interval of length $L_r$, starting at the predicted range $\bar{r}_k$

$$p\left(r_k|\theta_k(0), Z^{k-1}\right) = \frac{2}{L_r^2}(r_k - \bar{r}_k) \qquad \bar{r}_k \leq r_k \leq \bar{r}_k + L_r \tag{4.74}$$

The bearing measurement $\psi_k$ can be assumed uniformly distributed in an interval of length $2L_\psi$ around the predicted bearing $\bar{\psi}_k$

$$p\left(\psi_k|\theta_k(0), Z^{k-1}\right) = \frac{1}{2L_\psi} \qquad \bar{\psi}_k - L_\psi \leq \psi_k \leq \bar{\psi}_k + L_\psi \tag{4.75}$$

This way of modeling the wake-originated measurement is the motivation for the wake models presented in the included papers, **paper A**, **paper B** and **paper C**, in Part II.

# 5

# Multitarget Multisensor Tracking

THIS chapter considers tracking algorithms that can handle multiple targets in the surveillance region simultaneously. It should be noted that the methods presented in Chapter 4 are not "pure" single target tracking algorithms, but can also handle multiple targets as long as the targets' validation regions do not overlap. This is done by running separate filters in parallel, where each target has its own filter. The tracking algorithms in this chapter are developed to handle situations where the validation regions from two or more targets are overlapping. This is the requirement for a "pure" multitarget tracking algorithm. The joint probabilistic data association filter (JPDAF) is first derived, before a coupled version (JPDACF) assuming correlated targets is presented. Then, a brief review of the multiple hypothesis tracking (MHT) algorithm is given.

In recent years there has been an extensive interest in using multiple sensors in surveillance systems. The end of this chapter gives an introduction of the two fundamental multisensor architectures: the centralized configuration and the distributed (decentralized) configuration.

## 5.1 Joint Probabilistic Data Association Filter

In a multitarget environment the data association algorithm needs to handle situations where a measurement could originate from different targets. For this purpose, the joint probabilistic data association filter (JPDAF) [10], [28], [29] was developed to extend the PDAF to a known number of targets whose tracks have been established. The JPDAF evaluates the probabilities for all associations between the targets and the latest set of measurements, and then combines them into the state estimates. This JPDAF algorithm is presented next.

### 5.1.1 Assumptions

At time $k-1$ there is a known number $N_T$ of established targets. For each target $t$, where $t = 1, \ldots, N_T$, the target state is estimated as $\hat{x}^t_{k-1|k-1}$ with associated covariance $P^t_{k-1|k-1}$. The estimates are conditioned on the entire past up to time $k-1$, and the following assumptions are made:

(a) Measurements from one target can fall in the validation gate of a neighboring target.

(b) The past information about target $t$ is summarized approximately by the Gaussian pdf

$$p\left(x^t_k | Z^{k-1}\right) \approx \mathcal{N}\left(x^t_k; \hat{x}^t_{k|k-1}, P^t_{k|k-1}\right) \tag{5.1}$$

where $\hat{x}^t_{k|k-1}$ and $P^t_{k|k-1}$ is the predicted state and covariance, respectively.

(c) At time $k$ there are $m_k$ validated measurements in the union of their validation gates, but for each target $t$ at most one measurement can be target-originated. The rest are assumed to be due to i.i.d. uniformly distributed false alarms, independently across time.

(d) Each target has a dynamic and a measurement model as in (3.1) and (3.4). The models for the various targets do not have to be the same.

(e) Detections of the real targets occur independently over time with known detection probabilities $P^t_D$. The detection probabilities do not have to be the same for the various targets.

### 5.1.2 Joint Association Events

Define the validation matrix $\Omega$ to represent all feasible association events at time $k$ (the time index $k$ is omitted for simplicity where its omission does not cause confusion)

$$\Omega = [\omega(j,t)] \qquad j = 1, \ldots, m \quad \text{and} \quad t = 0, \ldots, N_T \tag{5.2}$$

Here, $\omega(j,t)$ is a binary element indicating whether measurement $j$ lies in the validation gate of target $t$. The index $t = 0$ means that the measurement is from none of the targets and therefore it is a false measurement. An example where a measurement may originate from either of two targets, i.e., it lies in both targets' validation gates, is shown with the corresponding validation matrix $\Omega$ in Figure 5.1.

A joint association event $\Theta$ describes an unambiguous association between the measurements and the targets at time $k$

$$\Theta = \bigcap_{j=1}^{m} \theta(j, t_j) \tag{5.3}$$

where

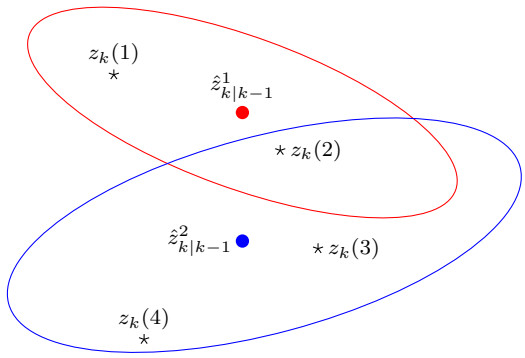


$$\Omega = \begin{array}{c|ccc} j\backslash t & 0 & 1 & 2 \\ \hline 1 & 1 & 1 & 0 \\ 2 & 1 & 1 & 1 \\ 3 & 1 & 0 & 1 \\ 4 & 1 & 0 & 1 \end{array}$$

***Figure 5.1:*** *Two targets with a measurement in the intersection of their validation gates are shown with corresponding validation matrix $\Omega$.*

- $\theta(j, t_j)$ is the event that measurement $j$ originates from target $t_j$.
- $t_j$ is the index of the target to which measurement $j$ is associated in the event under consideration.

The event $\Theta$ can also be represented by the matrix

$$\Omega_\Theta = [\omega_\Theta(j, t)] \tag{5.4}$$

consisting of the units in $\Omega$ corresponding to the associations in $\Theta$, where

$$\omega_\Theta(j, t) = \begin{cases} 1 & \text{if the event } \theta(j, t) \text{ is part of } \Theta \\ 0 & \text{otherwise} \end{cases} \tag{5.5}$$

Using this, a feasible association event needs to fulfill the following requirements:

1. A measurement can have only one source, i.e.

$$\sum_{t=0}^{N_T} \omega_\Theta(j, t) = 1 \qquad \forall \quad j \tag{5.6}$$

2. At most one measurement can originate from a target

$$\delta^t_\Theta \triangleq \sum_{j=1}^{m} \omega_\Theta(j, t) \leqslant 1 \qquad t = 1, \ldots, N_T \tag{5.7}$$

The binary variable $\delta^t_\Theta$ is called the target detection indicator since it indicates whether a measurement is associated to a target $t$ or not in event $\Theta$. It is also convenient to define

***Table 5.1:*** *Specific measurement association in the 11 feasible joint association events corresponding to Figure 5.1. Only measurement $z_k(2)$ can be associated to both targets since it is located inside both targets' validation gates.*

| $\Theta$ (hypothesis number) | Target 0 (false alarm) | | | | Target 1 | Target 2 |
|---|---|---|---|---|---|---|
| 1 | $z_k(1)$ | $z_k(2)$ | $z_k(3)$ | $z_k(4)$ | | |
| 2 | $z_k(2)$ | $z_k(3)$ | $z_k(4)$ | | $z_k(1)$ | |
| 3 | $z_k(3)$ | $z_k(4)$ | | | $z_k(1)$ | $z_k(2)$ |
| 4 | $z_k(2)$ | $z_k(4)$ | | | $z_k(1)$ | $z_k(3)$ |
| 5 | $z_k(2)$ | $z_k(3)$ | | | $z_k(1)$ | $z_k(4)$ |
| 6 | $z_k(1)$ | $z_k(3)$ | $z_k(4)$ | | $z_k(2)$ | |
| 7 | $z_k(1)$ | $z_k(4)$ | | | $z_k(2)$ | $z_k(3)$ |
| 8 | $z_k(1)$ | $z_k(3)$ | | | $z_k(2)$ | $z_k(4)$ |
| 9 | $z_k(1)$ | $z_k(3)$ | $z_k(4)$ | | | $z_k(2)$ |
| 10 | $z_k(1)$ | $z_k(2)$ | $z_k(4)$ | | | $z_k(3)$ |
| 11 | $z_k(1)$ | $z_k(2)$ | $z_k(3)$ | | | $z_k(4)$ |

two more binary variables

$$\tau_\Theta(j) \triangleq \sum_{t=1}^{N_T} \omega_\Theta(j,t) \tag{5.8}$$

$$\phi_\Theta \triangleq \sum_{j=1}^{m} [1 - \tau_\Theta(j)] \tag{5.9}$$

where $\tau_\Theta(j)$ is the measurement association indicator to indicate if measurement $j$ is associated to a target or not, and $\phi_\Theta$ is the number of false (unassociated) measurements in event $\Theta$.

In the example of Figure 5.1 it is possible to form 11 feasible joint association events, and the way the measurements are associated within these events is shown in Table 5.1. For all these possible joint association events, conditional probabilities have to be derived.

### 5.1.3 Joint Association Event Probabilities

The joint association event probabilities are derived using Bayes' formula

$$\begin{aligned} P\{\Theta_k|Z^k\} &= P\{\Theta_k|Z_k, m_k, Z^{k-1}\} \\ &= \frac{1}{c} p\left(Z_k|\Theta_k, m_k, Z^{k-1}\right) P\{\Theta_k|Z^{k-1}, m_k\} \\ &= \frac{1}{c} p\left(Z_k|\Theta_k, m_k, Z^{k-1}\right) P\{\Theta_k|m_k\} \end{aligned} \tag{5.10}$$

where $c$ is a normalizing constant. The prior probability of the joint association event is independent of the past measurements, and the conditioning term $Z^{k-1}$ has therefore been omitted in the last line of the above equation.

For the purpose of deriving the joint probabilities, no individual validation gates will be assumed for the various targets. Instead, the entire surveillance region will be used as the validation gate for each target. This approach is adopted in order to have the pdf of each false measurement the same, i.e., uniformly distributed in the validation region

$$p\left(z_k(j)|\theta_k(j,t_j),Z^{k-1}\right)=\frac{1}{V}\quad\text{for}\quad\tau_{\Theta_k}(j)=0 \tag{5.11}$$

where $V$ is the volume of the entire surveillance area. The pdf of a true target-originated measurement is assumed Gaussian distributed as in the PDAF, but since the validation gate coincides with the entire surveillance area, the gate probability in (4.16) is assumed to be unity, i.e., $P_G = 1$. The conditional pdf of a measurement given its origin is therefore

$$p\left(z_k(j)|\theta_k(j,t_j),Z^{k-1}\right)=\begin{cases}\mathcal{N}\left(z_k(j);\hat{z}^{t_j}_{k|k-1},S^{t_j}_k\right) & \text{if}\quad\tau_{\Theta_k}(j)=1\\ \frac{1}{V} & \text{if}\quad\tau_{\Theta_k}(j)=0\end{cases} \tag{5.12}$$

where $\hat{z}^{t_j}_{k|k-1}$ is the predicted measurement for target $t_j$ with associated innovation covariance $S^{t_j}_k$. Using the above equation, the pdf of the measurements in (5.10) can be written as

$$\begin{aligned}p\left(Z_k|\Theta_k,m_k,Z^{k-1}\right)&=\prod_{j=1}^{m_k}p\left(z_k(j)|\theta_k(j,t_j),Z^{k-1}\right)\\&=\prod_{j=1}^{m_k}\left\{\left(\frac{1}{V}\right)^{1-\tau_\Theta(j)}\mathcal{N}\left(z_k(j);\hat{z}^{t_j}_{k|k-1},S^{t_j}_k\right)^{\tau_\Theta(j)}\right\}\end{aligned} \tag{5.13}$$

where the states of the targets, conditioned on the past observations, are assumed mutually independent.

Next, the last term in (5.10) will be derived. Let $\delta_\Theta$ be the vector of detection indicators corresponding to event $\Theta_k$

$$\delta_\Theta=[\delta^1_\Theta,\ldots,\delta^{N_T}_\Theta] \tag{5.14}$$

The vector $\delta_\Theta$ and the number of false measurements $\phi_\Theta$ follow from the event $\Theta$ under consideration. Using the definition of conditional probabilities [52], this yields

$$P\{\Theta_k|m_k\}=P\{\Theta_k,\delta_\Theta,\phi_\Theta|m_k\}=P\{\Theta_k|\delta_\Theta,\phi_\Theta,m_k\}P\{\delta_\Theta,\phi_\Theta|m_k\} \tag{5.15}$$

The first term in (5.15) is obtained using combinatorics:

1. In event $\Theta_k$ there are assumed $m_k - \phi_\Theta$ targets detected.

2. The number of events $\Theta_k$, where the same targets are detected, is given by the number of ways of associating $m_k - \phi_\Theta$ measurements to the detected targets from a set of $m_k$ measurements.

By assuming each such event a priori equally likely, one has

$$P\{\Theta_k|\delta_\Theta, \phi_\Theta, m_k\} = \frac{1}{{}_{m_k}P_{m_k-\phi_\Theta}} = \frac{\phi_\Theta!}{m_k!} \tag{5.16}$$

The last term in (5.15) is, assuming $\delta$ and $\phi$ independent,

$$P\{\delta_\Theta, \phi_\Theta|m_k\} = \prod_{t=1}^{N_T} (P_D^t)^{\delta_\Theta^t} (1 - P_D^t)^{1-\delta_\Theta^t} \mu_F(\phi_\Theta) \tag{5.17}$$

where $P_D^t$ is the detection probability of target $t$ and $\mu_F(\phi_\Theta)$ is the prior pmf of the number of false measurements. The indicators $\delta_\Theta^t$ have been used to select the probabilities of detection and no-detection events according to the event $\Theta_k$ under consideration. Combining (5.16) and (5.17) into (5.15) yields the prior probability of a joint association event

$$P\{\Theta_k|m_k\} = \frac{\phi_\Theta!}{m_k!} \prod_{t=1}^{N_T} (P_D^t)^{\delta_\Theta^t} (1 - P_D^t)^{1-\delta_\Theta^t} \mu_F(\phi_\Theta) \tag{5.18}$$

The pmf of the number of false measurements $\mu_F(\phi)$ can, as in the case of the PDAF, have two versions, parametric or nonparametric.

1. Parametric JPDAF uses a Poisson pmf

$$\mu_F(\phi) = e^{-\lambda V} \frac{(\lambda V)^\phi}{\phi!} \tag{5.19}$$

   which requires the spatial density $\lambda$ of the false measurements.

2. Nonparametric JPDAF uses a diffuse prior

$$\mu_F(\phi) = \epsilon \qquad \forall \phi \tag{5.20}$$

   which does not require the parameter $\lambda$.

Using the nonparametric model and combining (5.18) and (5.13) into (5.10) yields the joint association event probabilities

$$P\{\Theta_k|Z^k\} = \frac{\phi_\Theta!}{c} \prod_{t=1}^{N_T} (P_D^t)^{\delta_\Theta^t} (1 - P_D^t)^{1-\delta_\Theta^t} \prod_{j=1}^{m_k} \left\{ V \, \mathcal{N}\left( z_k(j); \hat{z}_{k|k-1}^{t_j}, S_k^{t_j} \right) \right\}^{\tau_\Theta(j)} \tag{5.21}$$

where the constants $\epsilon$ and $m_k!$ are brought into the normalization constant $c$.

### 5.1.4 JPDAF Algorithm

Finally, marginal association probabilities are obtained by summing over all the joint association events in which the marginal event of interest occurs

$$\beta_k^t(j) \triangleq P\{\theta_k(j,t)|Z^k\} = \sum_{\Theta_k} P\{\Theta_k|Z^k\}\omega_\Theta(j,t) \tag{5.22}$$

$$\beta_k^t(0) \triangleq 1 - \sum_{j=1}^{m_k} \beta_k^t(j) \tag{5.23}$$

The joint association events are now decoupled into separate sets of association probabilities, one set for each target, where the probabilities in one set can be used as those association probabilities in the PDAF. By replacing the association probabilities in (4.63) with the probabilities calculated in (5.22) and (5.23), the JPDAF algorithm is the same as using the PDAF equations in Section 4.2.4 on each target $t$.

In **paper B** and **paper C** the JPDAF algorithm is modified to also handle false measurements that originate from the wakes behind the targets in a multitarget environment.

## 5.2 Coupled Joint Probabilistic Data Association Filter

The JPDAF is based on the assumption that the targets' states, conditioned on the past observations, are mutually independent. Because of this assumption, the filtering can be done decoupled. When measurements are inside the validation gates for two or more targets at the same time, we say that the targets are "sharing" measurements. For targets that share measurements for several sampling times, a dependence of their estimation error ensues, and this can be taken into account by calculating the resulting error correlations [15]. This leads to the joint probabilistic data association coupled filter (JPDACF) [7], [10], where the targets' states, given the past, are considered as correlated. The JPDACF algorithm does the filtering in a coupled manner, yielding a covariance matrix with cross-covariances that reflect the correlation between the targets' state estimation errors. However, this JPDACF approach does not account for situations with partial target detections since the association events where all targets are detected are not separated from events where only some of them are detected. This situation was accounted for in the coupled probabilistic data association (CPDA) filter, derived in [16], where the CPDA in combination with hypothesis pruning was developed to avoid track coalescence. In **paper C**, however, the CPDA approach did lead to numerical problems in the covariance calculations. An equivalent solution to the CPDA, but where the covariance calculation is in a symmetrical form, was therefore developed to avoid numerical problems. This modified JPDACF, accounting for partial target detections and the presence of wakes, is derived in **paper C**.

## 5.3 Multiple Hypothesis Tracking

The multiple hypothesis tracking (MHT) algorithm [10], [14] can be said to be the multitarget version of the OBA presented in Section 4.1, that also includes track initiation, track termination and different techniques to reduce memory and computational requirements. These techniques, which includes clustering, pruning and merging of tracks, are necessary to implement the MHT for use in practical tracking systems. In the MHT, alternative data association hypotheses are formed whenever there are measurement-to-track conflict situations such as shown in Figure 5.1. Then, rather than combining these hypotheses, as in the JPDAF presented in Section 5.1, the hypotheses are propagated in anticipation that subsequent measurements will resolve the uncertainties. Recall the example given in Figure 5.1 where two targets have overlapping validation regions such that one of the measurements is validated for both targets. As shown in Table 5.1, there are 11 possible association events $\Theta$, or hypotheses, in this example. The JPDAF uses the hypothesis probabilities to compute measurement-to-track assignment probabilities and then updates each track with a probabilistically weighted composite of all validated measurements. Thus, the 11 hypotheses would be effectively combined to update the two tracks. On the other hand, MHT will choose to maintain a subset of these 11 hypotheses and defer the decision so that subsequent scans of data can be used to resolve the uncertainty at the current time. The 11 hypotheses can be further expanded to include new tracks that can be formed by the measurements that are not used by the hypotheses for track update. When new measurements are validated in the next scan, each of the hypotheses from the current scan may spawn another set of hypotheses, and so on for subsequent scans. This creates the potential for an explosion in the number of hypotheses.

### 5.3.1 Assumptions

The following assumptions are made in the MHT approach:

(a) There is an unknown number of targets, and tracks have not necessarily been initialized.

(b) At each sampling time any measurement could have originated from either:

- an established track
- a new target
- a false alarm

(c) A measurement could have originated from at most one target.

(d) There can be at most one measurement from a target.

(e) Measurements associated with a track are Gaussian distributed around the corresponding predicted measurement.

(f) False measurements are uniformly distributed in the surveillance region, and appear according to a Poisson process with a certain rate.

(g) New targets can appear at each sampling time, uniformly distributed in the surveillance region (or according to some other pdf), and appear according to a Poisson process with a certain rate.

### 5.3.2 MHT Techniques to Limit the Number of Hypotheses

Hypotheses are collections of tracks that do not share measurements. To reduce the potential explosion of the number of hypotheses in the MHT, a number of techniques have been developed. The main techniques are:

1. **Clustering**
   Clusters are collections of tracks that share measurements, either directly or via other tracks. As an example, if Track 1 shares a measurement with Track 2, and Track 2 shares a measurement with Track 3, all three tracks are in the same cluster. Once clustering has been performed, the formation and evaluation of hypotheses within each cluster can be done independently from other clusters. In this way the processing of each cluster can be assigned to separate processors in a parallel processing implementation.

2. **Pruning**
   Hypotheses (and tracks) with probabilities lower than a given threshold are deleted.

3. **Merging**
   Hypotheses with similar effects, e.g., the same number of targets but with slightly different state estimates, can be combined. Another typical rule would be to merge tracks that have the last $N$ observations in common, where $N \geq 3$.

### 5.3.3 Track-Oriented vs. Hypothesis-Oriented Algorithms

There are two basic approaches to MHT implementation. The original MHT method, denoted Reid's algorithm [56], is a hypothesis-oriented approach that maintains the hypothesis structure from scan to scan and continually expands and cuts back (prunes) the hypotheses as new data is received. At each scan, a set of hypotheses will be carried over from the previous scan and composed of one or more tracks that do not share measurements with each other in the hypotheses. Then, on the receipt of new data, each hypothesis is expanded into a set of new hypotheses by considering all measurement-to-track assignments for the tracks within the hypotheses. On the other hand, the track-oriented approach [44] does not maintain hypotheses from scan to scan. The tracks formed on each scan are reformed into hypotheses and the tracks that survive pruning are predicted to the next scan where the process continues. The latter approach is, according to [5], the preferred one, since it is simpler and conveniently implementable via multidimensional assignment (MDA), using Lagrangian relaxation [53].

### 5.3.4 Optimality

The MHT is "optimal" in the sense that it makes no overt approximations or simplifications, but in order to implement it, hidden approximations and simplifications have to be made. This method is therefore not a panacea, and has to be treated cautiously and with a clear understanding of all its assumptions, like any other approach [10].

## 5.4 Multisensor Configurations

When more than one sensor is used to obtain measurements, there are several possible configurations or overall system architectures that relate to the sequence in which the data association and tracking are carried out [10], [35]. The key issue here is whether or not all measurements (from the multiple sensors) should be sent directly to a fusion center for track formation. In the centralized configuration, which gives the best performance,[1] all measurements are transmitted from the local sensors to a fusion center where the information processing is carried out. Primarily due to bandwidth constraints in real systems, the centralized configuration is sometimes not feasible because of its requirement to transmit all measurement information to a fusion center. This is the motivation for the interest in distributed configuration where each sensor has its own information processing system, and the processed data (including less information) at the local sensors is transmitted to the fusion center for further processing. Notice that the terms "distributed" and "decentralized" are often used interchangeably. In a distributed system the information processing is done at different locations, and if the information processors at these different locations do not all share the same information, the system is also decentralized. The centralized and distributed configurations have been compared in [21], [22].

### 5.4.1 Centralized Tracking

In a completely centralized tracking system, the fusion center has access to all measurements, yielding the best performance. However, the total amount of data received at the fusion center can be large, which increases the requirements for the communication system. An approach to make the centralized tracking more feasible for real systems, is to compress the measurement data in the local sensors before it is transmitted [23]. When the measurements are transmitted to a fusion center in the centralized tracking, there are two different schemes for the way the state is updated. In parallel filtering the measurements from all sensors (if synchronized) are taken into account at the same time. The other alternative is sequential filtering, where measurements from each sensor is processed one sensor at a time [10]. The first sensor updates the state (and covariance) based on predictions from the previous time step as in a single-sensor algorithm. Then, this new updated state is used as a zero-time prediction to update with the measurements

[1] It is assumed that the sensors are properly registered and have no biases.

from the second sensor and so on. A fundamental principle stated in [25] is that similar, properly aligned sources should be combined first. In [51] the sequential and parallel filtering schemes are compared in a multisensor JPDAF approach, and it is shown that sequential filtering is less computationally complex as the number of sensors increases. According to [51], the sequential method yields better tracking performance on the average when data association is needed. This is primarily due to the fact that better filtered estimates are available after processing each sensor's data. The centralized configuration with sequential update is used in the multisensor scenarios presented in **paper C**.

### 5.4.2 Distributed Tracking

In a distributed (decentralized) configuration, the local sensors are doing track estimation themselves. These local estimates are then transmitted to a fusion center (at a reduced rate), and a *track to track association* followed by track fusion is carried out. The *track to track association* decides whether two tracks from different systems represent the same target. If it is decided that these two tracks represent the same target, the track fusion combines their estimates.

In general there are $\mathcal{S}$ sensors, $s = 1, \ldots, \mathcal{S}$, where each sensor has $N_s$ local tracks. The different sensors have typically independent measurement noise, but due to the common process noise, the local estimates at the different sensors representing the same target should not be assumed independent. This dependence is characterized by the cross-covariance of the local estimation errors given by the Lyapunov equation. A *track to track association* method, using a likelihood-ratio based cost function in a $\mathcal{S}$-D assignment, was derived for tracks with dependent errors in [8]. This cost function allows simultaneous consideration of $\mathcal{S}$ tracks corresponding to the same target (one from each source) or any subset of this.

When the assignment algorithm has determined which tracks are going to be fused, the track fusion, assuming dependent track estimation errors, is done with the equations given in [22].

# 6

# Concluding Remarks

In this first part we have presented a framework for the research reported in this thesis. The aim has been to explain how the papers in Part II relate to each other and to the existing theory. The conclusions are given in Section 6.1, and some of the many interesting ideas for future research are discussed in Section 6.2.

## 6.1 Conclusions

The work presented in this thesis has mainly dealt with the association of measurements to their origin. This type of data association, called *measurement to track association*, is an important factor in practical tracking systems whenever false, non-target-originated measurements are likely to appear. These false measurements are due to noise and clutter. In this thesis we have introduced the measurements originating from the wake behind a target as a special kind of clutter. These wake-originated measurements are modeled with a probabilistic model which reflects the probability that a false measurement originated from the wake.

In **paper A**, a probabilistic model of the bubbles behind a diver is developed and incorporated in the PDAF algorithm presented in Chapter 4. The modified PDAF prevents measurements originating from the bubbles behind the diver to mislead the tracking algorithm by giving these measurements lower weights than in a regular PDAF. A linearly increasing bubble model was implemented, which results in an analytical expression for the probability that there are bubbles in the validation gate. The reported model was used in a real tracking scenario of two divers, and showed to be a valuable modification of the PDAF to maintain track continuity. A similar solution may be effective for the wake behind a ship or other vehicles with a wake effect.

In **paper B**, a probabilistic model is developed to account for multiple wakes in a multitarget scenario. This multitarget wake model is incorporated in the JPDAF algorithm presented in Chapter 5, and is formed by the sum of single models each linearly increasing behind their associated targets. Simulations of two crossing targets with various trajectory crossing angles between the targets show that this wake model is a useful modification of the JPDAF, especially when the trajectory crossing angle is small. The wake model is also necessary for higher trajectory crossing angles, but in these situations it seems to be enough to use a modified PDAF (developed in **paper A**) on each of the targets in parallel.

Four different simulation scenarios are examined in **paper C**, using the models developed in **paper A** and **paper B**, where two targets in the presence of wakes are:

1. Crossing each other.
2. Moving in parallel to each other.
3. One following after another.
4. Meeting and then passing each other.

The simulation scenarios consider two sensors, and the data association filters at the local sensors are compared with multisensor filters in a centralized tracking configuration with sequential updating (see Chapter 5.4). The results show that the data fusion provides significant improvement in the tracking performance. This paper also presents the coupled version of the JPDAF (JPDACF) presented in Chapter 5, and a modified JPDACF (with a wake model) is developed and tested, without showing any improvements compared to the modified JPDAF. **Paper C** also examines the effect of applying the wake model on point-targets without wakes. The results show that the modified JPDAF and JPDACF perform almost the same as the standard JPDAF. This makes the modification practical for real systems where both targets with wakes and targets without wakes are operating in the same environment.

## 6.2 Future Research

The wake models developed in this thesis are based on the assumption of a nearly constant velocity target. This leads to a wake model following a straight line behind the target. Further research should address robustness of this wake model in situations when a target is turning or performing different maneuvers. A suggestion is to make the probabilistic wake model adaptive to the trajectory of the target by following the last estimated positions rather than a straight line.

Due to continuously increasing sensor resolution, the problem of tracking extended targets becomes more and more important. An interesting idea would be to include the wake models developed in this thesis in an extended target tracking framework. This should be helpful especially for larger targets, like ships, that also have a wake.

In most classical tracking systems the detector and the tracker operate independently. An interesting approach would be to introduce a coordination between these two systems to improve the performance in the presence of a wake. For this purpose a CA-CFAR detector, presented in Chapter 2, with an adaptive window (the cells used to estimate the local noise parameter) could cooperate with a modified PDAF or JPDAF that informs the detector of the estimated target position and velocity. The averaging window should use the position and velocity information from the estimated track to exclude the wake-affected cells in the cell averaging process.

# Bibliography


[1] D. A. Abraham, "Choosing a non-Rayleigh reverberation model," in *OCEANS '99*, vol. 1, Seattle, WA, Sep. 1999, pp. 284–288.

[2] D. A. Abraham and A. P. Lyons, "Novel physical interpretations of K-distributed reverberation," *IEEE Journal of Oceanic Engineering*, vol. 27, no. 4, pp. 800–813, Oct. 2002.

[3] A. Asada, F. Maeda, K. Kuramoto, Y. Kawashima, M. Nanri, and K. Hantani, "Advanced surveillance technology for underwater security sonar systems," in *OCEANS 2007 - Europe*, Aberdeen, Scotland, UK, June 2007, pp. 1–5.

[4] M. Athans, R. H. Whiting, and M. Gruber, "A suboptimal estimation algorithm with probabilistic editing for false measurements with applications to target tracking with wake phenomena," *IEEE Transactions on Automatic Control*, vol. 22, no. 3, pp. 372–384, June 1977.

[5] Y. Bar-Shalom, "Dimensionless score function for multiple hypothesis tracking," *IEEE Transactions on Aerospace and Electronic Systems*, vol. 43, no. 1, pp. 392–400, Jan. 2007.

[6] Y. Bar-Shalom and W. D. Blair, Eds., *Multitarget-Multisensor Tracking: Applications and Advances*. Dedham, MA: Artech House, 2000, vol. III.

[7] Y. Bar-Shalom, K. C. Chang, and H. A. P. Blom, "Tracking of splitting targets in clutter using an interacting multiple model joint probabilistic data association filter," in *Proceedings of the 30th IEEE Conference on Decision and Control*, Brighton, UK, Dec. 1991, pp. 2043–2048.

[8] Y. Bar-Shalom and H. Chen, "Multisensor track-to-track association for tracks with dependent errors," in *Proceedings of the 43rd IEEE Conference on Decision and Control.*, vol. 3, Dec. 2004, pp. 2674–2679.

[9] Y. Bar-Shalom and X. R. Li, *Estimation and Tracking: Principles, Techniques, and Software.* Boston, MA: Artech House, 1993.

[10] ——, *Multitarget-Multisensor Tracking: Principles and Techniques.* Storrs, CT: YBS Publishing, 1995.

[11] Y. Bar-Shalom, X. R. Li, and T. Kirubarajan, *Estimation with Application to Tracking and Navigation.* New York: Wiley-Interscience, 2001.

[12] Y. Bar-Shalom and E. Tse, "Tracking in a cluttered environment with probabilistic data association," *Automatica*, vol. 11, no. 5, pp. 451–460, Sep. 1975.

[13] D. K. Barton, *Modern Radar System Analysis.* Norwood, MA: Artech House, 1988.

[14] S. S. Blackman and R. Popoli, *Design and Analysis of Modern Tracking Systems.* Norwood, MA: Artech House, 1999.

[15] S. Blake and S. Watts, "A multitarget track-while-scan filter," in *Proceedings of the IEE Radar 87 Conference*, London, UK, Oct. 1987.

[16] H. A. P. Blom and E. A. Bloem, "Probabilistic data association avoiding track coalescence," *IEEE Transactions on Automatic Control*, vol. 45, no. 2, pp. 247–259, Feb. 2000.

[17] M. Born and E. Wolf, *Principles of Optics*, 6th ed. London, UK: Pergamon Press, 1980.

[18] E. Brekke, O. Hallingstad, and J. Glattetre, "Target tracking in heavy-tailed clutter using amplitude information," in *Proceedings of the 12th International Conference on Information Fusion*, Seattle, WA, USA, July 2009, pp. 2153–2160.

[19] ——, "The signal-to-noise ratio of human divers," May 2010, to appear in IEEE Oceans Conference 2010.

[20] B. J. Bunin, A. Sutin, and M. S. Bruno, "Maritime security laboratory for maritime security research," in *Proceedings of the SPIE Conference on Optics and Photonics in Global Homeland Security III*, vol. 6540, May 2007.

[21] H. Chen, T. Kirubarajan, and Y. Bar-Shalom, "Comparison of centralized and distributed tracking algorithms using air-to-air scenarios," in *Proceedings of the SPIE Conference on Signal and Data Processing of Small Targets*, vol. 4048, July 2000, pp. 440–451.

[22] ——, "Performance limits of track-to-track fusion versus centralized estimation: Theory and application," *IEEE Transactions on Aerospace and Electronic Systems*, vol. 39, no. 2, pp. 386–400, Apr. 2003.

[23] H. Chen, K. Zhang, and X. R. Li, "Optimal data compression for multisensor target tracking with communication constraints," in *Proceedings of the 43rd IEEE Conference on Decision and Control*, vol. 3, Dec. 2004, pp. 2650–2655.

[24] A. M. Crawford and D. V. Crowe, "Observations from demonstrations of several commercial diver detection sonar systems," in *Oceans 2007*, Vancouver, BC, Canada, Sep./Oct. 2007, pp. 1–3.

[25] P. R. DeLong, "Ten principles of command and control system automation," *Naval Engineers Journal*, pp. 57–67, Jan. 1990.

[26] R. O. Duda, P. E. Hart, and D. G. Stork, *Pattern Classification*, 2nd ed. New York: Wiley-Interscience, 2001.

[27] M. Dwass, *Probability and Statistics*. New York: W. A. Benjamin, 1970.

[28] T. E. Fortmann, Y. Bar-Shalom, and M. Scheffe, "Multi-target tracking using joint probabilistic data association," in *19th IEEE Conference on Decision and Control including the Symposium on Adaptive Processes*, vol. 19, Dec. 1980, pp. 807–812.

[29] ——, "Sonar tracking of multiple targets using joint probabilistic data association," *IEEE Journal of Oceanic Engineering*, vol. 8, no. 3, pp. 173–184, July 1983.

[30] P. P. Gandhi and S. A. Kassam, "Analysis of CFAR processors in homogeneous background," *IEEE Transactions on Aerospace and Electronic Systems*, vol. 24, no. 4, pp. 427–445, July 1988.

[31] ——, "Optimality of the cell averaging CFAR detector," *IEEE Transactions on Information Theory*, vol. 40, no. 4, pp. 1226–1228, July 1994.

[32] A. Gelb, Ed., *Applied Optimal Estimation*. Boston, MA: MIT Press, 1974.

[33] G. B. Goldstein, "False-alarm regulation in log-normal and Weibul clutter," *IEEE Transactions on Aerospace and Electronic Systems*, vol. 9, pp. 84–92, Jan. 1973.

[34] M. Hadzagic, H. Michalska, and E. Lefebvre, "Track-before-detect methods in tracking low-observable targets: A survey," *Sensors & Transducers Magazine, Special Issue*, pp. 374 – 380, Aug. 2005.

[35] D. L. Hall and J. Llinas, Eds., *Handbook of Multisensor Data Fusion*. Florida: CRC Press, 2001.

[36] R. M. Haralick, S. R. Sternberg, and X. Zhuang, "Image analysis using mathematical morphology," *IEEE Transactions on Pattern Analysis and Machine Intelligence*, vol. 9, no. 4, pp. 532–550, July 1987.

[37] D. R. Iskander and A. M. Zoubir, "Estimation of the parameters of the K-distribution using higher order and fractional moments," *IEEE Transactions on Aerospace and Electronic Systems*, vol. 35, no. 4, pp. 1453–1457, Oct. 1999.

[38] D. H. Johnson and D. E. Dudgeon, *Array Signal Processing: Concepts and Techniques*, A. V. Oppenheim, Ed. New Jersey: Prentice Hall, 1993.

[39] J.-B. Jung, G. F. Denny, J. W. Tilley, A. B. Kulinchenko, and P. K. Simpson, "Broadband active sonar swimmer detection and identification," in *International Joint Conference on Neural Networks*, Vancouver, BC, July 2006, pp. 2600–2605.

[40] R. E. Kalman, "A new approach to linear filtering and prediction problems," *Journal of Basic Engineering*, vol. 82, pp. 35–46, Mar. 1960.

[41] S. A. Kassam, *Signal Detection in Non-Gaussian Noise*, J. B. Thomas, Ed. New York: Springer-Verlag, 1988.

[42] S. M. Kay, *Fundamentals of Statistical Signal Processing, Volume 2: Detection Theory*, A. V. Oppenheim, Ed. New Jersey: Prentice Hall, 1998.

[43] Y.-S. Kim, S.-L. Choi, and K.-S. Hong, "A suboptimal algorithm for the optimal bayesian filter using receding horizon FIR filter," in *Proceedings of the IEEE International Symposium on Industrial Electronics*, vol. 3, Pusan, Korea, June 2001, pp. 1860–1865.

[44] T. Kurien, "Issues in the design of practical multitarget tracking algorithms," in *Multitarget-Multisensor Tracking: Advanced Applications*, Y. Bar-Shalom, Ed. Norwood, MA: Artech House, 1990, ch. 3.

[45] H. Lew and D. M. Drumheller, "Estimation of non-Rayleigh clutter and fluctuating-target models," in *IEE Proceedings of Radar, Sonar and Navigation*, vol. 149, no. 5, Oct. 2002, pp. 231–241.

[46] Y. Li and L. Yu, "Group tracking using mathematical morphology and multiple clustering hypotheses," in *Proceedings of the SPIE Conference on MIPPR 2007: Automatic Target Recognition and Image Analysis; and Multispectral Image Acquisition.*, vol. 6786, paper 39, Nov. 2007.

[47] A. Lovik, A. R. Bakken, J. Dybedal, T. Knudsen, and J. Kjoll, "Underwater protection system," in *Oceans 2007*, Vancouver, BC, Canada, Sep./Oct. 2007, pp. 1–8.

[48] F. Maeda, A. Asada, K. Kuramoto, Y. Kurashige, M. Nanri, Y. Kawashima, R. Imai, and K. Hantani, "Development of diver detection and sensor integration for wharf surveillance software," in *Symposium on Underwater Technology and Workshop on Scientific Use of Submarine Cables and Related Technologies*, Tokyo, Japan, Apr. 2007, pp. 133–141.

[49] S. D. Meier and P. J. Moore, "Morphological filter assisted low amplitude impulse detector," in *IEEE International Symposium on Signal Processing and Information Technology*, Aug. 2006, pp. 950–954.

[50] D. Musicki, R. Evans, and S. Stankovic, "Integrated probabilistic data association," *IEEE Transactions on Automatic Control*, vol. 39, no. 6, pp. 1237–1241, June 1994.

[51] L. Y. Pao and C. W. Frei, "A comparison of parallel and sequential implementations of a multisensor multitarget tracking algorithm," in *Proceedings of the American Control Conference*, vol. 3, Seattle, WA, June 1995, pp. 1683–1687.

[52] A. Papoulis and S. U. Pillai, *Probability, Random Variables and Stochastic Processes*, 4th ed. New York: McGraw-Hill, 2002.

[53] A. Poore and N. Rijavec, "A lagrangian relaxation algorithm for multidimensional assignment problems arising from multitarget tracking," *SIAM Journal of Optimization*, vol. 3, no. 3, pp. 544–563, Aug. 1993.

[54] J. G. Postaire, R. D. Zhang, and C. Lecocq-Botte, "Cluster analysis by binary morphology," *IEEE Transactions on Pattern Analysis and Machine Intelligence*, vol. 15, no. 2, pp. 170–180, Feb. 1993.

[55] A. Rødningsby and Y. Bar-Shalom, "Tracking of divers in a noisy background using a bubble model," in *Proceedings of the SPIE Conference on Signal and Data Processing of Small Targets*, vol. 6699, paper 7, San Diego, CA, Aug. 2007.

[56] D. B. Reid, "An algorithm for tracking multiple targets," *IEEE Transactions on Automatic Control*, vol. 24, no. 6, pp. 843–854, Dec. 1979.

[57] B. Ristic, S. Arulampalam, and N. Gordon, *Beyond the Kalman Filter: Particle Filters for Tracking Applications*. Norwood, MA: Artech House, 2004.

[58] S. Sarangapani, J. H. Miller, G. R. Potty, D. B. Reeder, T. K. Stanton, and D. Chu, "Measurements and modeling of the target strength of divers," in *Oceans 2005 - Europe*, vol. 2, June 2005, pp. 952–956.

[59] J. P. Serra, *Image Analysis and Mathematical Morphology*. London, UK: Academic Press, 1982.

[60] M. Skolnik, *Introduction to Radar Systems*, 3rd ed. New York: McGraw-Hill, 2001.

[61] W. J. Smith, *Modern Optical Engineering: The Design of Optical Systems*, 2nd ed. New York: McGraw-Hill, 1990.

[62] R. J. Urick, *Principles of Underwater Sound*, 3rd ed. New York: McGraw-Hill, 1983.

# Part II

# Publications

# Paper A

## Tracking of Divers Using a Probabilistic Data Association Filter with a Bubble Model

**Authors:**
Anders Rødningsby and Yaakov Bar-Shalom.

Published in *IEEE Transactions on Aerospace and Electronic Systems*,
pp. 1181-1193, vol. 45, no. 3, July 2009

Preliminary version published as "Tracking of Divers in a Noisy Background Using a Bubble Model," in *Proceedings of the SPIE Conference on Signal and Data Processing of Small Targets*, vol. 6699, paper 7, San Diego, CA, USA, August 2007.

# Tracking of Divers Using a Probabilistic Data Association Filter with a Bubble Model

Anders Rødningsby[1] Yaakov Bar-Shalom[2]

[1]Department of Engineering Cybernetics,
Norwegian University of Science and Technology, NO-7491 Trondheim, Norway
[1]University Graduate Center, NO-2027 Kjeller, Norway
[2]Department of Electrical and Computer Engineering, University of Connecticut,
U-2157, Storrs, CT 06269, USA

**Abstract**

Detection and tracking of divers have become an important factor in port protection against underwater intruders. A problem arises from divers with open breathing systems because detections of the air bubbles they produce can mislead the tracking filter and sometimes result in a lost track. In this paper a probabilistic model is developed which reflects the probability that a false measurement originates from the bubbles. The novel contribution of this paper is the integration of this model in the probabilistic data association filter (PDAF) to improve the track continuity. The bubble detections may also cause confusion in the track initiation. To prevent this problem, a clustering method is proposed based on morphological operators which allows tracks to be initialized based on two-point differencing of the cluster centroids from succeeding scans. This morphological clustering method is included in a cell averaging constant false alarm rate (CA-CFAR) detector in such a way that both the point detections and their corresponding clusters can be fed to the tracking filter. These techniques are implemented and applied to real data of two divers, one with an open breathing system and the other with a closed breathing system, operating simultaneously in a coastal area. The real data were recorded from an active 90 kHz narrowband multibeam imaging sonar.

# 1 Introduction

In recent years the surveillance of divers near marine infrastructures such as bridges, power plants, port and harbor facilities has received renewed interest [2], [8], [9], [14], [16], [17]. The detection of divers is considered a challenging problem in underwater acoustics, and the target strength is the main unknown in assessing the feasibility of using a sonar to detect them. The target strength of a diver is a complicated function of aspect angle and frequency, where the human lungs and the oxygen tank are thought to be the largest contributors [22]. Especially for rebreathers with a fully closed breathing system, the target strength is particularly low. In addition, the surrounding environment could be noisy and nonstationary especially in ports and shallow water [24].

In a traditional tracking system only a small part of the information from the sonar signal processor is utilized in the tracking filter. This extraction of information is done by a detection process where only the most likely measurements that stand out from the background are passed on. In this paper we do not distinguish between noise, reverberation and clutter, but use the term background noise to include them all. It is often convenient to have some control on the measurements that originate from the background noise. For this purpose, a cell averaging constant false alarm rate (CA-CFAR) detector is frequently used in radar and sonar systems [11]. The detections resulting from a CA-CFAR detector are point measurements. However, some targets have a larger extent or they leave footprints (e.g. bubbles) which may result in more than one point detection. Sometimes it is desirable to gather these detections in a single cluster. Many possible algorithms for clustering are available, such as ISODATA and the K-means [10]. However, most of these suffer from the problem of requiring the knowledge of the number of clusters a priori. A technique from image analysis that does not requires this is called mathematical morphology [23]. This method may be used to connect or fill the empty space between several point detections to create a cluster. Mathematical morphology consists of set operations in Euclidean space for quantitative description of geometrical structures. This approach has been mainly concerned with image analysis to extract shape information from digital images [13]. Additional applications include low signal amplitude detection and pattern recognition [18], [20]. More interesting is the application of group tracking [15], where the morphological operators are used to cluster measurements into groups with a common activity. In this paper this method has been added to the CA-CFAR detector to create (in addition to single point measurements) clusters of the detections from the open breathing system diver and the bubbles he produces. We have therefore called this extended detection method as morphological CA-CFAR (MCA-CFAR). The clusters from the MCA-CFAR are used in the track initiation to avoid confusion of the many possibilities of two-point differencing [5] that could have been set up among the point detections. Instead, a two-point differencing is used for the cluster centroids from succeeding scans.

A sequence of sonar images from the data analyzed in this paper is shown in Figure 1. The two divers are pointed out and the detections are shown as black dots. To empha-

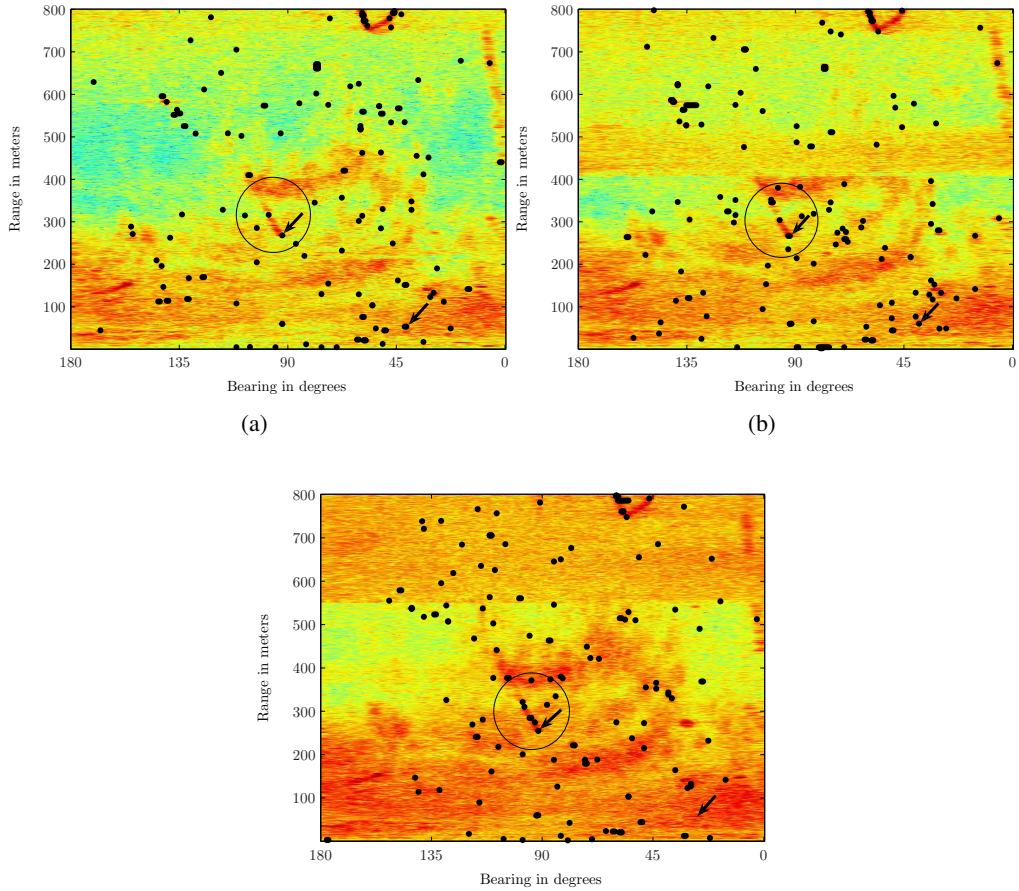


***Figure 1:*** *Sequence of sonar images showing amplitude (logarithmically scaled) of signal return in a nonhomogenous background. Each resolution cell is about* $0.8$ *m in range and* $0.7°$ *in bearing. Two divers, one with open breathing system and the other with closed breathing system, are pointed out by black arrows. The open breathing system diver and the cloud of bubbles behind him are circled. The detections are shown as black dots. Note that both divers are detected in images (a) and (b), but the closed breathing system diver is not detected in image (c). Moving directions are south-east for the open breathing system diver (circled) and east for the closed breathing system diver. Horizontal edges are due to interference from a fishing sonar operating at the same frequency as imaging sonar.*

size the time variation and nonhomogeneity in the background, the images have been logarithmically scaled. A low detection threshold is often required to achieve enough detections of the real targets in a nonhomogenous background. This results in a higher false alarm rate which makes it easier for false tracks to persist since there are more

spurious (false) measurements that are associated to these tracks. Especially in tracking of dim targets the higher false alarm rate is something that is almost impossible to avoid when the main goal is to have a continuous track of the real target.

For the purpose of tracking a target, there are several well-known methods [4], [5], [7]. However, the analysis and application of tracking methods applied to divers in the literature is rather scarce. Tracking is the estimation of the state of a moving target, and an important part is to determine which measurements to use in the estimation, i.e., data association. A well-known data association method is the probabilistic data association filter (PDAF) [4], [6] where the measurements are weighted according to how likely they originated from the target in a probabilistic sense. In the case when the diver uses an open breathing system, the produced bubbles may also stand out from the background and yield several detections. An example of this is shown in Figure 1. This makes it important to model the origination of the measurements to separate false measurements from target-originated ones. A similar problem has been discussed for a radar tracking a target in the presence of a wake [3], where a probabilistic editing method is used to handle the wake-dominated measurements in the tracking algorithm. This probabilistic editing method is based on a single measurement extracted for each time-step, and that this measurement originates from either the target or the wake. In this paper we have developed a method that does not restrict the number of measurements, but takes into account a set of measurements for each time-step, just as in the PDAF. Our method augments the regular PDAF to incorporate an additional probabilistic model for the bubbles behind the diver. The result is a lower weighting for bubble-originated measurements than what a regular PDAF would give. This makes it easier for the tracking algorithm to hold on to the true target and not lose it as a standard PDAF. A preliminary version of this work was presented in [21].

In Section 2 we describe the detection method, and how these detections can be clustered by using mathematical morphology. These measurements and corresponding clusters are handed over to the PDAF which is described in Section 3. In Section 4 we develop the modified PDAF to include a probabilistic model of the bubbles. The PDAF and the modified PDAF are applied to real data in Section 5, before conclusions are given in Section 6.

## 2 Morphological Cell Averaging Constant False Alarm Rate

In this section the detection method, and how these detections can be clustered by use of mathematical morphology, are described.

### 2.1 Detection

One of the most common detection methods in radar and sonar systems is the CA-CFAR processor [11]. By assuming that there are enough independent and identically dis-

tributed (i.i.d.) scatters contributing to the received signal in any given resolution cell (after beamforming and matched filtering) so that the central limit theorem (CLT) holds and the bandpass signal is Gaussian, the resulting amplitude is Rayleigh distributed [1]. This results in a Swerling I target model where the signal amplitude squared $A$ is exponentially distributed as

$$p(A|\text{noise}) = \frac{1}{\mu} \exp\left(-\frac{A}{\mu}\right) \tag{1}$$

for cells that originate from the background noise and

$$p(A|\text{target}) = \frac{1}{\mu(1+SNR)} \exp\left(-\frac{A}{\mu(1+SNR)}\right) \tag{2}$$

when the signal is reflected from a target [12]. Here the SNR is the signal-to-noise ratio in magnitude (not dB). Define $Y$ as the amplitude squared of the cell to be tested for possibly detection. Then, the background noise parameter $\mu$ is estimated by averaging over $n$ cells $A_i$ (amplitude squared), $i = 1, \ldots, n$, in a local neighborhood around the cell under test $Y$

$$\hat{\mu} = \frac{1}{n} \sum_{i=1}^{n} A_i \tag{3}$$

If the test signal cell has large enough signal intensity compared with the noise parameter estimate $\hat{\mu}$ in the following sense

$$\frac{Y}{\hat{\mu}} > \tau \tag{4}$$

then a detection will be declared. Let $P_{FA}$ be the average false alarm rate (probability of false alarm in a resolution cell). Based on [12] and the above assumptions, $P_{FA}$ is given by

$$P_{FA} = \frac{1}{\left(1+\frac{\tau}{n}\right)^n} \tag{5}$$

where $n$ is the number of cells used to estimate $\mu$. It is clear that $P_{FA}$ is independent of $\mu$, and from (5) the constant scale factor $\tau$ in (4) can be calculated as

$$\tau = nP_{FA}^{-\frac{1}{n}} - n \tag{6}$$

## 2.2 Mathematical Morphology

The resulting detections may be directly fed into a tracking algorithm as point measurements, but for targets that yield several detections, a form of clustering is useful. In this paper a clustering method based on mathematical morphology is included in the detection process such that both single point measurements and clusters of them are fed to the tracking system. This combined detection and clustering method is called MCA-CFAR.

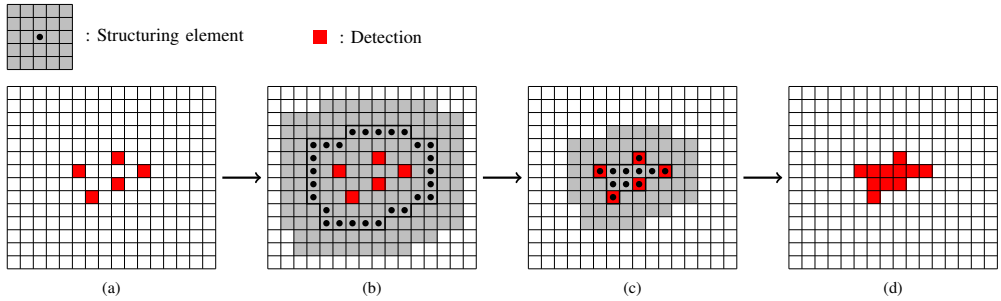


***Figure 2:*** *Clustering of detections by use of closing operation with specific* $5 \times 5$ *structuring element. (a) Detection image. (b) Expanded image after dilation. (c) Erosion of expanded image. (d) Cluster of detections.*

Mathematical morphology was originally developed in [23] and is principally based on the two set operations, erosion and dilation. These transformations involve the interaction between an image $X$ and a structuring set $B$, called the structuring element. Let $B_x$ be the translation of $B$ by $x$ defined as

$$B_x = \{z : z = b + x, \text{for } b \in B\} \tag{7}$$

Then dilation is defined as

$$\delta_B(X) = X \oplus B = \{x : B_x \cap X \neq \emptyset\} \tag{8}$$

where $B$ is usually a symmetric set around the origin and will expand the set $X$ depending on the form and size of the structuring element $B$. The erosion will shrink the set $X$ and is defined as

$$\epsilon_B(X) = X \ominus B = \{x : B_x \subseteq X\} \tag{9}$$

An important application of these two operations is called closing. It is produced by the dilation of $X$ by $B$, followed by the erosion of this result by $B$

$$\phi_B(X) = \epsilon_B(\delta_B(X)) = (X \oplus B) \ominus B \tag{10}$$

An example of clustering point measurements by use of the closing operation with a given structuring element is shown in Figure 2.

The important elements in the closing operation are the size and form of the structuring element. A larger structuring element will cluster together measurements that have a longer distance from each other. The size of the actual target should therefore be taken into account. If the orientation of the target is also known, a structuring element with the same shape and orientation as the target would be a good choice.

# 3 Probabilistic Data Association Filter

In this section the tracking model and the PDAF is described. The different steps in the PDAF are shown at the end.

## 3.1 Model of Tracking

The standard discrete linear model in tracking is

$$x_{k+1} = Fx_k + v_k \qquad z_k = Hx_k + w_k \tag{11}$$

where

| | | | |
|---|---|---|---|
| $x$ : | target state | $F$ : | transition matrix |
| $z$ : | measurement | $H$ : | measurement matrix |
| $v$ : | process noise | $w$ : | measurement noise |
| $k$ : | time index | | |

The process and measurement noises are assumed independent, white, and Gaussian with covariance matrices

$$E\{v_k v_k^T\} = Q_k \qquad E\{w_k w_k^T\} = R_k \tag{12}$$

In this system a Kalman filter would be optimal as long as there is only one single measurement $z_k$ at each time $k$. In real data this is unfortunately not true due to false measurements originating from the background noise. Instead, a set of $m_k$ measurements $Z_k = \{z_k(1), z_k(2), \ldots, z_k(m_k)\}$ is available at time $k$ and a form of data association is needed. A simple and effective method to solve this problem is the PDAF [4], [6].

## 3.2 Standard PDAF

The approach of the PDAF is to calculate the association probabilities for each validated measurement (that falls in a gate around the predicted measurement) at the current time to the target of interest. The posterior track probability density is therefore a mixture of Gaussian probability density functions (pdf), but is then forced back to Gaussianity by moment matching for the succeeding scan. For a derivation of the PDAF see [4]. In the following a brief overview of the PDAF is given.

Assume that the target state at time $k-1$ is estimated as $\hat{x}_{k-1|k-1}$ with associated covariance $P_{k-1|k-1}$. This means that the estimate is conditioned on the entire past up to time $k-1$. Then the following assumptions are made.

(a) The track is already initialized.

(b) The past information about the target is summarized approximately by the Gaussian distribution

$$p\left(x_k | Z^{k-1}\right) \approx \mathcal{N}\left(x_k; \hat{x}_{k|k-1}, P_{k|k-1}\right) \tag{13}$$

where

$$Z^{k-1} = \{Z_0, Z_1, \dots Z_{k-1}\} \tag{14}$$

(c) A validation region or gate is set up for each time step to select the candidate measurements for association.

(d) At time $k$ there are $m_k$ validated measurements but at most one of them can be target-originated. The remaining measurements are assumed due to i.i.d. uniformly spatially distributed false alarms, independent across time.

(e) Detections of the real target occur independently over time with known detection probability $P_D$.

At each time $k$, the algorithm goes through the following steps.

1. Predict the target state, associated covariance, and measurement at time $k$ based on the estimates at $k-1$:

$$\begin{aligned} \hat{x}_{k|k-1} &= F_k \hat{x}_{k-1|k-1} \\ P_{k|k-1} &= F_k P_{k-1|k-1} F_k^T + Q_k \\ \hat{z}_{k|k-1} &= H_k \hat{x}_{k|k-1} \end{aligned} \tag{15}$$

2. Compute the innovation covariance for the true target-originated measurement

$$S_k = H_k P_{k|k-1} H_k^T + R_k \tag{16}$$

and use $S_k$ to form the measurement validation gate where the validated measurements $Z_k$ result in $m_k$ innovations:

$$\nu_k(i) = z_k(i) - \hat{z}_{k|k-1} \qquad i = 1, \dots, m_k \tag{17}$$

3. Calculate the association probabilities $\beta_k(i)$, $i = 1, \dots, m_k$ that measurement $z_k(i)$ originates from the true target, and $\beta_k(0)$ as the probability that all measurements are false alarms:

$$\beta_k(i) = \begin{cases} c e^{-\frac{1}{2}\nu_k(i)^T S_k^{-1} \nu_k(i)} & i = 1, \dots, m_k \\ c\,|2\pi S_k|^{\frac{1}{2}}\, m_k \frac{1 - P_G P_D}{V_k P_D} & i = 0 \end{cases} \tag{18}$$

Here $c$ is the normalizing constant to ensure that $\sum_{i=0}^{m_k} \beta_k(i) = 1$, $V_k$ is the volume of the gate and $P_G$ is the probability that the true measurement falls inside the gate.

4. Calculate the Kalman gain and the combined innovation

$$W_k = P_{k|k-1} H_k^T S_k^{-1} \qquad \nu_k = \sum_{i=1}^{m_k} \beta_k(i) \nu_k(i) \tag{19}$$

to update the track according to

$$\hat{x}_{k|k} = \hat{x}_{k|k-1} + W_k \nu_k \tag{20}$$

5. The estimation covariance is updated by

$$\begin{aligned} P_{k|k} =& \beta_k(0) P_{k|k-1} + [1 - \beta_k(0)] \left( P_{k|k-1} - W_k S_k W_k^T \right) \\ &+ W_k \left[ \sum_{i=0}^{m_k} \beta_k(i) \nu_k(i) \nu_k(i)^T - \nu_k \nu_k^T \right] W_k^T \end{aligned} \tag{21}$$

where the last term in (21) is the “spread of the innovations."

# 4 PDAF with a Bubble Model

As mentioned earlier a diver with an open circuit breathing system will produce bubbles which may mislead the tracking algorithm. To prevent this, an extension of the regular PDAF incorporating a special probabilistic model of the bubbles is developed. In the PDAF each measurement that is not target-originated is modeled as i.i.d. uniformly spatially distributed inside the validation region. In a real sonar image a diver swimming in a given direction will often look like he is trailing a “cloud" behind him. The cloud is due to reflections from the bubbles he produces. This motivates the use of a pdf that reflects the increasing probability to get bubble-originated measurements behind the diver. The “bubble" pdf is the novelty added to the PDAF and is illustrated in Figure 3.

The PDAF with the bubble model takes into account that every false measurement can originate from either bubbles with a priori probability $P_B$ or from the background noise with a priori probability $1 - P_B$. Note that the a priori probability $P_B$ that a false measurement originates from bubbles is conditioned on a diver with an open breathing system being present. The assumptions for the bubble model PDAF are the same as in the standard PDAF as stated before with modification of point (d):

(d) At time $k$ there are $m_k$ validated measurements but at most one of them can be target-originated. The remaining measurements are assumed due to i.i.d. bubbles with pdf $p_B(\cdot)$ and a priori probability $P_B$, or from i.i.d. uniformly distributed background noise with a priori probability $1 - P_B$, independent across time.

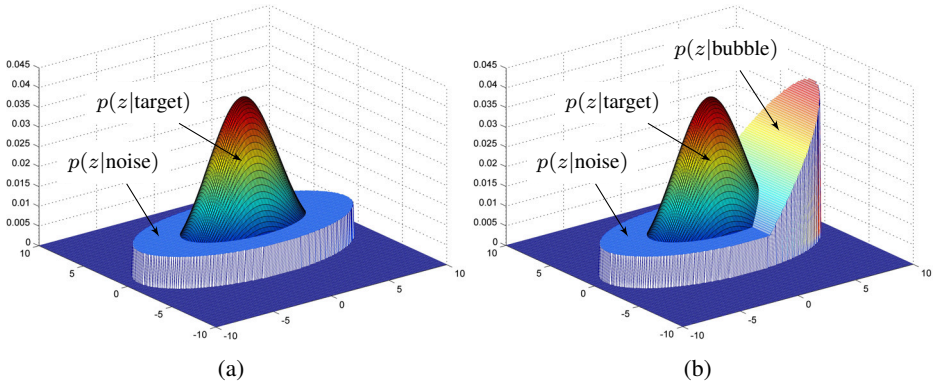


***Figure 3:*** *Illustration of pdfs for measurements originating from target, background noise, or bubbles. (a) In regular PDAF. (b) In modified PDAF with special bubble model.*

This modification will affect the PDAF in the calculation of the $\beta_k(i)$, which is derived in Appendix A, yielding

$$\beta_k(i) = \begin{cases} c \frac{e^{-\frac{1}{2}\nu_k(i)^T S_k^{-1} \nu_k(i)}}{\left[\frac{1-P_B}{V_k} + \frac{P_B}{P_{GB}} p_B(z_k(i))\right]} & i = 1, \ldots, m_k \\ c\,|2\pi S_k|^{\frac{1}{2}}\, m_k \frac{1-P_G P_D}{P_D} & i = 0 \end{cases} \tag{22}$$

Here $c$ is the normalizing constant to ensure that $\sum_{i=0}^{m_k} \beta_k(i) = 1$. In (22) a diffuse prior [4] is used for the point mass function (pmf) of the number of false measurements in the validation region. The denominator in $\beta_k(i)$ for $i = 1, \ldots, m_k$ is the pdf for a false measurement

$$p(z_k(i)|\theta_k(j), j \neq i) = \frac{1 - P_B}{V_k} + \frac{P_B}{P_{GB}} p_B(z_k(i)) \tag{23}$$

where $P_{GB}$ is used to account for restricting the density of the bubble model $p_B(z_k(i))$ to the validation gate. The calculation of $P_{GB}$ for a linear $p_B(\cdot)$ is presented in detail in Appendix B.

## 5 Results

In this section the methods described previously have been implemented and applied to real data recorded in the Oslo-fjord, Norway, during summer 2006.

## 5.1 Experimental Setup

The active sonar used in this experiment has a $180^\circ$ field of view and a maximum range of $800$ m, with resolution $0.703^\circ$ (256 cells) and $0.793$ m (1009 cells) in bearing and range respectively. The time $T$ between each scan is $1.089$ s, and the experiment lasted for 1792 scans (about $32.5$ min) in a single continuous run. Two divers, one with an open and the other with a closed breathing system, were located at two different positions in the water simultaneously. The divers are both attached to a GPS system, and are swimming well separated in a nearly straight line toward the sonar. In this case a two-dimensional direct discrete time nearly constant velocity model [5] is used in (11) and (12):

$$F = \begin{bmatrix} 1 & T & 0 & 0 \\ 0 & 1 & 0 & 0 \\ 0 & 0 & 1 & T \\ 0 & 0 & 0 & 1 \end{bmatrix} \qquad H = \begin{bmatrix} 1 & 0 & 0 & 0 \\ 0 & 0 & 1 & 0 \end{bmatrix} \tag{24}$$

$$R_c = \begin{bmatrix} \sigma_x^2 & \sigma_{xy}^2 \\ \sigma_{xy}^2 & \sigma_y^2 \end{bmatrix} \qquad R_p = \begin{bmatrix} \sigma_r^2 & 0 \\ 0 & \sigma_\psi^2 \end{bmatrix} \tag{25}$$

$$Q = \begin{bmatrix} \frac{1}{4}T^4 & \frac{1}{2}T^3 & 0 & 0 \\ \frac{1}{2}T^3 & T^2 & 0 & 0 \\ 0 & 0 & \frac{1}{4}T^4 & \frac{1}{2}T^3 \\ 0 & 0 & \frac{1}{2}T^3 & T^2 \end{bmatrix} \sigma_p^2 \tag{26}$$

For a target with bubbles behind it, situations may occur where the target is undetected but at the same time there are one or more detections of the bubbles. In these situations it is very hard to avoid that the track will accept the bubble-originated measurements and follow them even with the bubble model applied. It is therefore necessary to have a validation gate that is sufficiently large in the direction the target moves when a diver with bubbles behind it is tracked. To achieve this a larger measurement noise is used for the modified PDAF than the regular PDAF. Because the targets are moving toward the sonar, this difference is only in the range direction. The specifications of the parameters are given in Table 1.

The position measurements are originally in polar coordinates $(r, \psi)$ with (time-invariant) measurement noise covariance $R_p$, but are transformed to Cartesian coordinates $(x, y)$ with corresponding measurement noise covariance $R_c$ using the standard conversion [5]. This results in a purely linear model hence a standard Kalman filter can

be used in the tracking algorithm. In the detection process the MCA-CFAR detector is used with following parameters:

1. The average false alarm rate (probability of a false detection in a resolution cell) is set to $P_{FA} = 0.0005$ which corresponds to about 130 false detections in each scan (there are $1009 \cdot 256 = 258304$ cells).

2. The window of cells used to estimate the background noise parameter $\mu$ in (3) is shown in Figure 4a. There are 24 cells used to estimate $\mu$ in the averaging process for a given cell under test. To avoid the signal from the test cell affecting the estimation of $\mu$, some cells are defined as guard bands. It is critical that this window be sufficiently small due to the nonhomogenous background. The authors found the given size to be convenient.

3. The structuring element in the closing operation has size $5 \times 5$; see Figure 4(b).

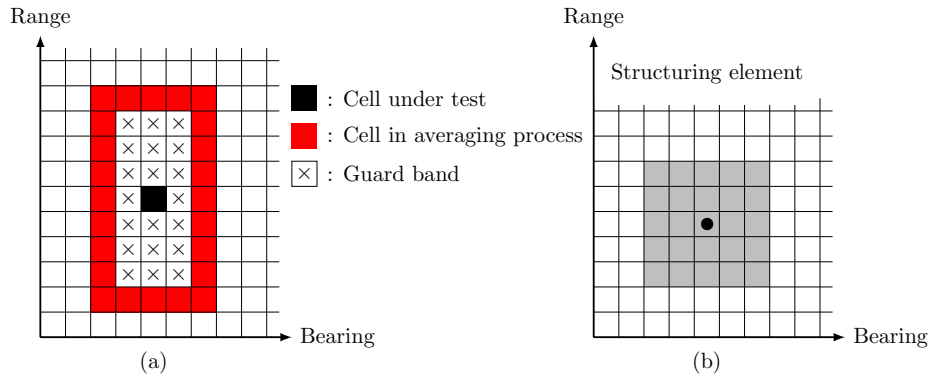


***Figure 4:*** *(a) Averaging window of cells used to estimate the background noise parameter $\mu$. (b) Structuring element. Resolution of each cell is about $0.8$ m in range and $0.7°$ in bearing.*

The measurements and corresponding clusters for each scan are handed over to the tracking algorithm. Tracks are initialized by two-point differencing of the cluster centroids. Any successive pair of clusters within a maximum distance based on target maximum motion parameters and cluster measurement noise variances initiates a preliminary track. For the motion parameters, a maximum distance $d_{max} = 0.5$ m together with the process noise matrix $Q$ in (12) is used. The measurement noise for the clusters is computed from the different cells included in the cluster as a Gaussian mixture [5]. A preliminary track then has to receive measurements for a minimum of 4 time steps during the first 6 scans to become a confirmed track. This is also referred to as a "$4/6$" logic-

based track formation procedure. In Table 1 the filter design parameters are specified with values and comments.

***Table 1:*** *Specification of parameters*

| Parameter | Value | Specification |
|---|---|---|
| $T$ | 1.089 s | Scan length |
| $N_S$ | 1792 | Number of scans |
| $P_D$ | 0.65 | Detection probability |
| $P_{FA}$ | 0.0005 | False alarm probability |
| $P_G$ | 0.999 | Gate probability |
| $P_B$ | 0.95 | Bubble probability |
| $\sigma_p^2$ | $0.0025$ m$^2$/s$^4$ | Process noise |
| $\sigma_r^2$ | $0.2$ m$^2$ | Measurement noise (range) for PDAF |
| $\sigma_r^2$ | $4.2$ m$^2$ | For the PDAF with a bubble model |
| $\sigma_\psi^2$ | $5 \cdot 10^{-5}$ rad$^2$ | Measurement noise (bearing) |

To terminate a track one of following events (termination events) must occur.

1. The estimated speed is outside the interval $[0.005, 2]$ m/s.
2. The average of the last $50$ estimated speeds is lower than $0.05$ m/s.
3. The estimate moves more than $10$ m between two scans.
4. The estimation error variance for one variable in the state exceeds $100$ m$^2$ (position variable) or $50$ m$^2$/s$^2$ (velocity variable).
5. There are no validated measurements received in a track within $20$ successive scans.
6. There are validated measurements in less than $10$ scans during the last $50$ scans.
7. A measurement in the validation region has already been associated to an older track.

The bubble model is meant to be applied only for the diver with an open breathing system. A simple test is used to decide which track this model should be applied to. For each scan, the number of measurements in front of the diver, $m_k^{\text{front}}$, is compared with

the number of measurements behind, $m_k^{\text{rear}}$. A threshold is set for how often $m_k^{\text{rear}}$ should be larger than $m_k^{\text{front}}$ before the bubble model is applied. A more sophisticated test could have been implemented, but this simple test worked well.

## 5.2 Experimental Results

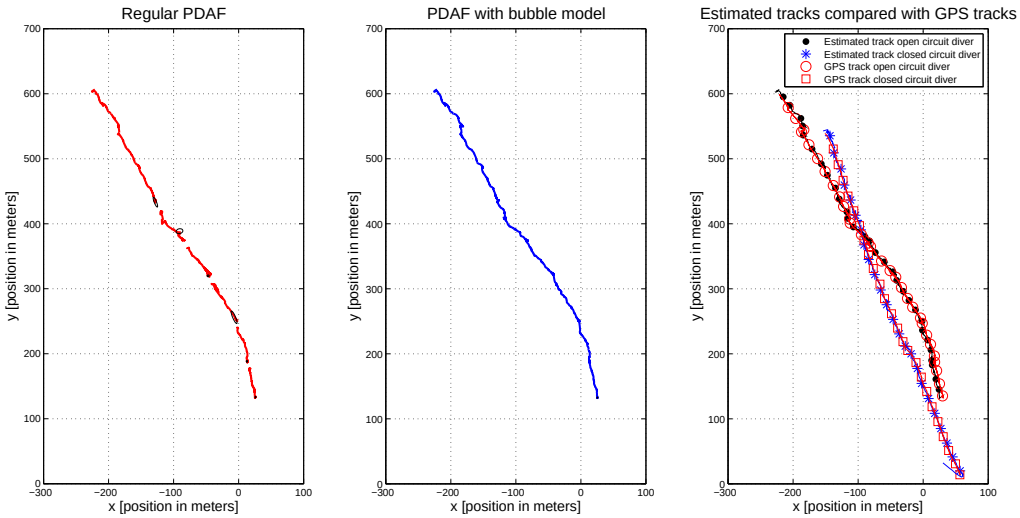


***Figure 5:*** *Estimated tracks of open breathing system diver using a regular PDAF (left) and PDAF with included bubble model (middle). Estimated tracks of both divers with GPS signal overlayed (right). The sonar is located in position (0,0), and both divers are recorded simultaneously in a single run.*

First a standard PDAF was tested on the data and it worked well on the closed breathing system diver. For the diver with the open breathing system the PDAF had problems when the real diver became undetected while at the same time false detections from the bubbles behind him showed up. This resulted in a lost track, and a new track had to be started. When the bubble model is included in the PDAF, the filter is able to handle this problem, and a lasting track is established. Figure 5 illustrates the difference between including the bubble model or not, and it shows how the track from the regular PDAF is broken into six segments. The first and longest track segment is terminated in position $(-130, 435)$ due to high velocity variance (termination event 4). The second segment loses the diver at position $(-85, 375)$. In that position the sonar return from the real diver becomes weaker and the detections from the bubbles start to affect the track. This makes the track turn around and move backwards through the cloud of bubbles. At position $(-90, 390)$ the bubbles are absent and the track terminates due to termination event 6. The third segment stops at position $(-45, 325)$ due to the weaker target and several bubble detections, and it “jumps" around in the local area between bubble detections for

a longer period before it terminates due to termination event 2. The fourth segment terminates for the same reason as the second (too large error variance). The fifth segment also stops by the bubble cloud and terminates due to a low speed (termination event 1), and the last is terminated by termination event 2. The linear bubble model pdf $p_B(\cdot)$ used in the modified PDAF is described in Appendix B.

The GPS systems supplied to the divers were floating on the surface attached to a rope about 15 m long connected to the divers. There is no further information about the position of the GPS relative to the diver so the GPS reported locations have been matched to the estimated tracks. Also since there is a bias between the GPS and the real diver, the GPS locations should not be considered as a ground truth but rather as helpful information to verify the accepted tracks, see Figure 5.

## 5.3 Track Life

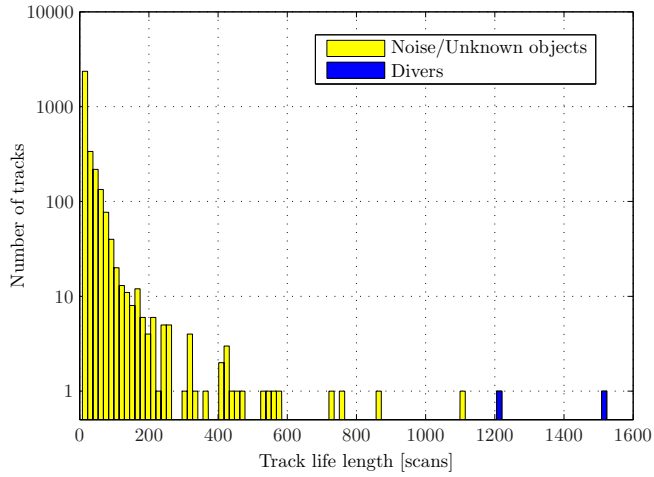


***Figure 6:*** *Histogram of track life length for all tracks. The two divers with life length 1217 scans (closed breathing system diver) and 1524 scans (open breathing system diver) are highlighted.*

In Figure 6 track life is illustrated for all tracks during the experiment. As can be seen, there are several tracks from unknown objects that have a long life length and the question arises as to whether they are false or not. Due to the nonhomogenous background a relatively low threshold (i.e., high false alarm rate) has to be used for the tracking algorithm to receive enough detections for the real diver tracks. The disadvantage of the high false alarm rate is that it makes it easier for false tracks to continue since there are several detections that may arise inside a validation region. Some of these false tracks are very difficult to exclude since they act similar to the targets of interest. As an example, the false track with longest life length, more than 1000 scans, has the following

behavior: It initializes by two spurious successive detections, and then “jumps" on false detections for a relatively far distance. At one point the track stops in an area with high background noise that yields constant detections which keep the track alive for a long time. Tracks that start in a position with high background noise are easier to exclude since they are standing still from the beginning.

The average length for a track was about 28 scans, and at average there are 51 active tracks at each scan. Defining only the two divers as real targets one could state that the average false track life length is also about 28 scans. Then, to indicate the average frequency of a false track in a particular cell $P_{FT}$, we approximate this probability as

$$P_{FT} \approx \frac{51-2}{\text{number of cells}} = \frac{49}{256 \cdot 1009} = 2 \cdot 10^{-4} \tag{27}$$

This is not very clear due to the fact that there could be other “targets" like fish in the area. There is also a question of how to define a target. This would be more of a classification problem, and is a topic for future work. By requiring a track to move a certain distance before declaring it a track, in this case 20 m, most of the false tracks are excluded. In that case, on the average, there are only 9 existing tracks at each scan, but still there are tracks from unknown objects or noise that would last for a long time due to the high false alarm rate and the nonhomogenous background. The focus of this paper has not been to minimize the number of false tracks. In state of the art sonar systems this problem is often solved by using target recognition.

## 6 Conclusions

An important factor in a tracking system is to correctly associate the measurements received from a detector to its origin. The PDAF has been a solution to this problem in many implemented systems due to its effectiveness and low computational demands. One assumption in the PDAF is that false measurements are due to i.i.d. uniformly spatially distributed background noise. In some situations such as in this paper this assumption is not adequate. The presented solution extends this to incorporate a model of the bubbles behind a diver. A similar solution may be effective for the wake behind a ship or other vehicles with a wake effect. Due to numerous detections from the bubbles behind the target, the tracking algorithm may be mislead and sometimes lose the target. To prevent this, the bubble model PDAF will weight these measurements behind the target lower than in a regular PDAF. It is important that the weights be sufficiently small so that the track is not forced to turn into the bubble cloud. To achieve this, we presented a bubble model with sufficient mass density behind the target. The model also includes an a priori probability for the bubble model conditioned on an open breathing system diver being present. A linearly increasing bubble model has been implemented, which results in an analytical expression for the probability that there are bubbles in the validation gate. The reported bubble model is shown to be a valuable modification of the PDAF to maintain track continuity, and the approach is a novel contribution to the state of the art sonar tracking systems.

## Acknowledgements

The authors would like to thank Dr. John H. Glattetre of Kongsberg Maritime for providing the sonar data recorded by the active 90 kHz narrowband SM2000 multibeam imaging sonar from Kongsberg Simrad Mesotech Ltd.

## Appendix A: The Association Probabilities in the Bubble PDAF

In this section the way the $\beta_k(i)$ are calculated in the modified PDAF is derived. Define the association events as

$$\theta_k(i) = \begin{cases} z_k(i) \text{ originates from the target} & i = 1, \ldots, m_k \\ \text{all measurements are false} & i = 0 \end{cases} \tag{28}$$

where $\theta_k(i)$ is mutually exclusive and exhaustive for the number of measurements $m_k \geq 1$. Using the total probability theorem, the conditional mean of the state at time $k$ is

$$\hat{x}_{k|k} = E\left\{x_k|Z^k\right\} = \sum_{i=0}^{m_k} E\left\{x_k|\theta_k(i), Z^k\right\} P\left\{\theta_k(i)|Z^k\right\} = \sum_{i=0}^{m_k} \hat{x}_{k|k}(i)\beta_k(i) \tag{29}$$

Here $\hat{x}_{k|k}(i)$, $i \neq 0$, is the updated state conditioned on the event that the $i$-th validated measurement is the correct target-originated one, and

$$\beta_k(i) \triangleq P\left\{\theta_k(i)|Z^k\right\} \qquad \text{for} \qquad i = 1, \ldots, m_k \tag{30}$$

is the conditional probability of this event. For the event that all measurements are false, event $i = 0$, the predicted state is used

$$\hat{x}_{k|k}(0) = \hat{x}_{k|k-1} \tag{31}$$

with the corresponding weight $\beta_k(0)$.

To derive the conditional probabilities, use Bayes' formula

$$\begin{aligned} \beta_k(i) &= P\left\{\theta_k(i)|Z^k\right\} = P\left\{\theta_k(i)|Z_k, m_k, Z^{k-1}\right\} \\ &= \frac{1}{c} p\left(Z_k|\theta_k(i), m_k, Z^{k-1}\right) P\left\{\theta_k(i)|m_k, Z^{k-1}\right\} \end{aligned} \tag{32}$$

The pdf of the target-originated measurement is

$$p\left(z_k(i)|\theta_k(i), m_k, Z^{k-1}\right) = \frac{1}{P_G}\mathcal{N}\left(z_k(i); \hat{z}_{k|k-1}, S_k\right) = \frac{1}{P_G}\mathcal{N}\left(\nu_k(i); 0, S_k\right) \tag{33}$$

where $P_G$ is used to account for restricting the normal density to the validation gate. Denote the events that a measurement originates from a target, background noise or

bubbles as $T$, $N$, and $B$, respectively, where these events are mutually exhaustive and exclusive. Then the pdf for a false measurement, with the time index $k$ omitted for simplicity, is given by the total probability theorem

$$p\left(z|\overline{T}\right) = p\left(z, N|\overline{T}\right) + p\left(z, B|\overline{T}\right) = P\left\{N|\overline{T}\right\} p\left(z|\overline{T}, N\right) + P\left\{B|\overline{T}\right\} p\left(z|\overline{T}, B\right) \tag{34}$$

where $\overline{T}$ is the complement [19] of $T$. Defining $p_B(\cdot)$ as the pdf for the bubble-originated measurements, and taking the time index $k$ into account, (34) yields

$$p(z_k(i)|\theta_k(j), j \neq i) = (1 - P_B)\frac{1}{V_k} + P_B\frac{p_B(z_k(i))}{P_{GB}} \tag{35}$$

Here $\frac{1}{V_k}$ is the uniform pdf for the background noise originated measurements and $P_{GB}$ is used to account for restricting the density of the bubble model to the validation gate. (The calculation of $P_{GB}$ for a linear $p_B(\cdot)$ is presented in detail in Appendix B.)

The joint density of the validated measurements conditioned on $\theta_k(i)$ in (32) is the product of the pdf for each measurement, given by (33) and (35), assuming that the measurements are independent

$$p\left(Z_k|\theta_k(i), m_k, Z^{k-1}\right) = \begin{cases} \prod_{\substack{j=1 \\ j\neq i}}^{m_k} \left[\frac{1-P_B}{V_k} + \frac{P_B}{P_{GB}} p_B(z_k(j))\right] & \\ \qquad \times \frac{1}{P_G}\mathcal{N}\left(\nu_k(i); 0, S_k\right) & i = 1, \ldots, m_k \\ \prod_{j=1}^{m_k} \left[\frac{1-P_B}{V_k} + \frac{P_B}{P_{GB}} p_B(z_k(j))\right] & i = 0 \end{cases} \tag{36}$$

The third term of (32) is the same as in the standard PDAF using a nonparametric model (diffuse prior) [4]

$$P\left\{\theta_k(i)|m_k\right\} = \begin{cases} \frac{1}{m_k} P_G P_D & i = 1, \ldots, m_k \\ (1 - P_G P_D) & i = 0 \end{cases} \tag{37}$$

The last step is to insert (36) and (37) into $\beta_k(i)$ in (32)

$$\beta_k(i) = \frac{1}{c} p\left(Z_k|\theta_k(i), m_k, Z^{k-1}\right) P\left\{\theta_k(i)|m_k, Z^{k-1}\right\}$$

$$= \frac{1}{c} \begin{cases} \prod_{\substack{j=1 \\ j\neq i}}^{m_k} \left[\frac{1-P_B}{V_k} + \frac{P_B}{P_{GB}} p_B(z_k(j))\right] \frac{P_D \mathcal{N}(\nu_k(i);0,S_k)}{m_k} & i = 1,\ldots,m_k \\ \prod_{j=1}^{m_k} \left[\frac{1-P_B}{V_k} + \frac{P_B}{P_{GB}} p_B(z_k(j))\right] (1 - P_G P_D) & i = 0 \end{cases} \tag{38}$$

$$= \frac{1}{c} \begin{cases} \prod_{j=1}^{m_k} \left[\frac{1-P_B}{V_k} + \frac{P_B}{P_{GB}} p_B(z_k(j))\right] \frac{P_D}{m_k} \frac{\mathcal{N}(\nu_k(i);0,S_k)}{\left[\frac{1-P_B}{V_k} + \frac{P_B}{P_{GB}} p_B(z_k(i))\right]} & i = 1,\ldots,m_k \\ \prod_{j=1}^{m_k} \left[\frac{1-P_B}{V_k} + \frac{P_B}{P_{GB}} p_B(z_k(j))\right] \frac{P_D}{m_k} \frac{m_k(1-P_G P_D)}{P_D} & i = 0 \end{cases}$$

$$= \frac{1}{c'} \begin{cases} \frac{\frac{1}{|2\pi S_k|^{\frac{1}{2}}} e^{-\frac{1}{2}\nu_k(i)^T S_k^{-1} \nu_k(i)}}{\left[\frac{1-P_B}{V_k} + \frac{P_B}{P_{GB}} p_B(z_k(i))\right]} & i = 1,\ldots,m_k \\ \frac{m_k(1-P_G P_D)}{P_D} & i = 0 \end{cases}$$

In the last step of (38) the product

$$\prod_{j=1}^{m_k} \left[\frac{1-P_B}{V_k} + \frac{P_B}{P_{GB}} p_B(z_k(j))\right] \frac{P_D}{m_k} \tag{39}$$

is brought into the constant $c'$, and the Gaussian distribution $\mathcal{N}(\nu_k(i);0,S_k)$ is substituted by the explicit expression

$$\mathcal{N}(\nu_k(i);0,S_k) = \frac{1}{|2\pi S_k|^{\frac{1}{2}}} e^{-\frac{1}{2}\nu_k(i)^T S_k^{-1} \nu_k(i)} \tag{40}$$

To summarize on the same form as (18)

$$\beta_k(i) = \begin{cases} c \frac{e^{-\frac{1}{2}\nu_k(i)^T S_k^{-1} \nu_k(i)}}{\left[\frac{1-P_B}{V_k} + \frac{P_B}{P_{GB}} p_B(z_k(i))\right]} & i = 1,\ldots,m_k \\ c\,|2\pi S_k|^{\frac{1}{2}}\, m_k \frac{1-P_G P_D}{P_D} & i = 0 \end{cases} \tag{41}$$

where $c$ is a normalizing constant to ensure that $\sum_{i=0}^{m_k} \beta_k(i) = 1$. Note that this is valid for the nonparametric PDAF, not for a parametric PDAF.

## Appendix B: Specification of the Bubble Model and Calculation of its Gate Probability

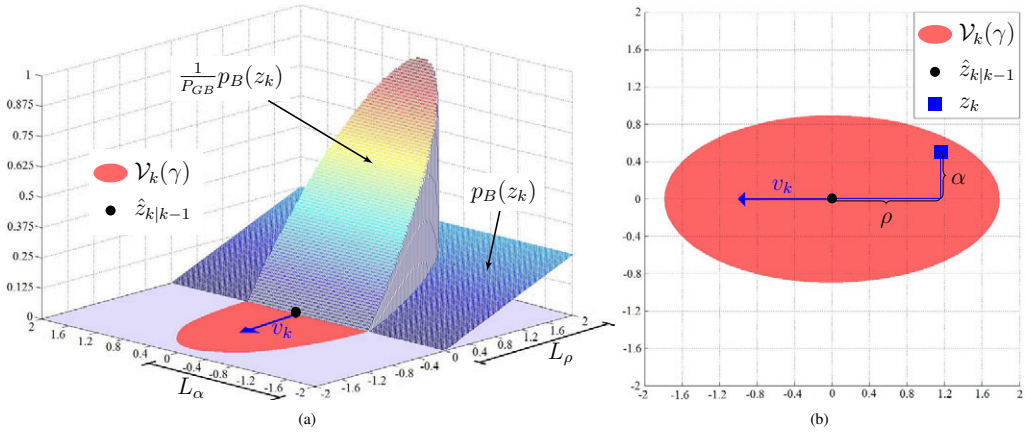


***Figure 7:*** *Illustration of elements used to calculate $P_{GB}$ in (a) 3D and (b) 2D (pdf $p_B(z_k)$ with boundaries $L_\rho$ and $L_\alpha$, the pdf $\frac{1}{P_{GB}} p_B(z_k)$ restricted by validation region $\mathcal{V}_k(\gamma)$, the target velocity $v_k$, its predicted measurement $\hat{z}_{k|k-1}$, and a measurement $z_k$ defined by its distances $\rho$ and $\alpha$).*

The probability $P_{GB}$ in (23), used to restrict the density of the bubble model $p_B(z_k)$ to the validation region, has to be calculated for each track at each scan. Let $v_k$ be the normalized target velocity with unit norm

$$v_k = \begin{bmatrix} v_{kx} \\ v_{ky} \end{bmatrix} \qquad \text{where} \qquad \|v_k\| = 1 \tag{42}$$

and define the measurement validation region as

$$\mathcal{V}_k(\gamma) = \left\{ z : [z - \hat{z}_{k|k-1}]^T S_k^{-1} [z - \hat{z}_{k|k-1}] \leq \gamma \right\} \tag{43}$$

where $\gamma$ is the gate threshold determined by the chosen gate probability $P_G$. To calculate $P_{GB}$ an integration of $p_B(z_k)$ inside the validation region $\mathcal{V}_k(\gamma)$ has to be done. The pdf $p_B(z_k)$ is assumed linear increasing in the direction opposite to $v_k$ and uniform in the direction perpendicular to $v_k$. Define the distances $\rho = -\nu_k^T v_k$ as the negative inner product of the innovation and the target velocity, and $\alpha = \left| \nu_k^T v_k^* \right|$ as the absolute value of the inner product of the innovation and $v_k^*$, where $v_k^*$ is perpendicular to $v_k$. Then

$$p_B(z_k) = p_\rho(\rho) p_\alpha(\alpha) = \frac{\rho}{L_\rho^2 L_\alpha} \tag{44}$$

where

$$p_\rho(\rho) = \frac{2}{L_\rho^2}\rho \qquad 0 \le \rho \le L_\rho \tag{45}$$

$$p_\alpha(\alpha) = \frac{1}{2L_\alpha} \qquad 0 \le \alpha \le L_\alpha \tag{46}$$

Reference to Figure 7 may be helpful here. The next step is to calculate the eigenvalue and eigenvector matrices $D_k$ and $M_k$ of $S_k$ so that

$$D_k = M_k S_k M_k^T = \begin{pmatrix} \sigma_x & 0 \\ 0 & \sigma_y \end{pmatrix} \tag{47}$$

and define the transformed velocity $\mathbf{v}_k$ as $\mathbf{v}_k = M_k v_k$. If $L_\rho$ and $L_\alpha$ are large enough to cover the whole validation region, $P_{GB}$ is found analytically by the following equation

$$P_{GB} = \int\limits_{\mathcal{V}_k(\gamma)} p_B(\omega)\mathrm{d}\omega = \frac{2}{3}\left|\frac{\sigma_x\sigma_y\gamma^{\frac{3}{2}}\sqrt{\sigma_x^2\mathbf{v}_{kx}^2 + \sigma_y^2\mathbf{v}_{ky}^2}}{L_\rho^2 L_\alpha}\right| \tag{48}$$

## References


[1] D. A. Abraham, "Signal excess in K-distributed reverberation," *IEEE Journal of Oceanic Engineering*, vol. 28, no. 3, pp. 526–536, July 2003.

[2] A. Asada, F. Maeda, K. Kuramoto, Y. Kawashima, M. Nanri, and K. Hantani, "Advanced surveillance technology for underwater security sonar systems," in *OCEANS 2007 - Europe*, Aberdeen, Scotland, UK, June 2007, pp. 1–5.

[3] M. Athans, R. H. Whiting, and M. Gruber, "A suboptimal estimation algorithm with probabilistic editing for false measurements with applications to target tracking with wake phenomena," *IEEE Transactions on Automatic Control*, vol. 22, no. 3, pp. 372–384, June 1977.

[4] Y. Bar-Shalom and X. R. Li, *Multitarget-Multisensor Tracking: Principles and Techniques.* Storrs, CT: YBS Publishing, 1995.

[5] Y. Bar-Shalom, X. R. Li, and T. Kirubarajan, *Estimation with Application to Tracking and Navigation.* New York: Wiley-Interscience, 2001.

[6] Y. Bar-Shalom and E. Tse, "Tracking in a cluttered environment with probabilistic data association," *Automatica*, vol. 11, no. 5, pp. 451–460, Sep. 1975.

[7] S. S. Blackman and R. Popoli, *Design and Analysis of Modern Tracking Systems.* Norwood, MA: Artech House, 1999.

[8] B. J. Bunin, A. Sutin, and M. S. Bruno, "Maritime security laboratory for maritime security research," in *Proceedings of the SPIE Conference on Optics and Photonics in Global Homeland Security III*, vol. 6540, May 2007.

[9] A. M. Crawford and D. V. Crowe, "Observations from demonstrations of several commercial diver detection sonar systems," in *Oceans 2007*, Vancouver, BC, Canada, Sep./Oct. 2007, pp. 1–3.

[10] R. O. Duda, P. E. Hart, and D. G. Stork, *Pattern Classification*, 2nd ed. New York: Wiley-Interscience, 2001.

[11] P. P. Gandhi and S. A. Kassam, "Analysis of CFAR processors in homogeneous background," *IEEE Transactions on Aerospace and Electronic Systems*, vol. 24, no. 4, pp. 427–445, July 1988.

[12] ——, "Optimality of the cell averaging CFAR detector," *IEEE Transactions on Information Theory*, vol. 40, no. 4, pp. 1226–1228, July 1994.

[13] R. M. Haralick, S. R. Sternberg, and X. Zhuang, "Image analysis using mathematical morphology," *IEEE Transactions on Pattern Analysis and Machine Intelligence*, vol. 9, no. 4, pp. 532–550, July 1987.

[14] J.-B. Jung, G. F. Denny, J. W. Tilley, A. B. Kulinchenko, and P. K. Simpson, "Broadband active sonar swimmer detection and identification," in *International Joint Conference on Neural Networks*, Vancouver, BC, July 2006, pp. 2600–2605.

[15] Y. Li and L. Yu, "Group tracking using mathematical morphology and multiple clustering hypotheses," in *Proceedings of the SPIE Conference on MIPPR 2007: Automatic Target Recognition and Image Analysis; and Multispectral Image Acquisition.*, vol. 6786, paper 39, Nov. 2007.

[16] A. Lovik, A. R. Bakken, J. Dybedal, T. Knudsen, and J. Kjoll, "Underwater protection system," in *Oceans 2007*, Vancouver, BC, Canada, Sep./Oct. 2007, pp. 1–8.

[17] F. Maeda, A. Asada, K. Kuramoto, Y. Kurashige, M. Nanri, Y. Kawashima, R. Imai, and K. Hantani, "Development of diver detection and sensor integration for wharf surveillance software," in *Symposium on Underwater Technology and Workshop on Scientific Use of Submarine Cables and Related Technologies*, Tokyo, Japan, Apr. 2007, pp. 133–141.

[18] S. D. Meier and P. J. Moore, "Morphological filter assisted low amplitude impulse detector," in *IEEE International Symposium on Signal Processing and Information Technology*, Aug. 2006, pp. 950–954.

[19] A. Papoulis and S. U. Pillai, *Probability, Random Variables and Stochastic Processes*, 4th ed. New York: McGraw-Hill, 2002.

[20] J. G. Postaire, R. D. Zhang, and C. Lecocq-Botte, "Cluster analysis by binary morphology," *IEEE Transactions on Pattern Analysis and Machine Intelligence*, vol. 15, no. 2, pp. 170–180, Feb. 1993.

[21] A. Rødningsby and Y. Bar-Shalom, "Tracking of divers in a noisy background using a bubble model," in *Proceedings of the SPIE Conference on Signal and Data Processing of Small Targets*, vol. 6699, paper 7, San Diego, CA, Aug. 2007.

[22] S. Sarangapani, J. H. Miller, G. R. Potty, D. B. Reeder, T. K. Stanton, and D. Chu, "Measurements and modeling of the target strength of divers," in *Oceans 2005 - Europe*, vol. 2, June 2005, pp. 952–956.

[23] J. P. Serra, *Image Analysis and Mathematical Morphology*. London, UK: Academic Press, 1982.

[24] R. J. Urick, *Principles of Underwater Sound*, 3rd ed. New York: McGraw-Hill, 1983.

# Paper B

## Multitarget Tracking in the Presence of Wakes

**Authors:**
Anders Rødningsby, Yaakov Bar-Shalom, Oddvar Hallingstad, and John Glattetre.

Edited version of paper originally published in *Proceedings of the 11th International Conference on Information Fusion*, pp. 1536-1543, Cologne, Germany, July 2008.

**Editing remarks:**

- The incorrect term $S_k^{-1}$ used in the original paper is replaced with the correct term $S_k$ in (11).
- The incorrect term $P\{\delta_\theta, \phi_\theta | m_k\}$ used in the original paper is replaced with the correct term $P\{\theta_k | \delta_\theta, \phi_\theta, m_k\}$ in (29).
- The joint association event $\Theta$, defined in (16), was denoted $\theta$ in the original paper. To agree with the notation in this thesis, the original term $\theta$ is substituted with the term $\Theta$ in Section 3.2 and Section 3.3.

This paper was nominated for Best Student Paper Award Fusion 2008.

# Multitarget Tracking in the Presence of Wakes

Anders Rødningsby[1] Yaakov Bar-Shalom[2] Oddvar Hallingstad[1] John Glattetre[3]

[1]University Graduate Center, NO-2027 Kjeller, Norway
[2]University of Connecticut, U-2157 Storrs, CT, USA
[3]Kongsberg Maritime, NO-3191 Horten, Norway

**Abstract**

In this paper we focus on targets which, in addition to reflecting signals themselves, also have a trailing path behind them, called a wake. When the detections are fed to a tracking system like the Probabilistic Data Association Filter, the estimated track can be misled and sometimes lose the real target because of the wake. This problem becomes even more severe in multitarget environments where targets are operating close to each other in the presence of wakes. To prevent this, we have developed a probabilistic model of the wakes in a multitarget environment. This model is used to augment the Joint Probabilistic Data Association Filter (JPDAF). Simulations of two crossing targets with wakes show that this modification gives good results and the number of lost tracks is significantly reduced.

**Keywords: Multitarget, tracking, data association, wake.**

# 1 Introduction

TARGETS in real tracking scenarios may be detected by their reflection of signals emitted from a radar [6], a sonar [14], or by the use of optical sensors [8], [13]. In addition to target-originated measurements there will also be a number of detections due to noise and clutter, called false alarms. A well-known tracking method to handle targets in clutter is the Probabilistic Data Association Filter (PDAF) [3], [5]. The PDAF accounts for the measurement origin uncertainty by calculating for each validated measurement at the current time the association probabilities to the target of interest.

In a multitarget environment [2] the association of measurements is more problematic because the individual targets no longer can be considered separately as in the PDAF. For this purpose the Joint Probabilistic Data Association Filter (JPDAF) [3], [10], [9] was developed to consider a known number of targets in the data association simultaneously. This method evaluates the measurement-to-target association probabilities for the latest set of measurements and then combines them into the state estimates.

A more powerful source of false measurements is the wake phenomenon that appears behind certain targets. This could be air bubbles from a diver, the wake behind a ship, or the wake from ballistic vehicles in the reentry stage. One possible approach to this problem is to handle both the target and the wake behind it as an extended target. A problem with this approach is the varying and unknown size of the wake which may reach far behind the target yielding a large bias. In this paper it is emphasized that the wake-dominated measurements should not be considered as part of the target, but rather as a special kind of clutter. When these measurements are fed to the tracking system, it becomes important to associate them correctly to prevent a lost track. In [1] a probabilistic editing method is used to handle the wake-dominated measurements in the tracking algorithm. This probabilistic editing method is based on a single measurement extracted for each time-step, and that this measurement originates from either the target or the wake. In [12] a modified PDAF is developed to handle false measurements originating from the bubbles behind a diver (the wake). This modified single target tracking method does not restrict the number of false measurements for each time-step, but assumes a set of measurements where each false measurement originates from either random clutter or the wake. In this paper we extend the modified PDAF to handle multiple targets in the presence of wakes. A probabilistic wake model is used for each target in the multitarget environment that has a wake behind it. These single wake models are combined to form a joint wake model, and the modified JPDAF is developed to incorporate this additional joint wake model.

In Section 2 the tracking model and data association is presented for a single target. In Section 3 the modified JPDAF is developed for a multitarget environment. The data association methods are then compared in Section 5 by simulations of two crossing targets, before conclusions are given in Section 6.

# 2 Background

## 2.1 Model of Tracking

The standard discrete linear model in tracking is

$$x_{k+1} = Fx_k + v_k \qquad \text{and} \qquad z_k = Hx_k + w_k \tag{1}$$

where

| | | | |
|---|---|---|---|
| $x$ : | target state | $F$ : | transition matrix |
| $z$ : | measurement | $H$ : | measurement matrix |
| $v$ : | process noise | $w$ : | measurement noise |
| $k$ : | time index | | |

The process and measurement noises are assumed independent, white and Gaussian with covariance matrices

$$E\{v_k v_k^T\} = Q \qquad \text{and} \qquad E\{w_k w_k^T\} = R \tag{2}$$

In this system, assuming equal process and filter model, a Kalman filter would be optimal as long as there is only one single measurement $z_k$ at each time $k$. In real data this is unfortunately not true due to false measurements originating from noise and clutter. Instead, a set of $m_k$ measurements $Z_k = \{z_k(1), z_k(2), \ldots, z_k(m_k)\}$ is available at time $k$ and a form of data association is needed.

## 2.2 Standard PDAF

The approach of the PDAF is to calculate the association probabilities for each validated measurement at the current time to the target of interest. The posterior track probability density is therefore a mixture of Gaussian probability density functions (pdf), but is then forced back to Gaussianity by moment-matching for the succeeding scan. For a derivation of the PDAF see [3], and in the following a brief overview of the PDAF will be given.

Assume that the target state at time $k-1$ is estimated as $\hat{x}_{k-1|k-1}$ with associated covariance $P_{k-1|k-1}$. This means that the estimate is conditioned on the entire past up to time $k-1$. Then the following assumptions are made:

(a) The track is already initialized.

(b) The past information about the target is summarized approximately by the Gaussian distribution

$$p\left(x_k | Z^{k-1}\right) \approx \mathcal{N}\left(x_k; \hat{x}_{k|k-1}, P_{k|k-1}\right) \tag{3}$$

where

$$Z^{k-1} = \{Z_0, Z_1, \ldots Z_{k-1}\} \tag{4}$$

(c) A validation region or gate is set up for each time step to select the candidate measurements for association.

(d) At time $k$ there are $m_k$ validated measurements but at most one of them can be target-originated. The rest are assumed due to i.i.d. uniformly spatially distributed false alarms, independent across time.

(e) Detections of the real target occur independently over time with known detection probability $P_D$.

At each time $k$, the algorithm goes through the following steps:

1. Predict the target state, associated covariance and measurement at time $k$ based on the estimates at $k-1$:

$$\begin{aligned} \hat{x}_{k|k-1} &= F\hat{x}_{k-1|k-1} \\ P_{k|k-1} &= FP_{k-1|k-1}F^T + Q \\ \hat{z}_{k|k-1} &= H\hat{x}_{k|k-1} \end{aligned} \tag{5}$$

2. Compute the innovation covariance for the true (target-originated) measurement

$$S_k = HP_{k|k-1}H^T + R \tag{6}$$

and use $S_k$ to form the measurement validation gate where the validated measurements $Z_k$ result in $m_k$ innovations:

$$\nu_k(i) = z_k(i) - \hat{z}_{k|k-1} \qquad i = 1, \ldots, m_k \tag{7}$$

3. Calculate the association probabilities $\beta_k(i)$, $i = 1 \ldots m_k$ that measurement $z_k(i)$ originates from the true target, and $\beta_k(0)$ as the probability that all measurements are false alarms

$$\beta_k(i) = \begin{cases} ce^{-\frac{1}{2}\nu_k(i)^T S_k^{-1}\nu_k(i)} & i = 1, \ldots, m_k \\ c\,|2\pi S_k|^{\frac{1}{2}}\, m_k \frac{1-P_G P_D}{V_k P_D} & i = 0 \end{cases} \tag{8}$$

Here $c$ is a normalizing constant to ensure that $\sum_{i=0}^{m_k} \beta_k(i) = 1$, $V_k$ is the volume of the gate and $P_G$ is the probability that the true measurement falls inside the gate. In (8) a diffuse prior [3] is used for the point mass function (pmf) of the number of false measurements in the validation region.

4. Calculate the Kalman gain and the combined innovation

$$W_k = P_{k|k-1}H^T S_k^{-1} \quad \text{and} \quad \nu_k = \sum_{i=1}^{m_k} \beta_k(i)\nu_k(i) \tag{9}$$

to update the track according to

$$\hat{x}_{k|k} = \hat{x}_{k|k-1} + W_k\nu_k \tag{10}$$

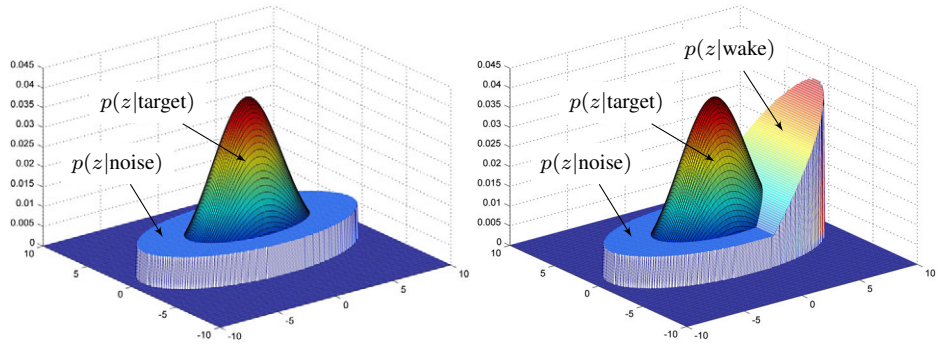


(a) Regular PDAF (b) Modified PDAF with wake model

***Figure 1:*** *Illustration of the pdfs for the measurements originating from the target, noise or wake in: (a) regular PDAF, and (b) modified PDAF with special wake model.*

5. The state estimation covariance is updated by[1]

$$\begin{aligned} P_{k|k} =& \beta_k(0) P_{k|k-1} + [1-\beta_k(0)] \left( P_{k|k-1} - W_k S_k W_k^T \right) \\ &+ W_k \left[ \sum_{i=0}^{m_k} \beta_k(i) \nu_k(i) \nu_k(i)^T - \nu_k \nu_k^T \right] W_k^T \end{aligned} \tag{11}$$

where the last term in (11) is the "spread of the innovations."

## 2.3 Modified PDAF

Targets with a wake behind them may cause detections from the wake that mislead the tracking algorithm and are likely to result in a lost track. To prevent this, an extension of the regular PDAF incorporating a special probabilistic model of the wake was developed in [12].

The PDAF with the wake model is illustrated in Figure 1, and takes into account that false measurements can originate from either the wake with pdf $p_W(\cdot)$ and a priori probability $P_W$, or from i.i.d. uniformly distributed noise/clutter with a priori probability $1-P_W$, independently across time. This modification affects the PDA in the calculation of the $\beta_k(i)$ in (8) and yields

$$\beta_k(i) = \begin{cases} c \frac{e^{-\frac{1}{2}\nu_k(i)^T S_k^{-1} \nu_k(i)}}{\left[ \frac{1-P_W}{V_k} + \frac{P_W}{P_{GW}} p_W(z_k(i)) \right]} & i = 1, \ldots, m_k \\ c \left| 2\pi S_k \right|^{\frac{1}{2}} m_k \frac{1-P_G P_D}{P_D} & i = 0 \end{cases} \tag{12}$$

[1]The incorrect term $S_k^{-1}$ used in the original paper is replaced with the correct term $S_k$ in (11).

The denominator in $\beta_k(i)$ for $i = 1, \ldots, m_k$ is the pdf of a false measurement

$$p(z_k(i)|\text{measurement } i \text{ is false}) = \frac{1 - P_W}{V_k} + \frac{P_W}{P_{GW}} p_W(z_k(i)) \tag{13}$$

where $P_{GW}$ is used to account for restricting the density of the wake model $p_W(z_k(i))$ to the validation gate. The calculation of $P_{GW}$ for a linear $p_W(\cdot)$ is presented in detail in [12]. As expected, in the limit as $P_W$ goes to zero, (12) becomes (8).

# 3 Probabilistic Data Association for Multiple Targets in the Presence of Wakes

In a multitarget environment the data association algorithm needs to handle situations where a measurement could originate from different targets. For this purpose, the JPDAF was developed, and a derivation of this standard algorithm is given in [3]. Another problem arises when these targets have wakes behind them that result in misleading wake detections. In this section we will modify the JPDAF to handle this problem.

## 3.1 Assumptions

Assume there are a known number $N_T$ of established targets at time $k-1$. For each target $t$, where $t = 1, \ldots, N_T$, the target state is estimated as $\hat{x}^t_{k-1|k-1}$ with associated covariance $P^t_{k-1|k-1}$. Then the following assumptions are made:

(a) Measurements from one target can fall in the validation gate of a neighboring target.

(b) The past information about target $t$ is summarized approximately by the Gaussian distribution

$$p\left(x^t_k | Z^{k-1}\right) \approx \mathcal{N}\left(x^t_k; \hat{x}^t_{k|k-1}, P^t_{k|k-1}\right) \tag{14}$$

(c) At time $k$ there are $m_k$ validated measurements in the union of their validation gates, but for each target $t$ at most one measurement can be target-originated. The rest are assumed due to the wakes with pdf $p_W(\cdot)$ and a priori probability $P_W$, or from i.i.d. uniformly distributed noise/clutter with a priori probability $1 - P_W$, independent across time.

In Figure 2 an example of the pdf's for two targets that are starting to cross each other is shown. Here both targets have a wake behind them, and the joint wake model (the sum of each target's single wake model) increases linearly behind the targets inside the joint validation region. The joint validation region contains all the candidate measurements, and restricts the spatially uniform distribution representing the noise/clutter. Further details about the joint wake model and the validation region are given in Appendix A.

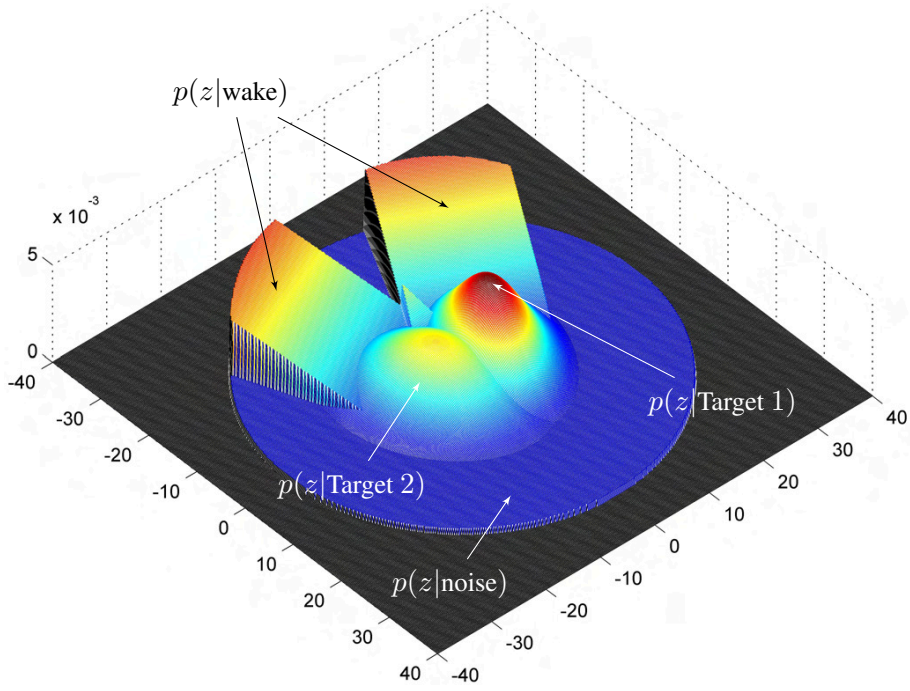


***Figure 2:*** *Probability density functions for two targets with crossing trajectories. The distribution of the targets are Gaussian and overlap each other. The wakes behind the targets are modeled as linear increasing pdf's, and the noise/clutter is uniformly spatially distributed inside the joint validation region.*

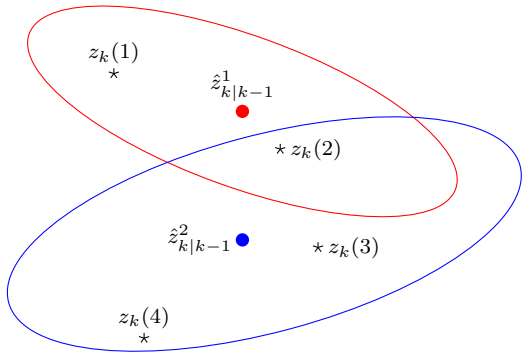


$$\Omega = \begin{array}{c|ccc} j\backslash t & 0 & 1 & 2 \\ \hline 1 & 1 & 1 & 0 \\ 2 & 1 & 1 & 1 \\ 3 & 1 & 0 & 1 \\ 4 & 1 & 0 & 1 \end{array}$$

***Figure 3:*** *Two targets with a measurement in the intersection of their validation gates are shown with corresponding validation matrix $\Omega$.*

### 3.2 Joint Association Events

Define the validation matrix $\Omega$ to represent all feasible association events at time $k$ (the time index $k$ is omitted for simplicity where it does not cause confusion)

$$\Omega = [\omega(j,t)] \qquad j = 1,\ldots,m \quad \text{and} \quad t = 0,\ldots,N_T \tag{15}$$

Here, $\omega(j,t)$ is a binary element indicating if measurement $j$ lies in the validation gate of target $t$. The index $t = 0$ means that the measurement is from none of the targets and therefore it is a false measurement. An example where a measurement may originate from two targets, i.e., it lies in both targets' validation gates, is shown with the corresponding validation matrix $\Omega$ in Figure 3. For all these possible joint association events, conditional probabilities have to be derived.

A joint association event[2] $\Theta$ describes an unambiguous association between the measurements and the targets at time $k$

$$\Theta = \bigcap_{j=1}^{m} \theta(j,t_j) \tag{16}$$

where

- $\theta(j,t)$ is the event that measurement $j$ originates from target $t$, where $j = 1,\ldots,m$ and $t = 0,1,\ldots,N_T$.
- $t_j$ is the index of the target to which measurement $j$ is associated in the event under consideration.

$\Theta$ can also be represented by the event matrix

$$\Omega_\Theta = [\omega_\Theta(j,t)] \tag{17}$$

consisting of the units in $\Omega$ corresponding to the associations in $\Theta$

$$\omega_\Theta(j,t) = \begin{cases} 1 & \text{if the event } \theta(j,t) \text{ is part of } \Theta \\ 0 & \text{otherwise} \end{cases} \tag{18}$$

Using this, a feasible association event needs to fulfill the following requirements:

1. a measurement can have only one source, i.e.

$$\sum_{t=0}^{N_T} \omega_\Theta(j,t) = 1 \qquad \forall \quad j \tag{19}$$

2. at most one measurement can originate from a target

$$\delta_\Theta^t \triangleq \sum_{j=1}^{m} \omega_\Theta(j,t) \leqslant 1 \qquad t = 1,\ldots,N_T \tag{20}$$

[2]The joint association event was denoted $\theta$ in the original paper, but is substituted with the term $\Theta$ throughout this paper. This is done to agree with the notation in this thesis.

The binary variable $\delta_\Theta^t$ is called the target detection indicator since it indicates whether a measurement is associated to a target $t$ or not in event $\Theta$. It is also convenient to define two more binary variables

$$\tau_\Theta(j) \triangleq \sum_{t=1}^{N_T} \omega_\Theta(j,t) \tag{21}$$

$$\phi_\Theta \triangleq \sum_{j=1}^{m} [1 - \tau_\Theta(j)] \tag{22}$$

where $\tau_\Theta(j)$ is the measurement association indicator to indicate if measurement $j$ is associated to a target or not, and $\phi_\Theta$ is the number of false (unassociated) measurements in event $\Theta$.

### 3.3 Modified JPDAF Including a Wake Model

The joint association event probabilities are derived using Bayes' formula

$$\begin{aligned} P\{\Theta_k|Z^k\} &= P\{\Theta_k|Z_k, m_k, Z^{k-1}\} \\ &= \frac{1}{c} p[Z_k|\Theta_k, m_k, Z^{k-1}] P\{\Theta_k|Z^{k-1}, m_k\} \\ &= \frac{1}{c} p[Z_k|\Theta_k, m_k, Z^{k-1}] P\{\Theta_k|m_k\} \end{aligned} \tag{23}$$

where $c$ is a normalizing constant. In the last line of the above equation the irrelevant conditioning term $Z^{k-1}$ has been omitted. The likelihood function of the measurements in (23) is derived by assuming that the states of the targets, conditioned on the past observations, are mutually independent

$$p[Z_k|\Theta_k, m_k, Z^{k-1}] = \prod_{j=1}^{m_k} p[z_k(j)|\theta_k(j,t_j), Z^{k-1}] \tag{24}$$

Measurements not associated with a target are assumed either from the wakes with pdf $p_W(z_k(j))$ and a priori probability $P_W$, or from uniformly distributed noise/clutter with a priori probability $(1 - P_W)$. Defining $V_k$ as the volume of the joint validation gate, the pdf of a measurement given its origin is

$$p[z_k(j)|\theta_k(j,t_j), Z^{k-1}] = \begin{cases} \mathcal{N}\left[z_k(j); \hat{z}_{k|k-1}^{t_j}, S_k^{t_j}\right] & \text{if} \quad \tau_{\Theta_k}(j) = 1 \\ P_W \frac{p_W(z_k(j))}{P_{GW}} + (1 - P_W)\frac{1}{V_k} & \text{if} \quad \tau_{\Theta_k}(j) = 0 \end{cases} \tag{25}$$

where $\hat{z}_{k|k-1}^{t_j}$ is the predicted measurement for target $t_j$ with associated innovation covariance $S_k^{t_j}$. The constant $P_{GW}$ is used for restricting $p_W(z_k(j))$ to the joint validation

region, and has an analytical expression derived in Appendix A. Using the above equation, (24) can be written as

$$p[Z_k|\Theta_k, m_k, Z^{k-1}] = \prod_{j=1}^{m_k} \left\{ \mathcal{N}\left[ z_k(j); \hat{z}_{k|k-1}^{t_j}, S_k^{t_j} \right] \right\}^{\tau(j)} \times \left\{ P_W \frac{p_W(z_k(j))}{P_{GW}} + (1 - P_W)\frac{1}{V_k} \right\}^{1-\tau(j)} \tag{26}$$

Next, the last term in (23) will be derived. Let $\delta_\Theta$ be the vector of detection indicators corresponding to event $\Theta_k$

$$\delta_\Theta = [\delta_\Theta^1, \ldots, \delta_\Theta^{N_T}] \tag{27}$$

The vector $\delta_\Theta$ and the number of false measurements $\phi_\Theta$ are both completely defined when $\Theta$ is given. This yields using the definition of conditional probabilities [11]

$$P\{\Theta_k|m_k\} = P\{\Theta_k, \delta_\Theta, \phi_\Theta|m_k\} = P\{\Theta_k|\delta_\Theta, \phi_\Theta, m_k\}P\{\delta_\Theta, \phi_\Theta|m_k\} \tag{28}$$

The first term in (28) is obtained using combinatorics:

1. In event $\Theta_k$ there are assumed $m_k - \phi_\Theta$ targets detected.
2. The number of events $\Theta_k$, where the same targets are detected, is given by the number of ways of associating $m_k - \phi_\Theta$ measurements to the detected targets from a set of $m_k$ measurements.

By assuming each such event a priori equally likely, one has [3]

$$P\{\Theta_k|\delta_\Theta, \phi_\Theta, m_k\} = \frac{1}{m_k P_{m_k - \phi_\Theta}} = \frac{\phi_\Theta!}{m_k!} \tag{29}$$

The last term in (28) is, assuming $\delta$ and $\phi$ independent,

$$P\{\delta_\Theta, \phi_\Theta|m_k\} = \prod_{t=1}^{N_T} (P_D^t)^{\delta_\Theta^t}(1 - P_D^t)^{1-\delta_\Theta^t}\mu_F(\phi) \tag{30}$$

where $P_D^t$ is the detection probability of target $t$ and $\mu_F(\phi)$ is the prior pmf of the number of false measurements. The indicators $\delta_\Theta^t$ have been used to select the probabilities of detection and no detection events according to the event $\Theta_k$ under consideration. Combining (29) and (30) into (28) yields the prior probability of a joint association event

$$P\{\Theta_k|m_k\} = \frac{\phi_\Theta!}{m_k!} \prod_{t=1}^{N_T} (P_D^t)^{\delta_\Theta^t}(1 - P_D^t)^{1-\delta_\Theta^t}\mu_F(\phi) \tag{31}$$

The pmf of the number of false measurements $\mu_F(\phi)$ can, as in the case of the PDA, have two versions, parametric or non-parametric.

[3] The incorrect term $P\{\delta_\Theta, \phi_\Theta|m_k\}$ used in the original paper is corrected to $P\{\Theta_k|\delta_\Theta, \phi_\Theta, m_k\}$ in (29).

1. Parametric JPDA uses a Poisson pmf

$$\mu_F(\phi) = e^{-\lambda V} \frac{(\lambda V)^\phi}{\phi!} \tag{32}$$

which requires the spatial density $\lambda$ of the false measurements.

2. Nonparametric JPDA uses a diffuse prior

$$\mu_F(\phi) = \epsilon \qquad \forall \phi \tag{33}$$

which does not require the parameter $\lambda$.

Using the nonparametric model and combining (31) and (26) into (23) yields the joint association event probabilities

$$\begin{aligned} P\{\Theta_k|Z^k\} =& \frac{\phi_\Theta!}{c} \prod_{t=1}^{N_T} (P_D^t)^{\delta_\Theta^t} (1-P_D^t)^{1-\delta_\Theta^t} \\ & \times \prod_{j=1}^{m_k} \left\{ \mathcal{N}\left[ z_k(j); \hat{z}_{k|k-1}^{t_j}, S_k^{t_j} \right] \right\}^{\tau(j)} \\ & \times \left\{ P_W \frac{p_W(z_k(j))}{P_{GW}} + (1-P_W)\frac{1}{V_k} \right\}^{1-\tau(j)} \end{aligned} \tag{34}$$

where the constants $\epsilon$ and $m_k!$ are brought into the normalization constant $c$. For comparison, the joint association event probabilities derived in [3] for the standard JPDAF is

$$P\{\Theta_k|Z^k\} = \frac{\phi_\Theta! \cdot V_k^{-\phi_\Theta}}{c} \prod_{t=1}^{N_T} (P_D^t)^{\delta_\Theta^t} (1-P_D^t)^{1-\delta_\Theta^t} \prod_{j=1}^{m_k} \left\{ \mathcal{N}\left[ z_k(j); \hat{z}_{k|k-1}^{t_j}, S_k^{t_j} \right] \right\}^{\tau(j)} \tag{35}$$

where the third line in (34) is substituted with $V_k^{-\phi_\Theta}$. As for the modified PDAF, (34) reduces to (35) in the limit as $P_W$ goes to zero. Finally, marginal association probabilities are obtained by summing over all the joint association events in which the marginal event of interest occurs

$$\beta_k^t(j) \triangleq P\{\theta_k(j,t)|Z^k\} = \sum_{\Theta_k} P\{\Theta_k|Z^k\} \omega_\Theta(j,t) \tag{36}$$

$$\beta_k^t(0) \triangleq 1 - \sum_{j=1}^{m_k} \beta_k^t(j) \tag{37}$$

By using these association probabilities in (8), the state estimation equations are exactly the same as in the PDAF, (5) - (11).

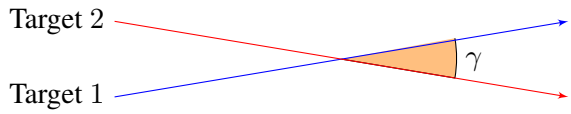


***Figure 4:*** *Trajectory crossing angle $\gamma$ between Target 1 and Target 2.*

## 4 Simulation Results

In this section we compare the data association methods described previously (PDAF, Modified PDAF, JPDAF and Modified JPDAF). To do this, a multitarget tracking problem of two crossing targets in the presence of wakes are simulated for varying trajectory crossing angles $\gamma$, see Figure 4. For both targets a two-dimensional direct discrete time nearly constant velocity model [4] is used in (1) and (2):

$$F = \begin{bmatrix} 1 & T & 0 & 0 \\ 0 & 1 & 0 & 0 \\ 0 & 0 & 1 & T \\ 0 & 0 & 0 & 1 \end{bmatrix} \qquad H = \begin{bmatrix} 1 & 0 & 0 & 0 \\ 0 & 0 & 1 & 0 \end{bmatrix}$$

$$Q = \begin{bmatrix} \frac{T^4}{4} & \frac{T^3}{2} & 0 & 0 \\ \frac{T^3}{2} & T^2 & 0 & 0 \\ 0 & 0 & \frac{T^4}{4} & \frac{T^3}{2} \\ 0 & 0 & \frac{T^3}{2} & T^2 \end{bmatrix} \sigma_p^2 \qquad R = \begin{bmatrix} \sigma_r^2 & 0 \\ 0 & \sigma_r^2 \end{bmatrix} \tag{38}$$

The parameters in (38) and other simulation design parameters are given in Table 1, and a standard Kalman filter is used as the tracking algorithm. Both targets are initialized with speed $0.5$ m/s and a course according to the trajectory crossing angle $\gamma$. To ensure a controlled crossing for the true trajectories, the added process noise $Q$ is set low, but not to zero. The small amount of process noise is used to exploit situations where the targets' positions are not totally overlapping at the crossing point, but where one target will cross in the wake from the other target. The measurements in real sonar and radar applications are obtained in polar coordinates yielding range dependent cross-range errors. By assuming a uniform measurement error inside a resolution cell, the variance is given by the squared size of the cell divided by $12$. This error can be approximated as Gaussian with the same variance. In this paper, the measurement noise is assumed constant over the surveillance area, with an approximately size of a resolution cell as $1.8$ m$^2$. This size is comparable to e.g a sonar system. Target-originated measurements are generated by adding measurement noise to the true trajectories, and then clutter and wake measurements (false alarms) are added. Denote the surveillance area covering the full trajectories of the targets as $S$, the wake area as $W$, and their respective volumes $V_S$ and $V_W$. Then, the number of clutter and wake measurements are both Poisson distributed

***Table 1:*** *Specification of parameters*

| Parameter | Value | Specification |
|---|---|---|
| $T$ | 1.0 s | Sampling period |
| $P_D$ | 0.6 | Detection probability |
| $P_G$ | 0.999 | Gate probability |
| $P_W$ | 0.9 | Wake probability |
| $P_{FA}$ | 0.005 | False alarm probability |
| $\sigma_p^2$ | $10^{-6}$ m$^2$/s$^4$ | Process noise (acceleration) |
| $\sigma_r^2$ | 0.15 m$^2$ | Measurement noise |
| $\sigma_w^2$ | 0.25 m$^2$ | Wake generation parameter, width |
| $\lambda_w$ | 10 m | Wake generation parameter, length |
| $S$ | $200 \times 100$ m | Surveillance area |
| $W$ | $5 \times 50$ m | Wake area |
| $V_S$ | 20000 m$^2$ | Volume of surveillance area |
| $V_W$ | 250 m$^2$ | Volume of wake area |

with parameters

$$\lambda_{\text{clutter}} = P_{FA} V_S \tag{39}$$

$$\lambda_{\text{wake}} = \frac{P_W}{1 - P_W} P_{FA} V_W \tag{40}$$

where $P_{FA}$ is the probability of false alarm in a unit volume. The clutter measurements are located uniformly in $S$, and wake measurements are distributed exponentially decreasing behind the target and Gaussian distributed sideways with parameters $\lambda_w$ and $\sigma_w^2$, respectively. One simulation run consists of 300 time-steps, and the true target-originated measurements are detected with probability $P_D$, independently over this period.

To reduce the computational load, the different versions of the multitarget tracking algorithms are substituted with their analogous single target tracking algorithms as long as targets are not "sharing" measurements. In other words, the standard PDAF is used instead of the JPDAF, and the modified PDAF is used instead of the modified JPDAF when the targets are apart.

Tracks are declared as lost if the position error exceeds 3 meters in front and to both sides of the true target, but are extended to 10 meters in the direction behind the target. This extension is to allow tracks with a small bias behind the true target due to the wake-originated measurements. The relatively low threshold at 3 meters is needed for small

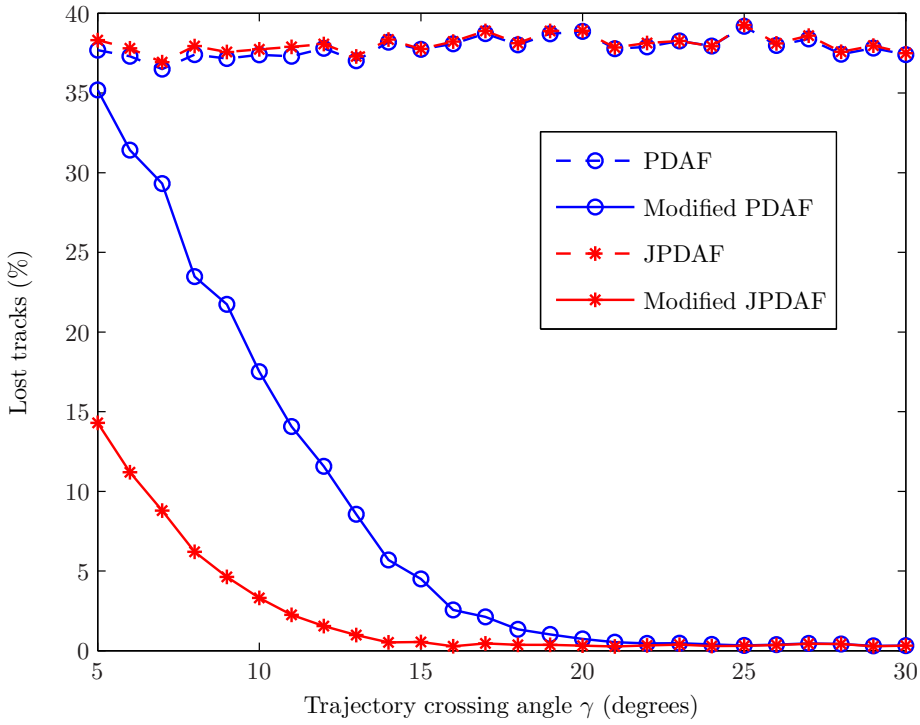


***Figure 5:*** *Lost tracks in % for various trajectory crossing angles $\gamma$ from 5000 Monte Carlo runs.*

trajectory crossing angles $\gamma$ so that tracks following the wrong target are declared as lost. At the same time 3 meters are sufficient not to declare tracks as lost in cases where they are able to get back on track again. The results of lost tracks after 5000 Monte Carlo runs for trajectory crossing angles $\gamma$ between $5°$ and $30°$, with $1°$ spacing, are shown in Figure 5. The standard filters (PDAF and JPDAF) have serious problems, and the JPDAF shows no improvement compared to the PDAF during the crossing period. For low trajectory crossing angles, $\gamma$ below $25°$, the modified JPDAF performs best. This is comparable to situations where two targets are moving almost together, and the targets are "sharing" measurements for a longer period of time. For $\gamma$ above $25°$ the modified single target tracking algorithm (PDAF) is preferable due to its equally good performance and lower computational load.

In Figure 6 the average position errors are shown for the different filters for Target 1 at trajectory crossing angle $\gamma = 15°$ (similar results for Target 2). These results are based only on tracks that are not declared as lost. The standard filters are outperformed by the modified filters, which are close to the filter with perfect data association (using only the true target-originating measurements). The different modified filters perform similarly, and only during the crossing period does the multitarget tracking algorithm

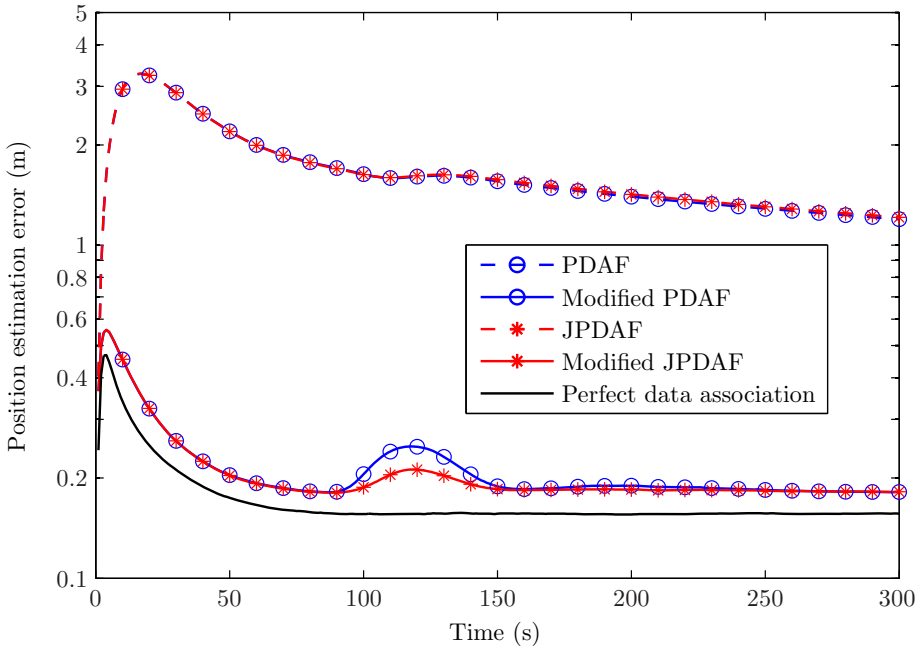


***Figure 6:*** *Position estimation error for Target 1 at trajectory crossing angle* $\gamma = 15°$ *from 50000 Monte Carlo runs.*

perform slightly better than the single target tracking filter. It is also interesting to see the RMS error in the directions parallel and perpendicular to the target's true velocity. This is shown in Figure 7 for $\gamma = 15°$. As expected, the error is much higher in the direction parallel to the velocity because this is the direction of the wakes. False detections from the wake, if not sufficiently accounted for, will draw the estimated position behind the target and into the wake, and create a bias in the estimate. The error in the direction perpendicular to the velocity is much smaller compared to the parallel direction, but during the crossing period the estimate for one target will be drawn towards the other target, also known as track coalescence [7]. This is most problematic for the modified single target tracking algorithm because it accounts for the wake behind its own target, but has no information about the nearby target which also has a wake behind it. Also notice that the perpendicular error before crossing is actually lower for the "non-perfect" data association filters, especially the standard filters, than the perfect data association filter. The reason for this is the high density of the wake measurements normally distributed (zero mean) in the direction perpendicular to the target's velocity. When these measurements are taken into the probabilistic data association, the weighted sum of all candidate measurements will give a smaller error in the perpendicular direction than using only the true target-originated measurement.

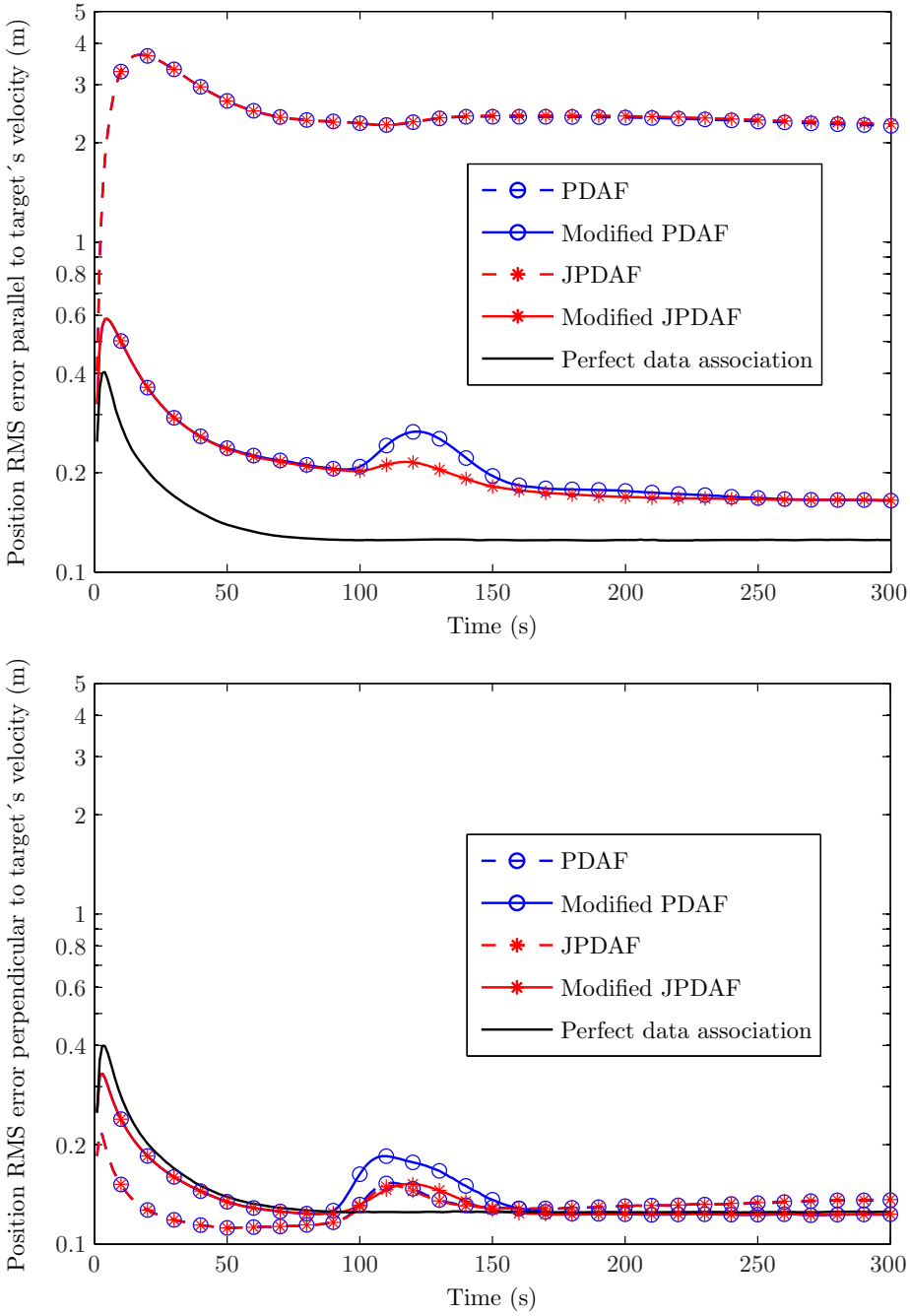


***Figure 7:*** *Position RMS error in the direction parallel and perpendicular to the target's true velocity from 50000 Monte Carlo runs. The trajectory crossing angle is* $\gamma = 15°$.

# 5 Conclusions

An important factor in a multitarget tracking system is to correctly associate each measurement received from a detector to its origin. The JPDAF has been a solution to this problem in many implemented systems due to its effectiveness and low computational demand. In the JPDAF all false measurements are assumed due to i.i.d. uniformly spatially distributed noise or clutter. This assumption is not adequate for targets in the presence of wakes, because detections originating from the wake may result in a lost track if they are not properly accounted for. The solution presented extends this to incorporate a model of the wakes behind the targets in a multitarget environment. The purpose of this wake model is to weight wake-originated measurements lower than in a regular JPDAF to avoid the tracks following these measurements and therefore be forced to turn into the wake. To achieve this, we presented a model formed by the sum of single models each linearly increasing behind their associated targets. Simulations of two crossing targets shows that the wake model presented is a useful modification of the JPDAF, especially when the trajectory crossing angle between the targets is small. The wake model is also necessary for higher trajectory crossing angles, but in these situations it seems to be enough with a modified single target tracking filter (PDAF).

## Appendix A: Specification of the Joint Wake Model

The probability $P_{GW}$ in (25), used to restrict the density of the joint wake model $p_W(z_k)$ to the joint validation region, has to be calculated for each scan by integration of $p_W(z_k)$ inside the region. The joint wake model is the sum of all single wake models $p_W^t(z_k)$ behind each target $t$ under consideration. Hence, the $P_{GW}^t$ has to be calculated for each target and then summed up

$$P_{GW} = \sum_{t=1}^{N_T} P_{GW}^t \quad \text{and} \quad p_W(z_k) = \frac{1}{N_T} \sum_{t=1}^{N_T} p_W^t(z_k) \tag{41}$$

In this section an analytical expression for the integration of a single wake model inside the joint validation region will be derived. Let $\bar{z}$ be the position of the predicted measurement of target $t$ with velocity $v$. The wake model is linear increasing with length $L$ behind the predicted position of the target, i.e., the direction opposite to $v$, and uniform with width $W$ in the direction perpendicular to the target's velocity $v$.

$$p_W^t(z_k) = p_l(l)p_w(w) = \frac{2l}{L^2 W} \tag{42}$$

where

$$p_l(l) = \frac{2l}{L^2} \quad 0 \le l \le L \qquad\qquad p_w(w) = \frac{1}{W} \quad 0 \le w \le \frac{W}{2} \tag{43}$$

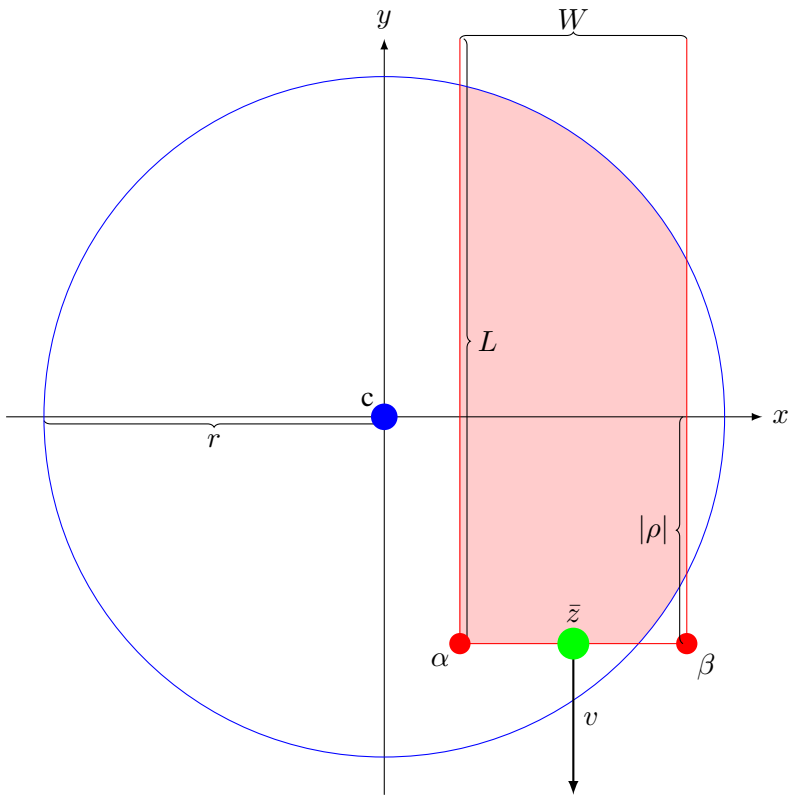


***Figure 8:*** *Specification of variables for integration of the wake model, with length $L$ and width $W$, inside the joint validation region with center $c$ and radius $r$. The wake has front corners $[\alpha\ \rho]$ and $[\beta\ \rho]$ and is oriented behind the target with position $\bar{z}$ and velocity $v$.*

and $l$ and $w$ are the respective distances behind and sideways (relative to $v$) to the target. The joint validation region containing all candidate measurements in the multitarget environment is a circle with radius $r$ and center $c$. Assume a Cartesian coordinate system with origin at position $c$ and $y$-axis parallel to $v$ but in the opposite direction, see Figure 8. Define the two front corners of the wake model with elements $\alpha$ and $\beta$ for the $x$-axis, and $\rho$ for the $y$-axis

$$\begin{aligned} \rho &= (c - \bar{z})^T v/|v| \\ \alpha &= \sqrt{|c - \bar{z}|^2 - \rho^2} - w/2 \\ \beta &= \sqrt{|c - \bar{z}|^2 - \rho^2} + w/2 \end{aligned} \tag{44}$$

The integration depends on if the front corners $[\alpha\ \rho]^T$ and $[\beta\ \rho]^T$ are inside or outside the joint validation region (circle), and will be broken into one, two or three parts. To do

this, define three binary variables $\delta_\rho$, $\delta_\alpha$ and $\delta_\beta$ as follows:

$$\delta_\rho = \begin{cases} 1 & \text{if} \quad \rho < 0 \\ 0 & \text{otherwise} \end{cases} \tag{45}$$

$$\delta_\alpha = \begin{cases} 1 & \text{if} \quad \sqrt{\alpha^2 + \rho^2} > r \\ 0 & \text{otherwise} \end{cases} \tag{46}$$

$$\delta_\beta = \begin{cases} 1 & \text{if} \quad \sqrt{\beta^2 + \rho^2} > r \\ 0 & \text{otherwise} \end{cases} \tag{47}$$

Then the integral can be written as

$$\begin{aligned} P_{GW}^t = & \frac{2}{L^2 W} \Bigg\{ \delta_\rho \delta_\alpha \int_{\max(\alpha,-r)}^{-\sqrt{r^2-\rho^2}} \int_{-\sqrt{r^2-x^2}}^{\sqrt{r^2-x^2}} (y-\rho) \mathrm{d}y \mathrm{d}x \\ & + \int_{\alpha(1-\delta_\alpha)-\delta_\alpha\sqrt{r^2-\rho^2}}^{\beta(1-\delta_\beta)+\delta_\beta\sqrt{r^2-\rho^2}} \int_{\rho}^{\sqrt{r^2-x^2}} (y-\rho) \mathrm{d}y \mathrm{d}x \\ & + \delta_\rho \delta_\beta \int_{\sqrt{r^2-\rho^2}}^{\min(\beta,r)} \int_{-\sqrt{r^2-x^2}}^{\sqrt{r^2-x^2}} (y-\rho) \mathrm{d}y \mathrm{d}x \Bigg\} \end{aligned} \tag{48}$$

For simplicity we substitute the limits of integration along the $x$-axis as follows:

$$\begin{aligned} a &= \max(\alpha, -r) \\ b &= -\sqrt{r^2 - \rho^2} \\ c &= \alpha(1-\delta_\alpha) - \delta_\alpha \sqrt{r^2 - \rho^2} \\ d &= \beta(1-\delta_\beta) + \delta_\beta \sqrt{r^2 - \rho^2} \\ e &= \sqrt{r^2 - \rho^2} \\ f &= \min(\beta, r) \end{aligned} \tag{49}$$

which yields

$$
\begin{aligned}
P_{GW}^{t} =& \frac{2}{L^2 W}\left\{\delta_\rho\delta_\alpha \int_{a}^{b}\int_{-\sqrt{r^2-x^2}}^{\sqrt{r^2-x^2}} (y-\rho)\mathrm{d}y\mathrm{d}x\right. \\
&+ \int_{c}^{d}\int_{\rho}^{\sqrt{r^2-x^2}} (y-\rho)\mathrm{d}y\mathrm{d}x \\
&\left.+ \delta_\rho\delta_\beta \int_{e}^{f}\int_{-\sqrt{r^2-x^2}}^{\sqrt{r^2-x^2}} (y-\rho)\mathrm{d}y\mathrm{d}x\right\} \qquad (50)\\
=& \frac{1}{L^2 W}\left\{\rho r^2\left(\arcsin\frac{c}{r}-\arcsin\frac{d}{r}\right)+\frac{c^3-d^3}{3}\right. \\
&+ 2\rho\delta_\alpha\delta_\rho\left(a\sqrt{r^2-a^2}-b\sqrt{r^2-b^2}\right)-c(\rho^2+r^2) \\
&+ 2\rho\delta_\beta\delta_\rho\left(e\sqrt{r^2-e^2}-f\sqrt{r^2-f^2}\right)+d(\rho^2+r^2) \\
&+ 2\rho\delta_\alpha\delta_\rho r^2\left(\arcsin\frac{a}{r}-\arcsin\frac{b}{r}\right)+\rho c\sqrt{r^2-c^2} \\
&\left.+ 2\rho\delta_\beta\delta_\rho r^2\left(\arcsin\frac{e}{r}-\arcsin\frac{f}{r}\right)-\rho d\sqrt{r^2-d^2}\right\}
\end{aligned}
$$

## References


[1] M. Athans, R. H. Whiting, and M. Gruber, "A suboptimal estimation algorithm with probabilistic editing for false measurements with applications to target tracking with wake phenomena," *IEEE Transactions on Automatic Control*, vol. 22, no. 3, pp. 372–384, June 1977.

[2] Y. Bar-Shalom, "Tracking methods in a multitarget environment," *IEEE Transactions on Automatic Control*, vol. 23, no. 4, pp. 618–626, Aug. 1978.

[3] Y. Bar-Shalom and X. R. Li, *Multitarget-Multisensor Tracking: Principles and Techniques.* Storrs, CT: YBS Publishing, 1995.

[4] Y. Bar-Shalom, X. R. Li, and T. Kirubarajan, *Estimation with Application to Tracking and Navigation.* New York: Wiley-Interscience, 2001.

[5] Y. Bar-Shalom and E. Tse, "Tracking in a cluttered environment with probabilistic data association," *Automatica*, vol. 11, no. 5, pp. 451–460, Sep. 1975.

[6] D. K. Barton, *Modern Radar System Analysis*. Norwood, MA: Artech House, 1988.

[7] E. A. Bloem and H. A. P. Blom, "Joint probabilistic data association methods avoiding track coalescence," in *Proceedings of the 34th IEEE Conference on Decision and Control*, vol. 3, New Orleans, LA, Dec. 1995, pp. 2752–2757.

[8] M. Born and E. Wolf, *Principles of Optics*, 6th ed. London, UK: Pergamon Press, 1980.

[9] T. E. Fortmann, Y. Bar-Shalom, and M. Scheffe, "Multi-target tracking using joint probabilistic data association," in *19th IEEE Conference on Decision and Control including the Symposium on Adaptive Processes*, vol. 19, Dec. 1980, pp. 807–812.

[10] ——, "Sonar tracking of multiple targets using joint probabilistic data association," *IEEE Journal of Oceanic Engineering*, vol. 8, no. 3, pp. 173–184, July 1983.

[11] A. Papoulis and S. U. Pillai, *Probability, Random Variables and Stochastic Processes*, 4th ed. New York: McGraw-Hill, 2002.

[12] A. Rødningsby and Y. Bar-Shalom, "Tracking of divers in a noisy background using a bubble model," in *Proceedings of the SPIE Conference on Signal and Data Processing of Small Targets*, vol. 6699, paper 7, San Diego, CA, Aug. 2007.

[13] W. J. Smith, *Modern Optical Engineering: The Design of Optical Systems*, 2nd ed. New York: McGraw-Hill, 1990.

[14] R. J. Urick, *Principles of Underwater Sound*, 3rd ed. New York: McGraw-Hill, 1983.

# Paper C

## Multitarget Multisensor Tracking in the Presence of Wakes

**Authors:**
Anders Rødningsby, Yaakov Bar-Shalom, Oddvar Hallingstad, and John Glattetre.

Published in *Journal of Advances in Information Fusion*,
pp. 117-145, vol. 4, no. 2, December 2009.

# Multitarget Multisensor Tracking in the Presence of Wakes

Anders Rødningsby[1] Yaakov Bar-Shalom[2] Oddvar Hallingstad[1] John Glattetre[3]

[1]University Graduate Center, NO-2027 Kjeller, Norway
[2]University of Connecticut, U-2157 Storrs, CT, USA
[3]Kongsberg Maritime, NO-3191 Horten, Norway

**Abstract**

In this paper we focus on targets which, in addition to reflecting signals themselves, also have a trailing path behind them, called a wake, which causes additional detections. When the detections are fed to a tracking system like the probabilistic data association filter (PDAF), the estimated track can be misled and sometimes lose the real target because of the wake. This problem becomes even more severe in multitarget environments where targets are operating close to each other in the presence of wakes. To prevent this, we have developed a probabilistic model of the wakes in a multitarget environment. This model is used to augment the joint probabilistic data association filter (JPDAF) for both coupled and decoupled filtering.

This paper provides a systematic comparison of the standard data association filters (PDAF and JPDAF) and their modified versions presented here in a multitarget multisensor environment. Simulations of two targets with wakes in four different scenarios show that this modification gives good results and the probability of lost tracks is significantly reduced. The targets are observed by two sensors and it is shown that tracks estimated in a centralized fusion configuration are better than those from the local sensors. It is also shown that applying the wake model to targets that do not generate a wake, yields almost no deterioration of the tracking performance.

# 1 Introduction

TARGETS in real tracking scenarios may be detected by their reflection of signals emitted from a radar [6], a sonar [26], or by the use of optical sensors [24]. In addition to target-originated measurements there will also be a number of detections due to noise and clutter, called false alarms. A well-known tracking method to handle targets in clutter is the probabilistic data association filter (PDAF) [4, ch. 3.4]. The PDAF accounts for the measurement origin uncertainty by calculating for each validated measurement at the current time the association probabilities to the target of interest.

In a multitarget environment [2] the association of measurements is more problematic because the individual targets no longer can be considered separately as in the PDAF. For this purpose the joint probabilistic data association filter (JPDAF) [4, ch. 6.2], [14] was developed to consider a known number of targets in the data association simultaneously. This method evaluates the measurement-to-target association probabilities for the latest set of measurements and then combines them into the state estimates. In the JPDAF the targets' states, conditioned on the past, are assumed independently distributed so that filtering can be done decoupled. As an alternative, the targets' states, given the past, can be considered as correlated. This leads to the joint probabilistic data association coupled filter (JPDACF) [3], [4, pp. 328-329], where the correlation between the targets' estimation errors is accounted for. A modified version of the JPDACF, called coupled data association filter (CPDA), was presented in [9] to also account for partial target detections. In this paper an equivalent filter to the CPDA, but where the covariance calculation is in symmetrical form (to avoid numerical problems experienced by the CPDA), is modified to also account for targets in the presence of wakes. This filter is called modified JPDACF.

A more powerful source of false measurements than those due to noise and clutter, is the wake phenomenon that appears behind certain targets. This could be air bubbles from a diver, the wake behind a ship, or the wake from ballistic vehicles in the reentry stage. One possible approach to this problem is to handle both the target and the wake behind it as an extended target. A problem with this approach is the varying and unknown size of the wake which may reach far behind the target yielding a large bias. In this paper the wake is not considered as part of the target, but rather as a special kind of clutter. When these measurements are fed to the tracking system, it becomes important to associate them correctly to prevent a lost track. In [1] a probabilistic editing method is used to handle the wake-dominated measurements in the tracking algorithm. This probabilistic editing method is based on a single measurement extracted for each time step, and that this measurement originates from either the target or the wake. In [21] a modified PDAF is developed to handle false measurements originating from the bubbles behind a diver (the wake). This modified single target tracking method does not restrict the number of false measurements for each time step, but assumes a set of measurements where each false measurement originates from either random clutter or the wake. In this paper we extend the modified PDAF to handle multiple targets in the presence of wakes.

A probabilistic wake model is used for each target in the multitarget environment that has a wake behind it. These single wake models are combined to form a joint wake model, and the modified JPDAF and JPDACF are developed to incorporate this additional joint wake model.

In recent years there has been an extensive interest in using multiple sensors in surveillance systems. This leads to data fusion where there exist several possible configurations [4, ch. 8.2]. Primarily due to the bandwidth constraints in real systems, it is sometimes not feasible to transmit all measurement information to a fusion center (centralized configuration). Instead, only local estimates are transmitted to a fusion center (at a reduced rate), and a track-to-track association followed by track fusion is carried out (decentralized configuration). However, the best performance is achieved using the centralized configurations where all measurements are transmitted from the local sensors to a fusion center. In this paper we use the centralized configuration with sequential filtering [4, p. 88] where the global estimate is updated by the measurements from each local sensor, one sensor at the time.

In Section 2 the tracking problem in the presence of a wake is reviewed for a single target. In Section 3 the modified JPDAF is developed for a multitarget environment, and the modified version of the JPDACF, which accounts for partial target detections, is derived. In Section 4 a brief review of multisensor tracking is given. The data association methods are then compared in Section 5 by simulations of two targets with wakes in four different multisensor scenarios, before conclusions are given in Section 6.

# 2 Background

## 2.1 Model of Tracking

The standard discrete linear model in tracking is

$$x_{k+1} = Fx_k + v_k \qquad z_k = Hx_k + w_k \tag{1}$$

where

| | | | |
|---|---|---|---|
| $x$ : | target state | $F$ : | transition matrix |
| $z$ : | measurement | $H$ : | measurement matrix |
| $v$ : | process noise | $w$ : | measurement noise |
| $k$ : | time index | | |

The process and measurement noises are assumed independent, white and Gaussian with covariance matrices

$$E\{v_k v_k^T\} = Q \qquad \text{and} \qquad E\{w_k w_k^T\} = R \tag{2}$$

For this system, a Kalman filter is optimal as long as the measurement $z_k$ originates from the target at each time $k$. In many real world problems this is unfortunately not true due to the presence of false measurements originating from noise and clutter. Instead, a set

of $m_k$ measurements $Z_k = \{z_k(1), z_k(2), \ldots, z_k(m_k)\}$ is available at time $k$ so that data association is needed. A simple and efficient method to solve this problem is the PDAF.

## 2.2 Standard PDAF

The approach of the PDAF is to calculate the association probabilities for each validated measurement (that falls in a gate around the predicted measurement) at the current time to the target of interest. The posterior track probability density is therefore a mixture of Gaussian probability density functions (pdf), but is then forced back to Gaussianity by moment-matching for the succeeding scan. For a derivation of the PDAF see [4, ch. 3.4], and in the following a brief overview of the PDAF will be given.

Assume that the target state at time $k-1$ is estimated as $\hat{x}_{k-1|k-1}$ with associated covariance $P_{k-1|k-1}$. This means that the estimate is conditioned on the entire past up to time $k-1$. Then the following assumptions are made:

(a) The track is already initialized.

(b) The past information about the target is summarized approximately by the Gaussian pdf

$$p\left(x_k|Z^{k-1}\right) \approx \mathcal{N}\left(x_k; \hat{x}_{k|k-1}, P_{k|k-1}\right) \tag{3}$$

where

$$Z^{k-1} = \{Z_0, Z_1, \ldots Z_{k-1}\} \tag{4}$$

(c) A validation region or gate is set up for each time step to select the candidate measurements for association.

(d) At time $k$ there are $m_k$ validated measurements but at most one of them can be target-originated. The rest are assumed to be due to i.i.d. uniformly spatially distributed false alarms, independently across time.

(e) Detections of the real target occur independently over time with known detection probability $P_D$.

At each time $k$, the algorithm goes through the following steps:

1. Predict the target state, associated covariance and measurement at time $k$ based on the estimates at $k-1$:

$$\begin{aligned} \hat{x}_{k|k-1} &= F\hat{x}_{k-1|k-1} \\ P_{k|k-1} &= FP_{k-1|k-1}F^T + Q \\ \hat{z}_{k|k-1} &= H\hat{x}_{k|k-1} \end{aligned} \tag{5}$$

2. Compute the innovation covariance for the true (target-originated) measurement

$$S_k = HP_{k|k-1}H^T + R \tag{6}$$

and use $S_k$ to form the measurement validation gate where the validated measurements $Z_k$ result in $m_k$ innovations:

$$\nu_k(i) = z_k(i) - \hat{z}_{k|k-1} \qquad i = 1, \ldots, m_k \tag{7}$$

3. Calculate the association probabilities $\beta_k(i)$, $i = 1 \ \ldots \ m_k$ that measurement $z_k(i)$ originates from the true target, and $\beta_k(0)$ as the probability that all measurements are false alarms

$$\beta_k(i) = \begin{cases} ce^{-\frac{1}{2}\nu_k(i)^T S_k^{-1}\nu_k(i)} & i = 1, \ldots, m_k \\ c\,|2\pi S_k|^{\frac{1}{2}}\, m_k \frac{1-P_G P_D}{V_k P_D} & i = 0 \end{cases} \tag{8}$$

Here $c$ is a normalizing constant to ensure that $\sum_{i=0}^{m_k} \beta_k(i) = 1$, $V_k$ is the volume of the gate and $P_G$ is the probability that the true measurement falls inside the gate. In (8) a diffuse prior [4, p. 135] is used for the point mass function (pmf) of the number of false measurements in the validation region.

4. Calculate the Kalman gain and the combined innovation

$$W_k = P_{k|k-1}H^T S_k^{-1} \quad \text{and} \quad \nu_k = \sum_{i=1}^{m_k} \beta_k(i)\nu_k(i) \tag{9}$$

to update the track according to

$$\hat{x}_{k|k} = \hat{x}_{k|k-1} + W_k\nu_k \tag{10}$$

5. The state estimation covariance is updated by

$$\begin{aligned} P_{k|k} =& \beta_k(0)P_{k|k-1} + [1 - \beta_k(0)]\left(P_{k|k-1} - W_k S_k W_k^T\right) \\ &+ W_k \left[\sum_{i=0}^{m_k} \beta_k(i)\nu_k(i)\nu_k(i)^T - \nu_k\nu_k^T\right] W_k^T \end{aligned} \tag{11}$$

where the last term in (11) is the "spread of the innovations."

## 2.3 Modified PDAF

Targets with a wake behind them may cause detections from the wake that mislead the tracking algorithm and are likely to result in a lost track. This is because the uniform distribution assumption for the false measurements (assumption (d) in Section 2.2) is

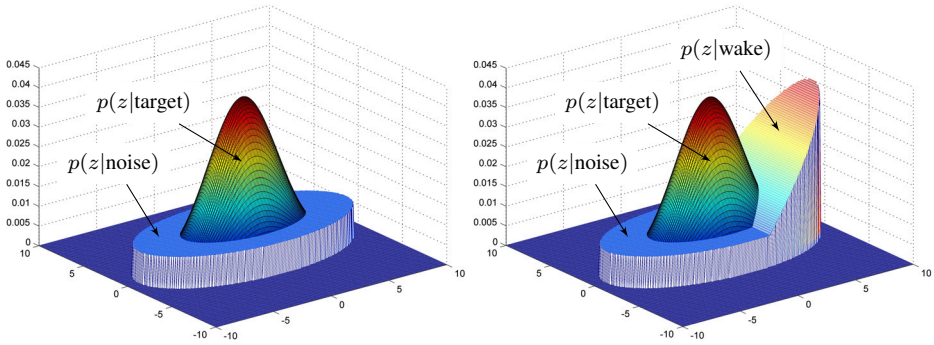


(a) Regular PDAF (b) Modified PDAF with wake model

***Figure 1:*** *Illustration of the pdfs for the measurements originating from the target, noise or wake in: (a) regular PDAF, and (b) modified PDAF with special wake model.*

violated. To prevent this, an extension of the regular PDAF incorporating a special probabilistic model of the wake was developed in [21]. The PDAF with the wake model is illustrated in Figure 1. The modified PDAF takes into account that the false measurements can originate from either the wake with pdf $p_W(\cdot)$ with a priori probability $P_W$, or from i.i.d. uniformly distributed noise/clutter with a priori probability $1 - P_W$, independently across time. This modification affects the PDA in the calculation of the $\beta_k(i)$ in (8) and yields

$$\beta_k(i) = \begin{cases} c\dfrac{e^{-\frac{1}{2}\nu_k(i)^T S_k^{-1}\nu_k(i)}}{V_k\left[\frac{1-P_W}{V_k}+\frac{P_W}{P_{GW}}p_W(z_k(i))\right]} & i = 1,\ldots,m_k \\ c\,|2\pi S_k|^{\frac{1}{2}}\, m_k \dfrac{1-P_G P_D}{V_k P_D} & i = 0 \end{cases} \tag{12}$$

The bracketed parenthesis in the denominator in $\beta_k(i)$ for $i = 1,\ldots,m_k$ is the pdf of a false measurement

$$p(z_k(i)|\text{measurement } i \text{ is false}) = \frac{1-P_W}{V_k} + \frac{P_W}{P_{GW}}p_W(z_k(i)) \tag{13}$$

where $P_{GW}$ is used to account for restricting the density of the wake model $p_W(z_k(i))$ to the validation gate. The calculation of $P_{GW}$ for a linear $p_W(\cdot)$ is presented in detail in [21]. As expected, in the limit as $P_W$ goes to zero, (12) becomes (8).

## 2.4 Track Formation and Termination

The data association filters discussed above assume that the track is already initialized, and when a track is established, there are no included rules for how to terminate the track.

Hence, procedures for formation and termination of tracks are necessary. A simple and common method to initialize tracks is the two-point differencing method [5, p. 247]. Any successive pair of detections within a maximum distance based on target maximum motion parameters and measurement noise variances initiates a preliminary track. This preliminary track, containing the initial state and the corresponding covariance, can now initialize the PDAF. To reduce the amount of false tracks, a "$p/q$" logic-based track formation procedure can be used. In this procedure a preliminary track has to receive measurements for a minimum of $p$ time steps during the first $q$ scans to become valid.

To terminate a track a logic suitable for the application is needed, and a set of rules has to be made. The rules used in this paper, called termination events, are described in Section 5.4. It should also be noted that in some filters, such as the integrated probabilistic data association filter (IPDAF) [18] or the version of the interacting multiple model probabilistic data association filter (IMMPDAF) presented in [4, ch. 4.4], the track formation and termination are included.

# 3 Probabilistic Data Association for Multiple Targets in the Presence of Wakes

In a multitarget environment the data association algorithm needs to handle situations where a measurement could originate from different targets. For this purpose, the JPDAF was developed, and a derivation of this standard algorithm is given in [4, ch. 6.2]. Another problem arises when these targets have wakes behind them that result in misleading wake detections. In this section we will modify the JPDAF to handle this problem.

## 3.1 Assumptions

Assume there is a known number $N_T$ of established targets at time $k-1$. Notice that these targets are already initialized, e.g., by the method in Section 2.2. For each target $t$, where $t = 1, \ldots, N_T$, the target state is estimated as $\hat{x}^t_{k-1|k-1}$ with associated covariance $P^t_{k-1|k-1}$. Then the following assumptions are made:

(a) Measurements from one target can fall in the validation gate of a neighboring target.

(b) The past information about target $t$ is summarized approximately by the Gaussian pdf

$$p\left(x^t_k | Z^{k-1}\right) \approx \mathcal{N}\left(x^t_k; \hat{x}^t_{k|k-1}, P^t_{k|k-1}\right) \tag{14}$$

(c) At time $k$ there are $m_k$ validated measurements in the union of their validation gates, but for each target $t$ at most one measurement can be target-originated. The rest are assumed to be due to the wakes with pdf $p_W(\cdot)$ with a priori probability $P_W$, or from i.i.d. uniformly distributed noise/clutter with a priori probability $1 - P_W$, independently across time.

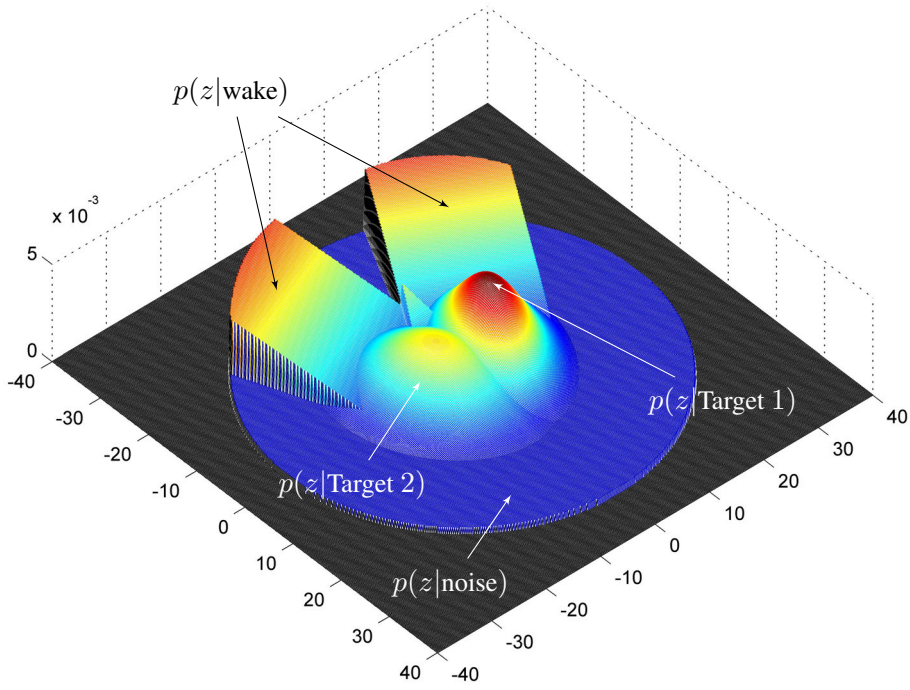


***Figure 2:*** *Probability density functions for two targets with crossing trajectories. The distributions of the targets are Gaussian and overlap each other. Each wake behind the two targets is modeled as a pdf, linearly increasing from the target and backwards, and the sum of each single target's wake model forms the joint wake model. The noise/clutter is uniformly spatially distributed inside the joint validation region.*

In Figure 2 an example of the pdfs for two targets that are starting to cross each other is shown. Here both targets have a wake behind them, and the joint wake model (the sum of each target's single wake model) increases linearly behind the targets inside the joint validation region. The joint validation region contains all the candidate measurements, and restricts the spatially uniform distribution representing the noise/clutter. It should be noted that the linearly increasing wake models are not developed to approach the true density of the wake since the wake density would seemingly be higher close to the targets rather than farther away. Such an approach would easily misassociate true target-originated measurements as wake-originated ones. At the same time, in practice, a false wake-originated measurement is less detrimental when it is very close to the true target than farther behind. The adopted wake model is therefore a pragmatic approach to let the probability of having a wake-originated measurement instead of a target-originated one increase with the distance behind the true target. Further details about the joint wake model and the validation region are given in Appendix A.

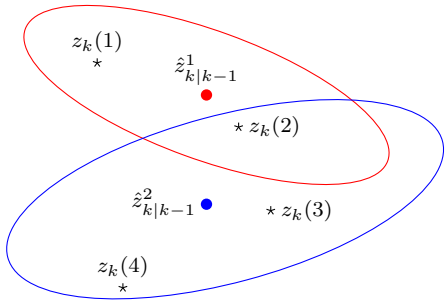


$$\Omega = \begin{array}{c|ccc} j\backslash t & 0 & 1 & 2 \\ \hline 1 & 1 & 1 & 0 \\ 2 & 1 & 1 & 1 \\ 3 & 1 & 0 & 1 \\ 4 & 1 & 0 & 1 \end{array}$$

***Figure 3:*** *Two targets with a measurement in the intersection of their validation gates are shown with corresponding validation matrix $\Omega$.*

## 3.2 Joint Association Events

Define the validation matrix $\Omega$ to represent all feasible association events at time $k$ (the time index $k$ is omitted for simplicity where it does not cause confusion)

$$\Omega = [\omega(j,t)] \qquad j = 1,\ldots,m \quad \text{and} \quad t = 0,\ldots,N_T \tag{15}$$

Here, $\omega(j,t)$ is a binary element indicating whether measurement $j$ lies in the validation gate of target $t$. The index $t = 0$ means that the measurement is from none of the targets and therefore it is a false measurement. An example where a measurement may originate from either of two targets, i.e., it lies in both targets' validation gates, is shown with the corresponding validation matrix $\Omega$ in Figure 3. For all these possible joint association events, conditional probabilities have to be derived.

A joint association event $\Theta$ describes an unambiguous association between the measurements and the targets at time $k$

$$\Theta = \bigcap_{j=1}^{m} \theta(j,t_j) \tag{16}$$

where

- $\theta(j,t_j)$ is the event that measurement $j$ originates from target $t_j$.
- $t_j$ is the index of the target to which measurement $j$ is associated in the event under consideration.

The event $\Theta$ can also be represented by the matrix

$$\Omega_\Theta = [\omega_\Theta(j,t)] \tag{17}$$

consisting of the units in $\Omega$ corresponding to the associations in $\Theta$

$$\omega_\Theta(j,t) = \begin{cases} 1 & \text{if the event } \theta(j,t) \text{ is part of } \Theta \\ 0 & \text{otherwise} \end{cases} \tag{18}$$

Using this, a feasible association event needs to fulfill the following requirements:

1. A measurement can have only one source, i.e.

$$\sum_{t=0}^{N_T} \omega_\Theta(j,t) = 1 \qquad \forall \quad j \tag{19}$$

2. At most one measurement can originate from a target

$$\delta_\Theta^t \triangleq \sum_{j=1}^{m} \omega_\Theta(j,t) \leqslant 1 \qquad t = 1, \ldots, N_T \tag{20}$$

The binary variable $\delta_\Theta^t$ is called the target detection indicator since it indicates whether a measurement is associated to a target $t$ or not in event $\Theta$. It is also convenient to define two more binary variables

$$\tau_\Theta(j) \triangleq \sum_{t=1}^{N_T} \omega_\Theta(j,t) \tag{21}$$

$$\phi_\Theta \triangleq \sum_{j=1}^{m} [1 - \tau_\Theta(j)] \tag{22}$$

where $\tau_\Theta(j)$ is the measurement association indicator to indicate if measurement $j$ is associated to a target or not, and $\phi_\Theta$ is the number of false (unassociated) measurements in event $\Theta$.

### 3.3 Modified JPDAF with a Wake Model

The joint association event probabilities are derived using Bayes' formula

$$\begin{aligned} P\{\Theta_k|Z^k\} &= P\{\Theta_k|Z_k, m_k, Z^{k-1}\} \\ &= \frac{1}{c} p\left(Z_k|\Theta_k, m_k, Z^{k-1}\right) P\{\Theta_k|Z^{k-1}, m_k\} \\ &= \frac{1}{c} p\left(Z_k|\Theta_k, m_k, Z^{k-1}\right) P\{\Theta_k|m_k\} \end{aligned} \tag{23}$$

where $c$ is a normalizing constant. In the last line of the above equation the irrelevant conditioning term $Z^{k-1}$ has been omitted. The pdf of the measurements in (23) is derived by assuming that the states of the targets, conditioned on the past observations, are mutually independent

$$p\left(Z_k|\Theta_k, m_k, Z^{k-1}\right) = \prod_{j=1}^{m_k} p\left(z_k(j)|\theta_k(j,t_j), Z^{k-1}\right) \tag{24}$$

Measurements not associated to a target are assumed either from the wakes with pdf $p_W(z_k(j))$ with a priori probability $P_W$, or from uniformly distributed noise/clutter with a priori probability $(1 - P_W)$. Defining $V_k$ as the volume of the joint validation gate, the pdf of a measurement given its origin is

$$p\left(z_k(j)|\theta_k(j,t_j), Z^{k-1}\right) = \begin{cases} \mathcal{N}\left(z_k(j); \hat{z}^{t_j}_{k|k-1}, S^{t_j}_k\right) & \text{if} \quad \tau_{\Theta_k}(j) = 1 \\ P_W \frac{p_W(z_k(j))}{P_{GW}} + (1 - P_W)\frac{1}{V_k} & \text{if} \quad \tau_{\Theta_k}(j) = 0 \end{cases} \tag{25}$$

where $\hat{z}^{t_j}_{k|k-1}$ is the predicted measurement for target $t_j$ with associated innovation covariance $S^{t_j}_k$. The constant $P_{GW}$ is used for restricting $p_W(z_k(j))$ to the joint validation region, and has an analytical expression derived in Appendix A. Using the above equation, (24) can be written as

$$\begin{aligned} p\left(Z_k|\Theta_k, m_k, Z^{k-1}\right) = &\prod_{j=1}^{m_k} \left\{\mathcal{N}\left(z_k(j); \hat{z}^{t_j}_{k|k-1}, S^{t_j}_k\right)\right\}^{\tau_\Theta(j)} \\ &\times \left\{P_W \frac{p_W(z_k(j))}{P_{GW}} + (1 - P_W)\frac{1}{V_k}\right\}^{1-\tau_\Theta(j)} \end{aligned} \tag{26}$$

Next, the last term in (23) will be derived. Let $\delta_\Theta$ be the vector of detection indicators corresponding to event $\Theta_k$

$$\delta_\Theta = [\delta^1_\Theta, \ldots, \delta^{N_T}_\Theta] \tag{27}$$

The vector $\delta_\Theta$ and the number of false measurements $\phi_\Theta$ follow from the event $\Theta$ under consideration. Using the definition of conditional probabilities [20, p. 28], this yields

$$P\{\Theta_k|m_k\} = P\{\Theta_k, \delta_\Theta, \phi_\Theta|m_k\} = P\{\Theta_k|\delta_\Theta, \phi_\Theta, m_k\}P\{\delta_\Theta, \phi_\Theta|m_k\} \tag{28}$$

The first term in (28) is obtained using combinatorics:

1. In event $\Theta_k$ there are assumed $m_k - \phi_\Theta$ targets detected.
2. The number of events $\Theta_k$, where the same targets are detected, is given by the number of ways of associating $m_k - \phi_\Theta$ measurements to the detected targets from a set of $m_k$ measurements.

By assuming each such event a priori equally likely, one has

$$P\{\Theta_k|\delta_\Theta, \phi_\Theta, m_k\} = \frac{1}{{}_{m_k}P_{m_k-\phi_\Theta}} = \frac{\phi_\Theta!}{m_k!} \tag{29}$$

The last term in (28) is, assuming $\delta$ and $\phi$ independent,

$$P\{\delta_\Theta, \phi_\Theta|m_k\} = \prod_{t=1}^{N_T} (P^t_D)^{\delta^t_\Theta}(1 - P^t_D)^{1-\delta^t_\Theta}\mu_F(\phi_\Theta) \tag{30}$$

where $P_D^t$ is the detection probability of target $t$ and $\mu_F(\phi_\Theta)$ is the prior pmf of the number of false measurements. The indicators $\delta_\Theta^t$ have been used to select the probabilities of detection and no detection events according to the event $\Theta_k$ under consideration. Combining (29) and (30) into (28) yields the prior probability of a joint association event

$$P\{\Theta_k|m_k\} = \frac{\phi_\Theta!}{m_k!}\prod_{t=1}^{N_T}(P_D^t)^{\delta_\Theta^t}(1-P_D^t)^{1-\delta_\Theta^t}\mu_F(\phi_\Theta) \tag{31}$$

The pmf of the number of false measurements $\mu_F(\phi)$ can, as in the case of the PDA, have two versions, parametric or nonparametric.

1. Parametric JPDA uses a Poisson pmf

$$\mu_F(\phi) = e^{-\lambda V}\frac{(\lambda V)^\phi}{\phi!} \tag{32}$$

   which requires the spatial density $\lambda$ of the false measurements.

2. Nonparametric JPDA uses a diffuse prior

$$\mu_F(\phi) = \epsilon \qquad \forall\phi \tag{33}$$

   which does not require the parameter $\lambda$.

Using the nonparametric model and combining (31) and (26) into (23) yields the joint association event probabilities

$$\begin{aligned} P\{\Theta_k|Z^k\} =& \frac{\phi_\Theta!}{c}\prod_{t=1}^{N_T}(P_D^t)^{\delta_\Theta^t}(1-P_D^t)^{1-\delta_\Theta^t} \\ &\times \prod_{j=1}^{m_k}\left\{\mathcal{N}\left(z_k(j);\hat{z}_{k|k-1}^{t_j}, S_k^{t_j}\right)\right\}^{\tau_\Theta(j)} \\ &\times \left\{P_W\frac{p_W(z_k(j))}{P_{GW}} + (1-P_W)\frac{1}{V_k}\right\}^{1-\tau_\Theta(j)} \end{aligned} \tag{34}$$

where the constants $\epsilon$ and $m_k!$ are brought into the normalization constant $c$. For comparison, the joint association event probabilities derived in [4, p. 318] for the standard JPDAF is

$$P\{\Theta_k|Z^k\} = \frac{\phi_\Theta!\cdot V_k^{-\phi_\Theta}}{c}\prod_{t=1}^{N_T}(P_D^t)^{\delta_\Theta^t}(1-P_D^t)^{1-\delta_\Theta^t}\prod_{j=1}^{m_k}\left\{\mathcal{N}\left(z_k(j);\hat{z}_{k|k-1}^{t_j}, S_k^{t_j}\right)\right\}^{\tau_\Theta(j)} \tag{35}$$

where the third line in (34) is replaced by $V_k^{-\phi_\Theta}$. As for the modified PDAF, (34) reduces to (35) in the limit as $P_W$ goes to zero. Finally, marginal association probabilities are

obtained by summing over all the joint association events in which the marginal event of interest occurs

$$\beta_k^t(j) \triangleq P\{\theta_k(j,t)|Z^k\} = \sum_{\Theta_k} P\{\Theta_k|Z^k\}\omega_\Theta(j,t) \tag{36}$$

$$\beta_k^t(0) \triangleq 1 - \sum_{j=1}^{m_k} \beta_k^t(j) \tag{37}$$

By using these association probabilities in (8), the state estimation equations are exactly the same as in the PDAF, (5) - (11).

### 3.4 Modified JPDACF

The state estimation above is based on the assumption that the targets, conditioned on the past observations, are mutually independent. When measurements are inside the validation gates for two or more targets at the same time, we say that the targets are "sharing" measurements. For targets that share measurements for several sampling times, a dependence of their estimation error ensues, and this can be taken into account by calculating the resulting error correlations [7]. The resulting JPDACF algorithm [4, pp. 328-329] does the filtering in a coupled manner, yielding a covariance matrix with cross-covariances that reflect the correlation between the targets' state estimation errors. The effectiveness of the JPDACF approach in combination with the IMM was demonstrated on splitting targets in [3]. This JPDACF approach does not account for situations with partial target detections since the association events where all targets are detected are not separated from events where only some of them are detected. The association events need to be separated in groups where the group member events have the same vector of detection indicators $\delta_\Theta$, see (27). This situation was accounted for in the CPDA filter, derived in [9], where the CPDA in combination with hypothesis pruning was developed to avoid track coalescence. In our simulations, however, the CPDA approach did lead to numerical problems in the covariance calculations. An equivalent solution to the CPDA, but where the covariance calculation is in a symmetrical form, is therefore developed and used in this paper to avoid numerical problems. The modified JPDACF accounting for partial target detections and the presence of wakes, is derived next.

Assuming only two targets, the stacked state vector and its associated covariance are denoted as

$$\hat{x}_{k|k-1}^S = \begin{bmatrix} \hat{x}_{k|k-1}^1 \\ \hat{x}_{k|k-1}^2 \end{bmatrix} \quad \text{and} \quad P_{k|k-1}^S = \begin{bmatrix} P_{k|k-1}^1 & P_{k|k-1}^{12} \\ P_{k|k-1}^{21} & P_{k|k-1}^2 \end{bmatrix} \tag{38}$$

where $P_{k|k-1}^{12}$ is the cross-covariance between target 1 and 2. This cross-covariance will be zero before these targets become coupled, i.e., start to share measurements. The

updated state estimate is

$$\hat{x}^S_{k|k} = \hat{x}^S_{k|k-1} + \sum_{\Theta_k} P\{\Theta_k|Z^k\} I^x_\Theta W^S_k I^z_\Theta \nu^S_k(\Theta) \tag{39}$$

where

$$\nu^S_k(\Theta) = z^S_k(\Theta) - \hat{z}^S_{k|k-1} \tag{40}$$

$$z^S_k(\Theta) = \begin{bmatrix} z_k(j_1(\Theta)) \\ z_k(j_2(\Theta)) \end{bmatrix} \tag{41}$$

$$\hat{z}^S_{k|k-1} = H^S \hat{x}^S_{k|k-1} \tag{42}$$

and $j_t(\Theta_k)$ is the index of the measurement associated with target $t$ in the event $\Theta_k$ at time $k$. The filter gain in (39) is

$$W^S_k = P^S_{k|k-1} H^{S^T} \left[ H^S P^S_{k|k-1} H^{S^T} + R^S \right]^{-1} \tag{43}$$

where

$$H^S = \begin{bmatrix} H^1 & 0 \\ 0 & H^2 \end{bmatrix} \quad \text{and} \quad R^S = \begin{bmatrix} R^1 & 0 \\ 0 & R^2 \end{bmatrix} \tag{44}$$

The matrices $I^x_\Theta$ and $I^z_\Theta$ in (39) are used to choose only the innovation from the target(s) that are detected, given by the detection indicator in (20), such that

$$I^x_\Theta = \begin{bmatrix} \delta^1_\Theta I_{n_x} & 0 \\ 0 & \delta^2_\Theta I_{n_x} \end{bmatrix} \qquad I^z_\Theta = \begin{bmatrix} \delta^1_\Theta I_{n_z} & 0 \\ 0 & \delta^2_\Theta I_{n_z} \end{bmatrix} \tag{45}$$

Here, $I_{n_x}$ and $I_{n_z}$ are $n_x \times n_x$ and $n_z \times n_z$ identity matrices, where $n_x$ and $n_z$ are the dimensions of a single target state vector and a single target measurement, respectively. Notice that if a target is undetected in the joint association event $\Theta_k$ under consideration, the corresponding part of the innovation vector needs to be set to zero even though $I^x_\Theta$ is multiplied to the Kalman gain $W^S_k$. This is accomplished by $I^z_\Theta$.

The updated stacked covariance $P^S_{k|k}$, conditioned on all measurements up to time $k$, $Z^k$, is derived in Appendix B and yields

$$\begin{aligned} P^S_{k|k} = & \sum_{\Theta_k} P\{\Theta_k|Z^k\} \\ & \times \left\{ I^x_\Theta W^S_k I^z_\Theta \left( \nu^S_k(\Theta) \nu^S_k(\Theta)^T + R^S \right) I^z_\Theta W^{S^T}_k I^x_\Theta \right. \\ & \left. + \left( I - I^x_\Theta W^S_k I^z_\Theta H^S \right) P^S_{k|k-1} \left( I - I^x_\Theta W^S_k I^z_\Theta H^S \right)^T \right\} \\ & - \left( \sum_{\Theta_k} P\{\Theta_k|Z^k\} I^x_\Theta W^S_k I^z_\Theta \nu^S_k(\Theta) \right) \\ & \times \left( \sum_{\Theta_k} P\{\Theta_k|Z^k\} I^x_\Theta W^S_k I^z_\Theta \nu^S_k(\Theta) \right)^T \end{aligned} \tag{46}$$

The joint association event probabilities $P\{\Theta_k|Z^k\}$ are calculated as for the decoupled filter in Section 3.3, and the prediction step is as in (5), but with stacked state and covariance.

## 4 Multisensor Tracking

The best performance in multisensor data fusion is achieved using centralized configurations where all measurements are transmitted from the local sensors to a fusion center.[1] Primarily due to the bandwidth constraints in real systems, the centralized configuration is sometimes not feasible because its requirement to transmit all measurement information to a fusion center. This is the motivation for the interest in decentralized tracking, with track-to-track association followed by track fusion, which has been compared to centralized tracking in [10], [11]. To make the centralized tracking more feasible for real systems, the measurement data can be compressed in the local sensors before they are transmitted [12]. When the measurements are transmitted to a fusion center in the centralized tracking, there are two different schemes for the way the state is updated. In parallel filtering the measurements from all sensors (if synchronized) are taken into account at the same time. The other alternative is sequential filtering where measurements from each sensor is processed one sensor at a time. The first sensor updates the state (and covariance) based on predictions from the previous time step as in a single-sensor algorithm. Then, this new updated state is used as a zero-time prediction to update with the measurements from the second sensor and so on. In [19] the sequential and parallel filtering schemes are compared in a multisensor JPDAF approach, and it is shown that sequential filtering is less computationally expensive as the number of sensors increases. According to [19], the sequential method yields better tracking performance on the average when data association is needed. This is primarily due to the fact that better filtered estimates are available after processing each sensor's data.

Another problem regarding multisensor systems is the positioning of the sensors, where there are several aspects to consider:

- The sensors' joint ability to cover the required area.
- The sensor specifications.
- The most likely target locations and trajectories.
- The possibility of tracking the targets from various view angles.

These factors, among others, have to be considered separately and in light of the main purpose of each specific tracking problem.

[1] It is assumed that the sensors are properly registered and have no biases.

# 5 Simulations and Results

In this section the data association methods described previously (PDAF, Modified PDAF, JPDAF, Modified JPDAF and Modified JPDACF) are compared in four different multitarget simulation scenarios in the presence of wakes. These simulations consider an underwater surveillance system with active sonar sensors and scuba divers as the targets. The wakes are generated by the air bubbles from the divers. Results are shown using two sensors, working both as independent single sensors and together in a centralized tracking system. When the filters discussed above are used in multisensor (MS) situations in the centralized tracking configuration, they will be denoted as MSPDAF, Modified MSPDAF, MSJPDAF, Modified MSJPDAF and Modified MSJPDACF.

## 5.1 Simulation Scenarios

The four simulation scenarios are shown in Figure 4, and are in the sequel denoted as:

1. Crossing scenario:
   The targets are starting in positions $(25, 32.5)\,\mathrm{m}$ and $(25, 67.5)\,\mathrm{m}$ with speed $1\,\mathrm{m/s}$ and course according to the trajectory crossing angle $\gamma = 20°$, see Figure 4. The nearly straight trajectories are crossing the $200\,\mathrm{s}$ run midway. In [22] a similar scenario with varying trajectory crossing angle $\gamma = [5°, 6°, \ldots, 30°]$ is simulated for a single sensor, showing significant reduction of track loss for the modified filters.

2. Parallel scenario:
   The targets are starting in positions $(25, 40)\,\mathrm{m}$ and $(25, 60)\,\mathrm{m}$ with speed $1\,\mathrm{m/s}$ and course according to the trajectory crossing angle $\gamma = 15°$. When the distance between the targets is less than $3\,\mathrm{m}$, their velocities are both set to $[1, 0]\,\mathrm{m/s}$, creating parallel trajectories with $3\,\mathrm{m}$ spacing. Then, after $130\,\mathrm{s}$ they separate in the same way as they joined each other.

3. Sequential scenario:
   The targets are starting in positions $(22.5, 40)\,\mathrm{m}$ and $(27.5, 60)\,\mathrm{m}$ with speed $1\,\mathrm{m/s}$ and course according to the trajectory crossing angle $\gamma = 15°$. When the distance between the targets is less than $0.5\,\mathrm{m}$ in the $y$-direction their velocities are both set to $[1, 0]\,\mathrm{m/s}$. Since the first target started $5\,\mathrm{m}$ behind the second target in the $x$-direction, they will now move after each other in the same direction with about $5\,\mathrm{m}$ spacing. Then, after $130\,\mathrm{s}$ they separate in the same way as they joined each other. Note that Target 1 is moving inside the wake created by Target 2 before they separate.

4. Meeting scenario:
   The targets are starting in positions $(25, 50)\,\mathrm{m}$ and $(225, 50)\,\mathrm{m}$ with speed $1\,\mathrm{m/s}$ and course directly towards each other. The targets are passing each other without changing course. Note that both targets are moving inside the wake of the other one after the passing.

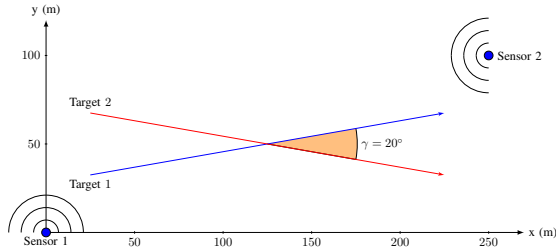


(a) Scenario 1: Crossing trajectories with trajectory crossing angle $\gamma = 20°$

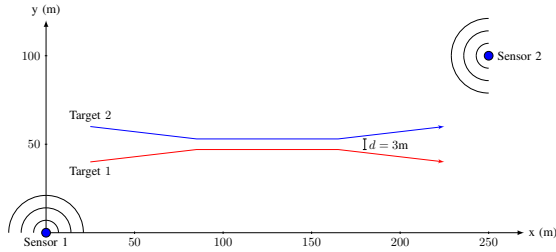


(b) Scenario 2: Parallel trajectories with spacing $d = 3\,\mathrm{m}$

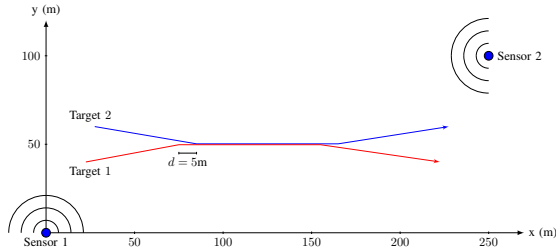


(c) Scenario 3: Sequential trajectories with spacing $d = 5\,\mathrm{m}$

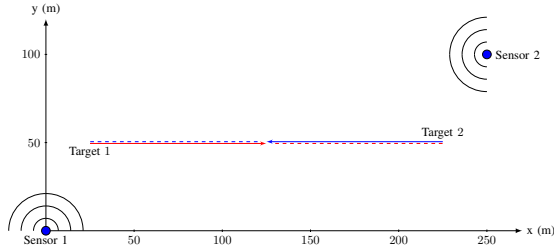


(d) Scenario 4: Meeting trajectories

***Figure 4:*** *Simulation scenarios of two targets observed by two sensors. Four different scenarios are shown: (a) Crossing trajectories with trajectory crossing angle $\gamma = 20°$; (b) Parallel trajectories where the targets are moving side by side with spacing $d = 3\,\mathrm{m}$; (c) Sequential trajectories where Target 1 is moving behind in the wake created by Target 2, with spacing $d = 5\,\mathrm{m}$; and (d) Meeting trajectories where the targets are moving towards each other, and passing each other inside the wake of the other target.*

## 5.2 Simulation Setup

Two sensors, with the same specifications, are located in the positions $(0, 0)$ m and $(250, 100)$ m respectively. The sensors have $180^\circ$ field of view with resolution about $0.7^\circ$ in bearing (256 non-overlapping beams) and $0.2$ m in range. Their maximum range of 250 m is assumed large enough to cover the targets throughout the 200 s long runs, consisting of 200 scans with sampling period $T = 1$ s. For both targets a two-dimensional direct discrete time nearly constant velocity model [5] is used in (1) and (2):

$$F = \begin{bmatrix} 1 & T & 0 & 0 \\ 0 & 1 & 0 & 0 \\ 0 & 0 & 1 & T \\ 0 & 0 & 0 & 1 \end{bmatrix} \qquad H = \begin{bmatrix} 1 & 0 & 0 & 0 \\ 0 & 0 & 1 & 0 \end{bmatrix} \tag{47}$$

$$R_c = \begin{bmatrix} \sigma_x^2 & \sigma_{xy}^2 \\ \sigma_{xy}^2 & \sigma_y^2 \end{bmatrix} \qquad R_p = \begin{bmatrix} \sigma_r^2 & 0 \\ 0 & \sigma_\psi^2 \end{bmatrix} \tag{48}$$

$$Q = \begin{bmatrix} \frac{1}{4}T^4 & \frac{1}{2}T^3 & 0 & 0 \\ \frac{1}{2}T^3 & T^2 & 0 & 0 \\ 0 & 0 & \frac{1}{4}T^4 & \frac{1}{2}T^3 \\ 0 & 0 & \frac{1}{2}T^3 & T^2 \end{bmatrix} \sigma_p^2 \tag{49}$$

The parameters in (47)-(49) and other simulation design parameters are given in Table 1.

Originally, the position measurements are in polar coordinates $(r, \psi)$ with (time invariant) measurement noise covariance $R_p$, but are transformed to Cartesian coordinates $(x, y)$ with corresponding measurement noise covariance $R_c$ using the standard conversion [5, pp. 397-399]. This results in a purely linear model so that a Kalman filter can be used in the tracking algorithm. The measurement noise matrix $R_p$ is calculated assuming a uniformly distributed position error inside the resolution cell. Hence, the variance of the uniformly distributed error is given by the resolution, and this variance is heuristically used as the variance in the Gaussian distributed $R_p$

$$\sigma_r^2 = \frac{0.2^2}{12}\ \text{m}^2 \qquad \text{and} \qquad \sigma_\psi^2 = \frac{(\pi/256)^2}{12}\ \text{rad}^2 \tag{50}$$

Due to the high resolution in range (0.2 m), the targets will cover several resolution cells in the range direction, resulting in extended targets. Because of this, the actual range resolution is used as the standard deviation ($\sigma_r = 0.2$ m) instead of the calculation in (50). This modification of $\sigma_r$ in the simulations seems more reasonable since the targets (scuba divers) are extended in the range direction. To ensure controlled trajectories for

***Table 1:*** *Specification of parameters*

| Parameter | Value | Specification |
|---|---|---|
| $T$ | $1.0\,\mathrm{s}$ | Sampling period |
| $P_D$ | $0.7$ | Detection probability |
| $P_G$ | $0.99999$ | Gate probability |
| $P_W$ | $0.9$ | Wake probability |
| $P_{FA}$ | $0.001$ | False alarm probability |
| $\sigma_p^2(\mathrm{s})$ | $\left(0.001\,\mathrm{m/s^2}\right)^2$ | Process noise (simulation model) |
| $\sigma_p^2(\mathrm{f})$ | $\left(0.05\,\mathrm{m/s^2}\right)^2$ | Process noise (filter model) |
| $\sigma_r^2$ | $(0.2\,\mathrm{m})^2$ | Measurement noise (range) |
| $\sigma_\psi^2$ | $(3.5 \cdot 10^{-3}\,\mathrm{rad})^2$ | Measurement noise (bearing) |
| $N$ | $256 \times 1250$ | Number of resolution cells |
| $S$ | 180°, 250 m range | Sensor coverage area |
| $M$ | $250 \times 40\,\mathrm{m}$ | Measurement generation area |
| $W$ | $5 \times 30\,\mathrm{m}$ | Wake area |
| $V_S$ | $98174\,\mathrm{m}^2$ | Volume of S |
| $V_M$ | $10000\,\mathrm{m}^2$ | Volume of M |
| $V_W$ | $150\,\mathrm{m}^2$ | Volume of W |
| $\lambda_{\texttt{clutter}}$ | $16.3$ | Expected number of correlated clutter measurements |

the true targets, the added process noise in the simulation model $\sigma_p^2(\mathrm{s}) = \left(0.001\,\mathrm{m/s^2}\right)^2$ is set low, but not to zero. The process noise in the filter model $\sigma_p^2(\mathrm{f}) = \left(0.05\,\mathrm{m/s^2}\right)^2$ is set to approximate about 5 cm/s change in the velocity components between each scan.

When the targets are following after each other in the sequential scenario, there will be a problem using the filter modifications as described above. This problem especially affects the target following behind the first target, because there will be wake detections surrounding this target both in front and behind it. If the wake model is used in this situation, the wake-dominated measurements behind the target will get lower weights than the wake-dominated measurements in front. These measurements in front, which originate from the wake of the first target, will mislead the tracker, and the estimated track will speed up until it catches up with the target in front. It is therefore likely that this target will be lost. An approach to prevent this is to only apply the wake model to the target in front, and use a regular data association filter for the target that is following

the first one. By handling the two targets separately in two single-target tracking filters, the track of the target behind the first one will have better chance to survive in this hard situation. In the simulations a target following behind another one will therefore not use the wake model if the following criteria are fulfilled:

1. The target is inside the wake area $W$ of the target in front. The wake area $W$ is defined as a rectangle, $L_w$ wide and reaching $L_l$ backwards from the target ($L_w = 5\,\text{m}$, $L_l = 30\,\text{m}$).
2. The target is at least 2 m behind the target in front.
3. The difference between the moving direction of the following target and the target in front is less than $10^\circ$.

To reduce the computational load, the different versions of the multitarget tracking algorithms are substituted with their analogous single target tracking algorithms as long as targets are not "sharing" measurements. In other words, the standard PDAF is used instead of the JPDAF, and the modified PDAF is used instead of the modified JPDAF and JPDACF when the targets are apart. The multisensor (MS) filters are treated in the same way, i.e., the MSPDAF is used instead of the MSJPDAF.

## 5.3 Measurement Generation

The directional information (bearing) in an active sonar is given by the beamforming. Since no beamforming can achieve an ideal directivity pattern, there will be a leakage or scattering of the signal in one beam to the neighboring beams [16, ch. 5.3]. This is also known as the point spread function (psf) [25], and may yield detections from a point target in more than one bearing cell. In [22] the true target-originated measurements are simulated as single point detections, which, as described above, is a simplification of the real world. To generate measurements from the targets and their wakes in this paper, detections from a *real data set* of a scuba diver with an open breathing system are used. The data set consists of $500$ scans, and is recorded by an active sonar with the same specifications as the sensors used in the simulations. The diver is swimming in a nearly straight line, and its trajectory is estimated mainly by using a modified PDAF [21], but some manual corrections are done to get better position estimates. For each scan a cell averaging - constant false alarm rate (CA-CFAR) detector [15] is used to obtain the detections. The parameters of the CA-CFAR algorithm are the same as in [21], except for the following parameters:

- The average false alarm rate (probability of a false detection in a resolution cell) is set to $P_{FA} = 0.001$.
- The size of the averaging window used to estimate the local background noise parameter is increased to 51 cells in the range direction due to the increased resolution of the sensors used in this paper.

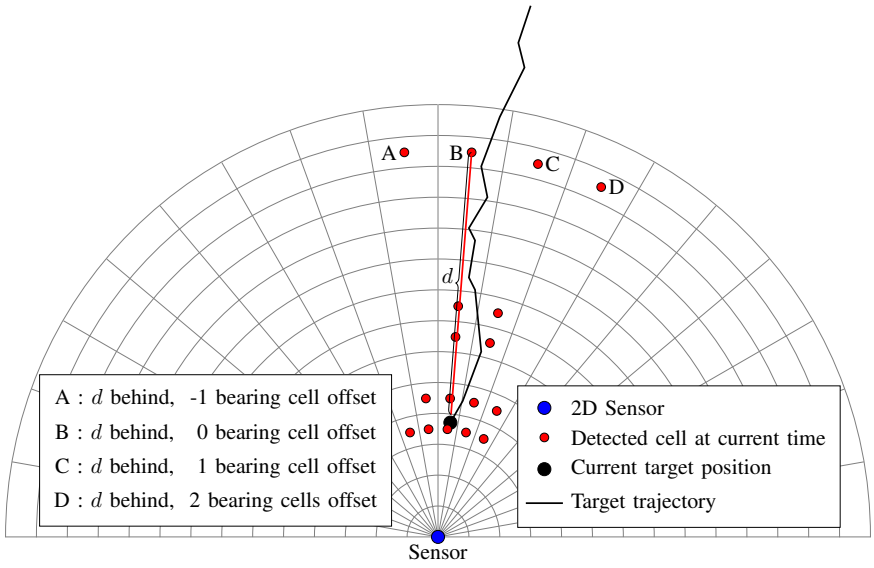


***Figure 5:*** *Illustration of how each detection is specified by using the distance behind the target $d$ and a bearing offset. The bearing offset describes the number of cells in the bearing direction between a detected cell and the cell where the target trajectory passes through, and with the same range as the detected one. As an example, the four detections marked with A, B, C and D are the same distance behind the target, but with offsets -1, 0, 1 and 2 respectively.*

For each scan, the detections are stored and specified by a distance $d$ behind the true target position and a bearing offset, see Figure 5. The bearing offset describes the number of cells in the bearing direction between a detected cell and the cell where the target trajectory passes through, and with the same range as the detected one. As an example, the four detections marked with A, B, C and D in Figure 5 are the same distance behind the target, but with bearing offsets -1, 0, 1 and 2 respectively. Finally, after going through the 500 scans in the *real data set*, this gives $500$ different sets of detections of the true target and its wake, where the scattering in the bearing-direction is accounted for. In the simulations the detections originating from the target and its wake are generated by drawing from these $500$ sets according to a first order Markov model. If set $s$ was drawn at scan $k$, the probability of drawing the succeeding set $s+1$ at time $k+1$ is $\pi_{s,s+1} = 0.7$, and the probability of a random drawing $u \in [1, 500]$ (uniformly distributed) is $\pi_{s,u} = 1 - \pi_{s,s+1} = 0.3$. The targets' states are generated directly from (1), and with the position and velocity known, the target and wake originated measurements are added.

Another part of the measurements is the clutter or false measurements, and a standard assumption in simulations is that clutter is uniformly distributed in the surveillance area. In this paper the generation of clutter is done in two steps. The first step is under the standard assumption, where the probability of generating a clutter measurement in a resolution cell is $\frac{P_{FA}}{2} = 0.005$, uniformly distributed across all cells in range and bear-

ing. The second step is to generate spatially correlated clutter. These measurements are generated from a multimodal Gaussian pdf with equal weights for the different modes. This is an approach to reflect that some areas in the surveillance region yields more clutter, due to, e.g., a rough surface of the sea bed, banks, hills, large stones and other objects that creates variation in the surveillance area. The multimodal Gaussian pdf is regenerated for each run, and the number of modes is drawn as a uniform discrete variable between 1 and 10. The mean of each Gaussian mode is drawn uniformly in the surveillance area, and the covariance matrix is diagonal with standard deviations in the $x$ and $y$ directions drawn as uniform variables between 0 and 10. The number of correlated clutter measurements for each scan is Poisson distributed with parameter $\lambda_{\text{clutter}}$. Denote the coverage area for a sensor as $S$ (180°, 250 m range), and the measurement area covering the full trajectories of the targets as $M$ ($250 \times 40$ m), with volume $V_S$ and $V_M$ respectively. The Poisson parameter $\lambda_{\text{clutter}}$ is then given by

$$\lambda_{\text{clutter}} = 0.5 P_{FA} N \frac{V_M}{V_S} \approx 16.3 \tag{51}$$

where $P_{FA}$ is the probability of a false alarm in a resolution cell, and $N$ is the number of resolution cells in $S$. Hence, in average there will be 16.3 correlated clutter measurements in $M$ for each scan. An example of all measurements in one time frame for the crossing scenario is given in Figure 6. Notice that the detections of the targets are more spread out sideways in Sensor 2 than in Sensor 1. At this time the targets are closer to Sensor 1 than Sensor 2, and they are therefore better resolved by Sensor 1. The targets are also moving towards Sensor 2, and because of the scattering of the signal to the neighboring beams, the detections will be spread out more sideways from the direction of motion. Also notice how in some places the detections are located in groups due to the non-uniform spatial distribution of the clutter measurements. It is also possible that a target can be undetected, which is the case for the lower target at Sensor 1 in Figure 6.

## 5.4 Track Formation and Termination

As can be seen in Figure 6, the targets are often determined by a cluster of detections rather than a single point detection. In the simulations the tracks are initialized by two-point differencing [5], p. 247] of the cluster centroids from succeeding scans. The reason for this is to avoid confusion due to the many possibilities of two-point differencing that could have been set up among the point detections from one single target. The clustering method of the single point detections is described in [21], and is based on mathematical morphology [23]. Any successive pair of clusters within a maximum distance based on target maximum motion parameters and cluster measurement noise variances initiates a preliminary track. For the motion parameters, a maximum distance $d_{\max} = 1$ m together with the process noise matrix $Q$ in (2) is used. The measurement noise for the clusters is computed from the different cells included in the cluster as a Gaussian mixture [5, pp. 55-56]. A preliminary track has to receive measurements for a minimum of 4 time steps during the first 6 scans to become a confirmed track. This is also referred to as a "$4/6$"

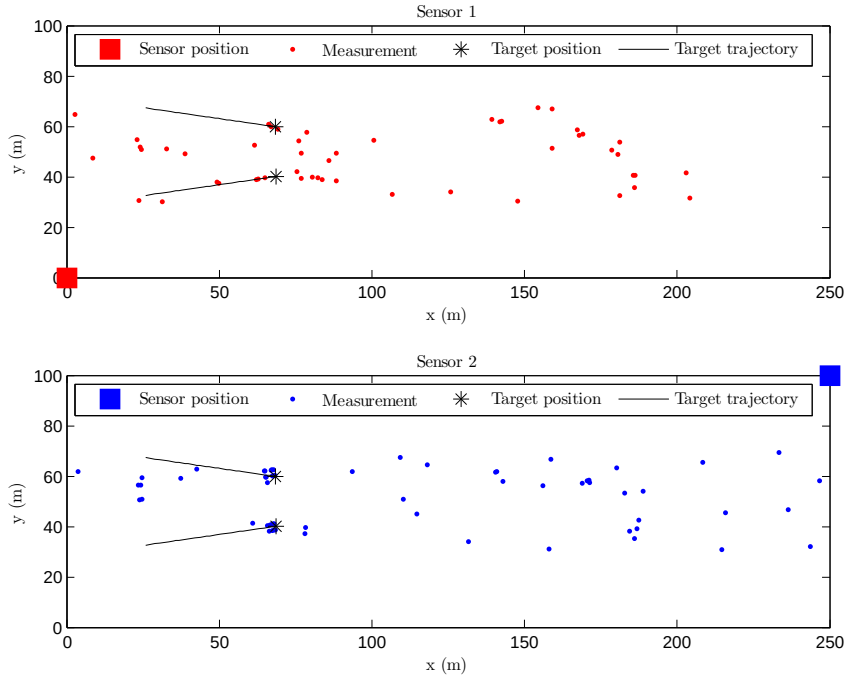


***Figure 6:*** *Snapshot of all detections/measurements at Sensor 1 and Sensor 2 during a run in the crossing scenario.*

logic-based track formation procedure. Note that the clustering method is only used for the two-point differencing in the track initialization.

In the centralized tracking the multisensor filtering is described in Section 4, first updating with measurements from Sensor 1 and then with measurements from Sensor 2 in a sequential updating scheme. The track initialization in the centralized tracking algorithm is based on measurements that also contain velocity information. First, the two-point differencing is used at Sensor 1 to make an initial state. Then, the two-point differencing is used at Sensor 2, but these initial states are now used as measurements (including both position and velocity) to update the initial state from Sensor 1. The updating is done as in a regular PDAF, but since these measurements are formed by two-point differencing of cluster centroids from succeeding scans, they will not have the same measurement noise, yielding a varying innovation covariance ($S_k$ in (6)). The innovation covariance is normally used to form the measurement validation gate in the PDAF, but in this case a fixed matrix

$$S_{\text{fix}} = \begin{bmatrix} \sigma^2_{\text{pos}} & 0 & 0 & 0 \\ 0 & \sigma^2_{\text{pos}} & 0 & 0 \\ 0 & 0 & \sigma^2_{\text{vel}} & 0 \\ 0 & 0 & 0 & \sigma^2_{\text{vel}} \end{bmatrix} \tag{52}$$

is used instead of the non-constant innovation covariance to form a constant measure-

ment validation gate. The values used in $S_{\text{fix}}$ is set based on the assumption that the standard deviation for these measurements are about 1 m for the position elements, and 0.5 m for the velocity elements ($\sigma_{\text{pos}} = 1\,\text{m}$ and $\sigma_{\text{vel}} = 0.5\,\text{m}$).

In the modified filters, the wake assumption also affects the track initialization in the way that measurements inside the wake area $W$ (defined in Section 5.2) are excluded in the initialization procedure.

To terminate a track one of the following events (termination events) must occur:

1. The estimated speed is outside the interval $[v_{\min}, v_{\max}]$, where $v_{\min} = 0.1\,\text{m/s}$ and $v_{\max} = 3\,\text{m/s}$.
2. The estimate moves more than $5\,\text{m}$ between two scans.
3. The position state estimation variance exceeds $\sigma^2_{\text{pos max}}$, where $\sigma^2_{\text{pos max}} = 50\,\text{m}^2$.
4. There are no validated measurements received in a track within $5$ successive scans.
5. The track is closer than $d_{\min}$ to another older track during 10 succeeding scans, where $d_{\min} = 0.5\,\text{m}$.

These track termination criteria are adopted rather than using more rigorous methods, such as the joint version of the IPDAF [17], because of their sensitivity to inaccurate estimates of the clutter density. In real sensor measurements, the signal is often scattered resulting in more than one target-originated detection. This will increase the clutter density resulting in an unrealistic low probability for the track to survive. This may be solved by the use of clustering, but for targets in the presence of wakes it is undesirable to blend the wake-originated detections together with the target-originated ones. The above termination criteria are more strict than those used in [21] due to the higher sensor resolution used in this paper.

## 5.5 Performance Analysis

The performance evaluation of a multitarget tracking system is always a difficult problem, and the quality of the results is difficult to quantify in terms of a few variables. When the evaluation is based on real data, where not all parameters are known, this problem becomes even harder. The results also depend on the simulation scenarios, and the performance of the JPDAF may, according to [13], show large local maxima and minima as a function of scenario parameters. However, by considering the basic scenarios described above and using a relatively large set of measures of performance (MOP), a certain amount of meaningful information should be obtained. The MOP considered are the following:

1. The percentage of lost tracks among all true tracks.
2. The percentage of swapped tracks among all true tracks (measured only when the targets are closer than 10 m).

3. The average fraction of each trajectory's total duration where the target is tracked (by a true track).
4. The average life length of a true track relative to its true target's life length.
5. The average time for target acquisition.
6. The number of false tracks per scan.
7. The average life length of a false track.
8. The position RMS error.

This section describes how these MOP are obtained before the corresponding results, based on 500 Monte Carlo runs for each of the four given scenarios, are shown. At a given time $k$ there might exist several tracks, but for each target, at most one of them can be defined as true. The rest of the tracks are therefore by definition false. A track is first defined as true if the position estimation error is less than $1$ m during the next $5$ scans, and at the same time there are no other true track associated to the target. If there is more than one track fulfilling these requirements at the same time, the track with lowest average position estimation error during these 5 scans is defined as the true one. The true track will stay as such until either the position estimation error exceeds 5 m, or the position estimation error associated to a neighboring target is less than $1$ m during the next 5 scans. In both situations the track will be declared as lost, but in the latter case it will also be defined as a swapped track.

#### The percentage of lost tracks among all true tracks

In Figure 7 the percentage of lost tracks is shown. The standard filters (PDAF and JPDAF) have the highest track loss percentage, and the JPDAF shows no improvement compared to the PDAF. The modified single target tracking algorithm (PDAF) performs better than the standard filters, but the best performance is achieved with the modified JPDAF and JPDACF. The difference between the standard filters and the modified PDAF is largest in the meeting and crossing scenarios where the targets are close to each other during a short time. When the targets stay together for a longer period of time, the modified PDAF is not significantly better than the standard filters because it does not account for the neighboring target and its wake like the modified JPDAF and JPDACF do. Also notice that there is almost no difference between the decoupled and coupled modified JPDAF, which indicates that the correlation between the targets' estimation errors is insignificant.

In the different scenarios considered the best performance is achieved for the meeting scenario. This is maybe a bit surprising since the density of the joint wake model after the passing is lowest between the targets, the area opposite to their moving direction. However, the high wake density in the whole joint validation region will at the same time give more confidence in the predicted target motion than the measurements. Because

of this, and the fact that the velocities of the two targets are totally opposite to each other, the tracks will be less affected by the false measurements. The percentage of the lost tracks in the crossing scenario is the next best, and the good performance in both the meeting and crossing scenarios is as expected since the targets are only close to each other a short time. In these scenarios the results from the single sensor filters are almost as good as from the multisensor filters in the centralized tracking. This is not true for the parallel scenario where the performance is significantly improved by fusing the sensors' data in the modifed MSJPDAF and MSJPDACF. In this scenario the targets are separated by only 3 m, which is close to the limit for having multiple targets in a single resolution cell (unresolved targets). By using two sensors in this situation, Sensor 1 resolves the targets relatively good in the beginning of the run, and Sensor 2 does the same at the end of the run. Because of this, the fusion of these two sensors data improves the performance significantly.

The most difficult scenario is the sequential, where a target is moving behind another target, surrounded by the wake. In this case the centralized tracking performs best, and a track loss under 40% is achieved by the modified MSJPDAF and MSJPDACF. In practice this means that, even in a hard case like this, at least one track will be kept throughout the run.

### The percentage of swapped tracks among all true tracks (measured only when the targets are closer than 10 m)

The percentage of the swapped tracks, shown in Figure 8, is only measured when the distance between the targets is less than 10 m. The reason for this is to find the percentage of swapping among only the tracks where the two associated targets are close to each other. The swapping is, as expected, highest in the parallel scenario where the tracks are moving in parallel for a longer period of time. In this situation it is easy for a track to switch over to the neighboring target only 3 m away. In the meeting scenario the swapping phenomenon is totally absent for the modified filters, and practically absent for the standard filters (PDAF and JPDAF). The reason for this is the same as discussed under the previous MOP.

The modified PDAF has the most problems, especially in the parallel scenario, since it accounts for its own wake, but does not take into consideration that there is another target in the surrounding area. The standard filters, which do not consider the wakes, are more disposed to turn into their own wake than to swap to the neighboring target. Therefore, even if their track loss is higher, they have a lower swapping percentage than the modified PDAF.

The best performance is achieved by the modified MSJPDAF and MSJPDACF in the centralized tracking. This improvement is most significant in the parallel scenario, where the percentage of swapped tracks are almost halved for the modified MSJPDAF and MSJPDACF compared to the other filters.

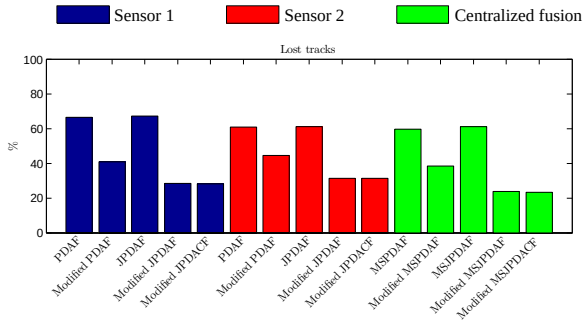


(a) Scenario 1: Crossing trajectories

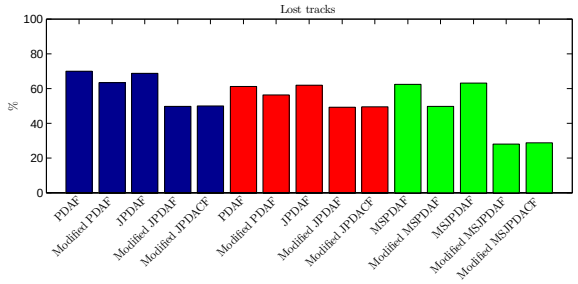


(b) Scenario 2: Parallel trajectories

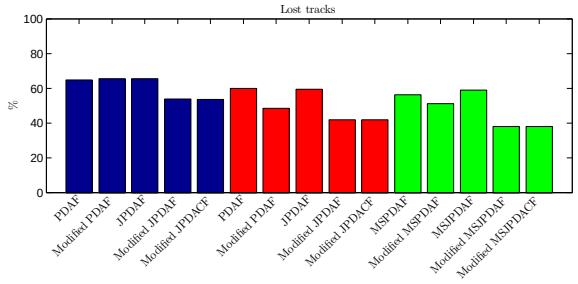


(c) Scenario 3: Sequential trajectories

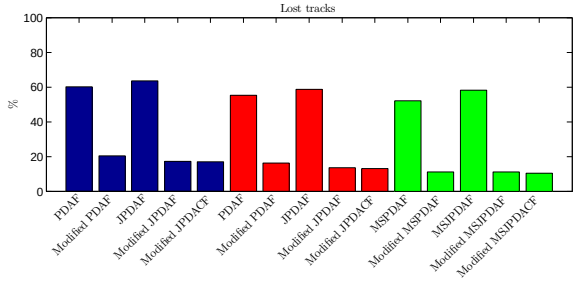


(d) Scenario 4: Meeting trajectories

***Figure 7:*** *Average percentage of lost tracks in the four simulation scenarios: (a) crossing trajectories, (b) parallel trajectories, (c) sequential trajectories, and (d) meeting trajectories.*

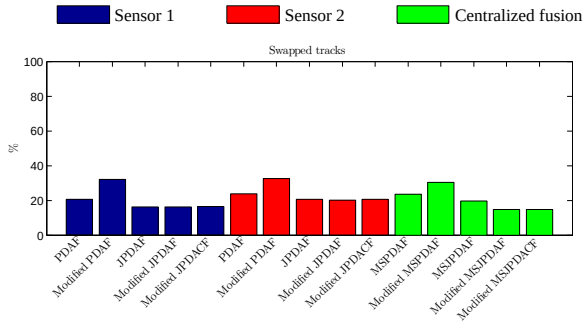


(a) Scenario 1: Crossing trajectories

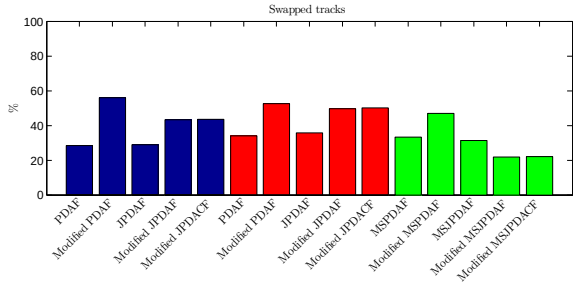


(b) Scenario 2: Parallel trajectories

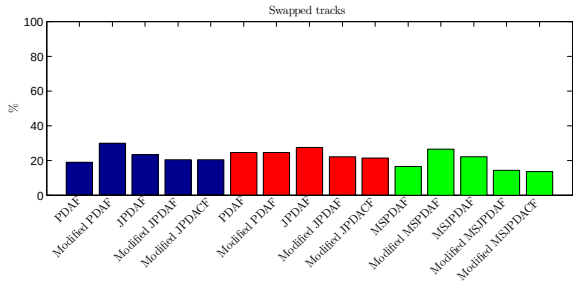


(c) Scenario 3: Sequential trajectories

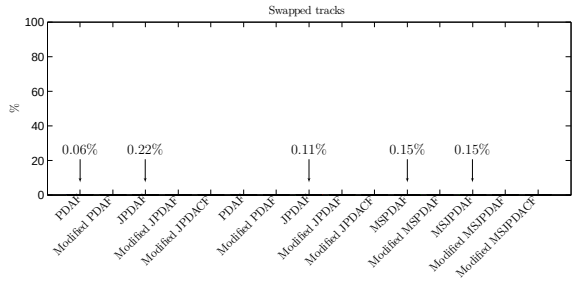


(d) Scenario 4: Meeting trajectories

***Figure 8:*** *Average percentage of swapped tracks in the three simulation scenarios: (a) crossing trajectories, (b) parallel trajectories, (c) sequential trajectories, and (d) meeting trajectories.*

### The average fraction of each trajectory's total duration where the target is tracked (by a true track)

In Figure 9 the average percentage of the tracked part of the trajectories' duration is shown. Also here the modified JPDAF and JPDACF perform best, and by using the modified MSJPDAF or MSJPDACF in the centralized tracking, about 90% of the trajectories are tracked. Notice that the percentage of the tracked trajectory can be very good even with a high track loss percentage if tracks are quickly reacquired after a loss. It is therefore important to consider other MOP to get the total picture.

### The average life length of a true track relative to its true target's life length

In Figure 10 the average life length (in %) of the true tracks is shown. It is clear that the track length is significantly increased by the modified filters, and most by the modified multitarget tracking filters (JPDAF and JPDACF). The best performance is achieved by the modified filters in the meeting scenario, where the average track length is about 80% of the true target's life length, more than twice as long as for the standard PDAF and JPDAF. The improvement by using multiple sensors is most significant for the modified MSJPDAF and MSJPDACF in the parallel scenario. In this situation the combination of both using the multitarget wake model, and for the targets to be well resolved by at least one sensor all the time throughout the run, is vital. In the sequential scenario the best track length is almost 60% for the same modified multisensor filters. This is due to the fact that when a track is first lost inside the wake of another target in front, it is very hard to reacquire a track on the rear target.

### The average time for target acquisition

In many situations it is important to quickly initiate tracks and reacquire them once lost. Let the time for target acquisition be the time before a track is defined as true either in the beginning of a run or after a track was lost. The average time for target acquisition (or reacquisition) is shown in Figure 11. For the crossing, the parallel and the meeting scenarios, the modified filters perform slightly better than the standard filters. At the sequential scenario the behavior is different in the way that the standard filters outperform the modified filters. This is due to the assumption that the measurements behind a target originate from a wake and not a target. Therefore, when the target following the target in front is lost, the real target-originated measurements will not be considered for a new track as long as they are inside the wake area $W$ of the target in front.

In the first three scenarios it is harder to initiate/reacquire true tracks at Sensor 2 than for Sensor 1. The reason for this is that tracks are starting close to Sensor 1, and far from Sensor 2, and the detections of the targets (and wakes) will therefore be more spread out in the view of Sensor 2. This can be seen in Figure 6, and makes it harder to acquire tracks in the two-point differencing of the cluster centroids from succeeding scans.

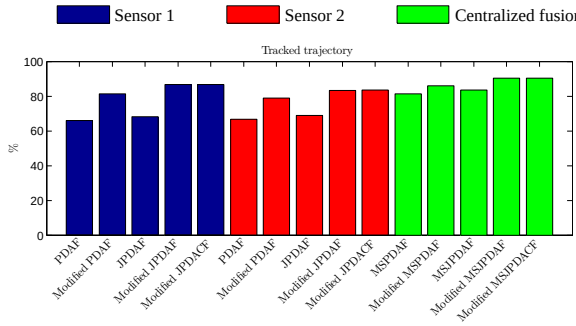


(a) Scenario 1: Crossing trajectories

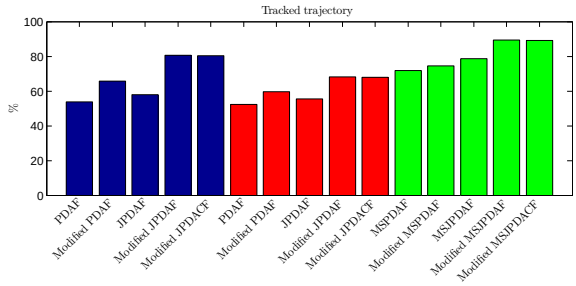


(b) Scenario 2: Parallel trajectories

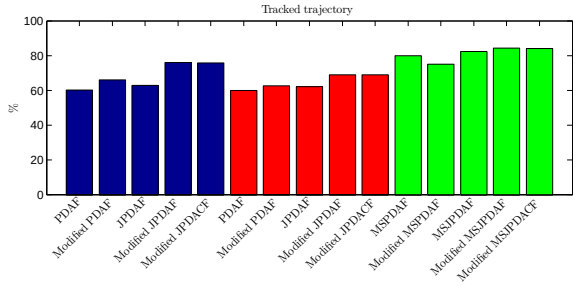


(c) Scenario 3: Sequential trajectories

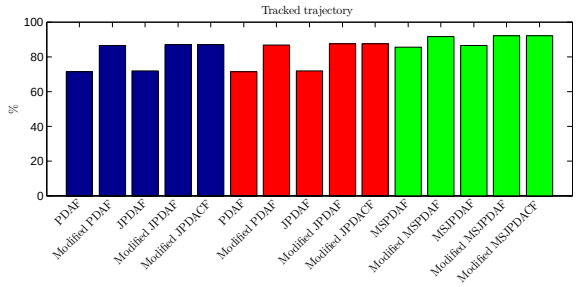


(d) Scenario 4: Meeting trajectories

***Figure 9:*** *Average percentage of tracked trajectory in the four simulation scenarios: (a) crossing trajectories, (b) parallel trajectories, (c) sequential trajectories, and (d) meeting trajectories.*

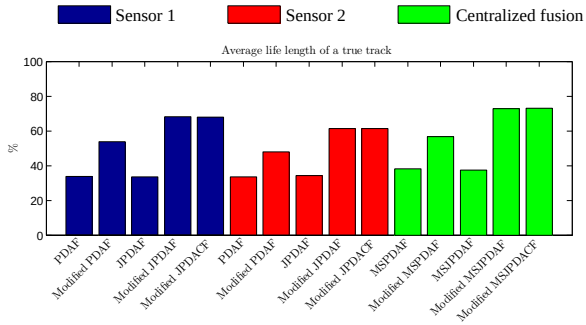


(a) Scenario 1: Crossing trajectories

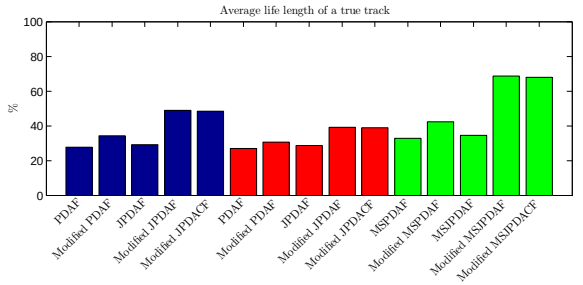


(b) Scenario 2: Parallel trajectories

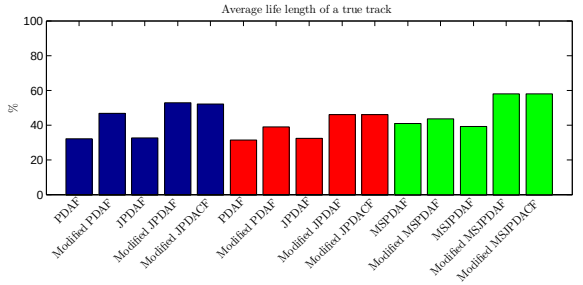


(c) Scenario 3: Sequential trajectories

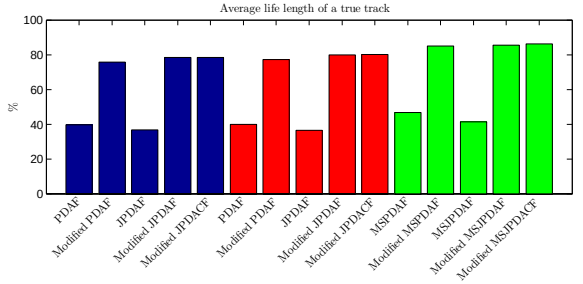


(d) Scenario 4: Meeting trajectories

***Figure 10:*** *Average life length of a true track relative to its true target's life length in the four simulation scenarios: (a) crossing trajectories, (b) parallel trajectories, (c) sequential trajectories, and (d) meeting trajectories.*

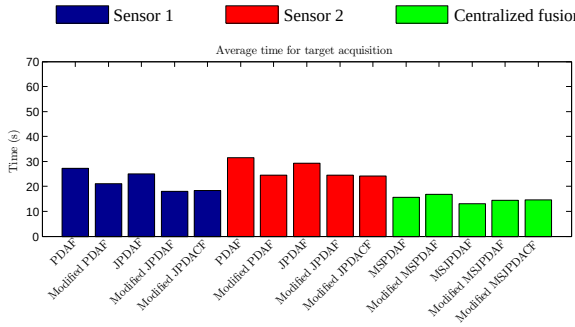


(a) Scenario 1: Crossing trajectories

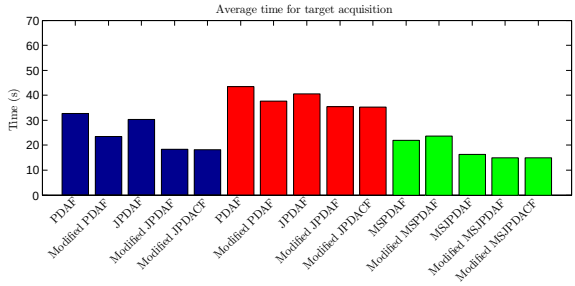


(b) Scenario 2: Parallel trajectories

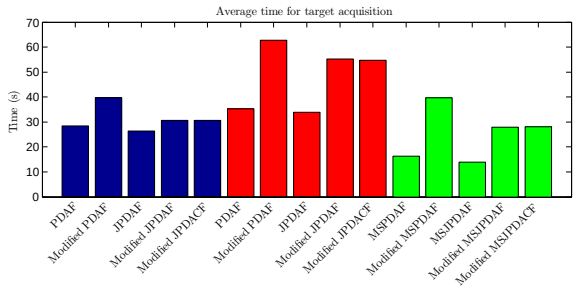


(c) Scenario 3: Sequential trajectories

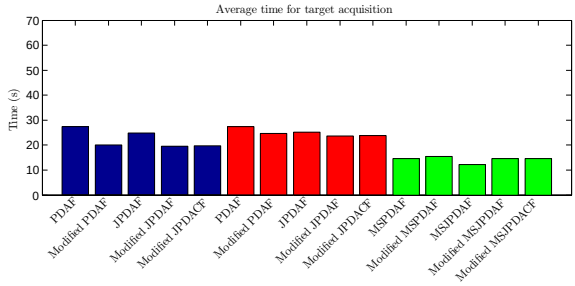


(d) Scenario 4: Meeting trajectories

***Figure 11:*** *Average time for target acquisition in the four simulation scenarios: (a) crossing trajectories, (b) parallel trajectories, (c) sequential trajectories, and (d) meeting trajectories.*

### The average life length of a false track

As mentioned above, all tracks that are not defined as true, are considered false. The average life length of a false track is shown in Figure 12, and the performance is almost the same for all filters, with an insignificant tendency for shorter life length of the false tracks in the modified filters.

### The number of false tracks per scan

Another MOP considering the false tracks, is the average number of false tracks per scan, shown in Figure 13. This number is higher for the standard filters than for the modified ones because the standard filters do not restrict the track formation inside the wake areas behind the targets. Also, there are more false tracks for the centralized tracking due to the fact that this tracking algorithm takes into account false measurements from both sensors.

### The position RMS error

The last MOP in this analysis is the position RMS error, given in Figure 14. The RMS error is based only on the true tracks in the simulation scenarios. In all scenarios the position RMS error is larger for the standard filters than for the modified filters. This is because the standard filters do not consider the wake-originated measurements like the modified filters do, and the state estimate is therefore likely to be drawn into the wake. It can also be seen that the RMS error, at least for the modified JPDAF and JPDACF, is slightly reduced in the centralized tracking.

In the two first scenarios (crossing and parallel), the error increases during the periods when the targets are close to each other. For the crossing scenario this is seen as a "jump" in the error when the targets are crossing between 80 s and 120 s. In the parallel scenario, this jump starts at about 60 s and ends at 140 s, which are the period the targets are moving in parallel. In these situations the estimate for one target will be drawn towards the other target, also known as track coalescence [8]. Among the modified filters, this is most problematic for the single target tracking algorithm because it accounts for the wake behind its own target, but has no information about the nearby target which also has a wake behind it. The modified multitarget filters perform similarly, and their RMS errors are almost constant throughout the run.

In the meeting scenario only a small tendency of the jump phenomenon is noticeable shortly after the passing. As discussed above, the totally opposite velocities of the two targets and the high wake density in the whole joint validation region, make the targets' passing relatively easy.

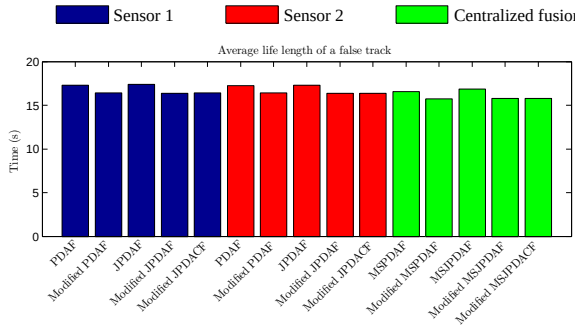


(a) Scenario 1: Crossing trajectories

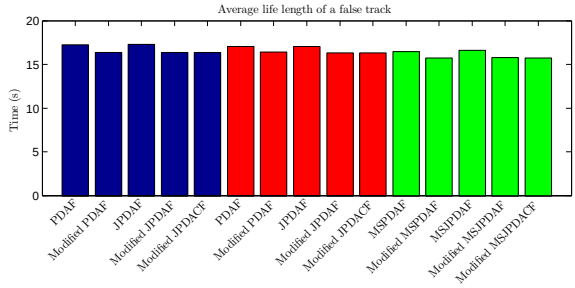


(b) Scenario 2: Parallel trajectories

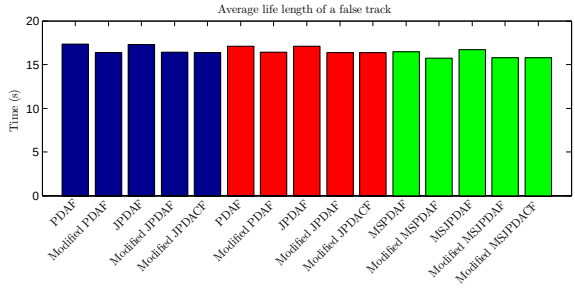


(c) Scenario 3: Sequential trajectories

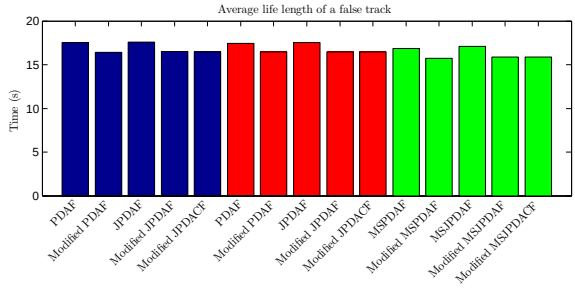


(d) Scenario 4: Meeting trajectories

***Figure 12:*** *Average track length for a false track in the four simulation scenarios: (a) crossing trajectories, (b) parallel trajectories, (c) sequential trajectories, and (d) meeting trajectories.*

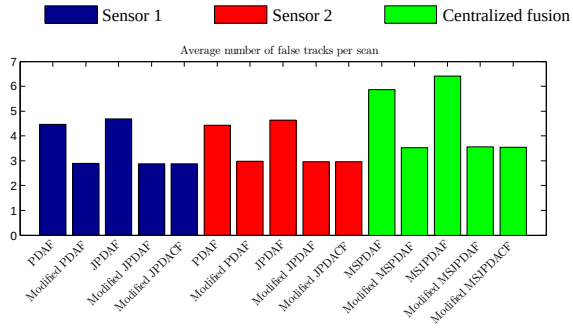


(a) Scenario 1: Crossing trajectories

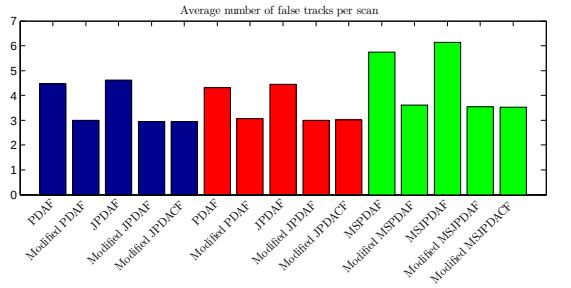


(b) Scenario 2: Parallel trajectories

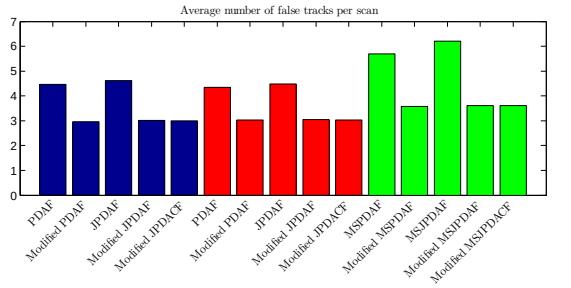


(c) Scenario 3: Sequential trajectories

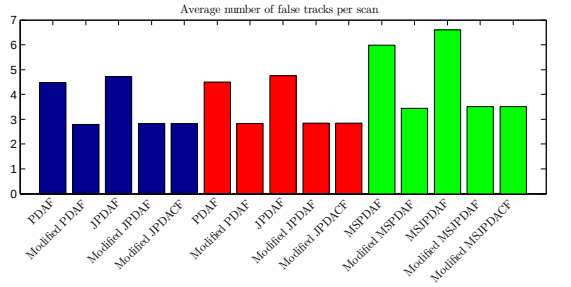


(d) Scenario 4: Meeting trajectories

***Figure 13:*** *Average number of false tracks per scan in the four simulation scenarios: (a) crossing trajectories, (b) parallel trajectories, (c) sequential trajectories, and (d) meeting trajectories.*

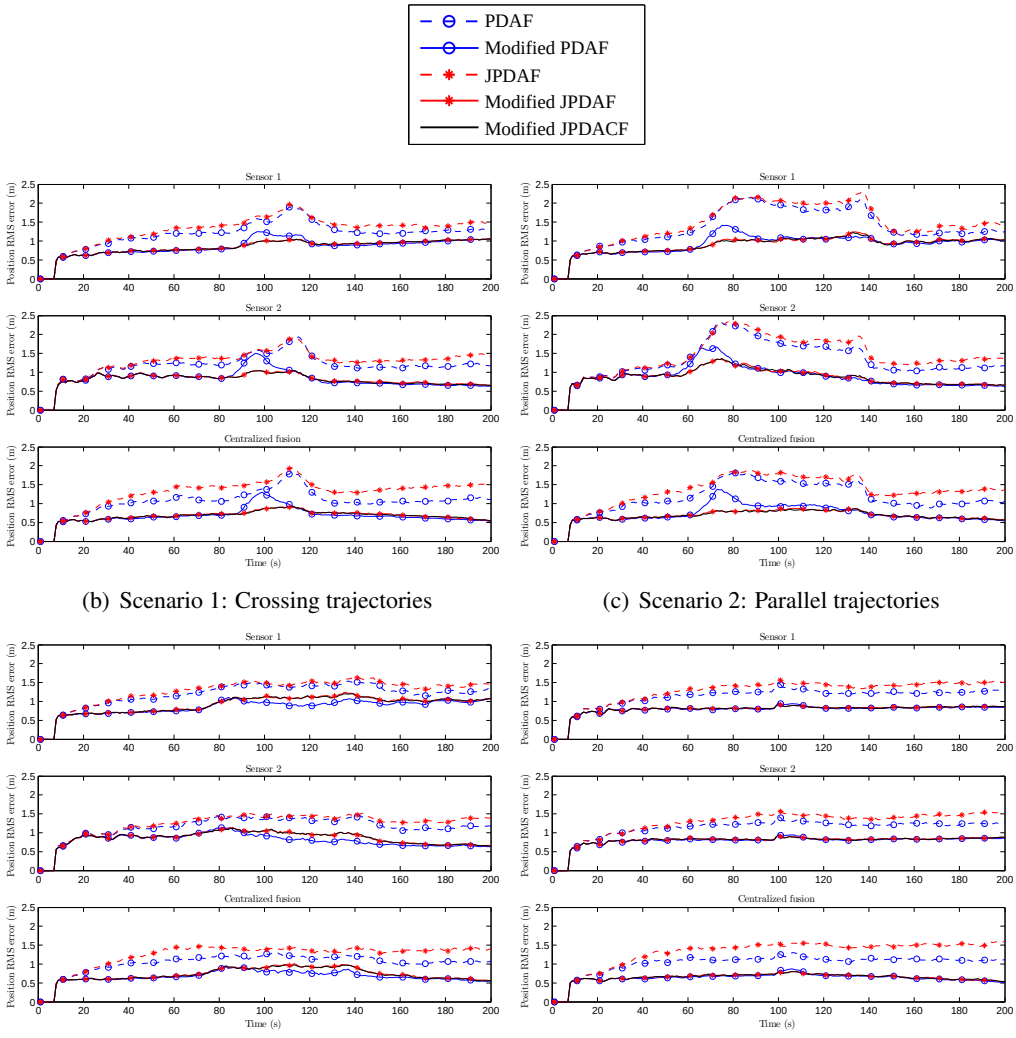


(b) Scenario 1: Crossing trajectories

(c) Scenario 2: Parallel trajectories

(d) Scenario 3: Sequential trajectories

(e) Scenario 4: Meeting trajectories

***Figure 14:*** *Position RMS error from 500 Monte Carlo runs in: (a) crossing trajectories, (b) parallel trajectories, (c) sequential trajectories, and (d) meeting trajectories.*

In the sequential scenario the targets are never closer than about 5 m, so the RMS error does not increase much during the period the tracks are following after each other. In this scenario, the modified single target tracking filter performs better than the modified multitarget tracking filters. The reason for this is because the RMS error is measured only among the true tracks, not when they become lost. In this scenario, where the targets are following after each other, the estimation error is larger for the target behind the one in front, because it is surrounded by wakes. From the percentage of lost tracks in Figure 7, the modified single target filter will lose the target more often than the modified multitarget filters, and it is most likely that the lost target is the one with largest estimation error. Therefore, when the RMS error is calculated, the modified multitarget filters are based on tracks with larger estimation error than what the modified single target filter is based on, only because these tracks were not lost.

## 5.6 Usage of the Wake Model on Targets Without Wakes

In this section the erroneous use of wake models on targets without wakes is considered. The crossing scenario (see Figure 4) is used as before, but without wakes behind the targets.[2] Each target is simulated as a point-target (only one measurement) with detection probability $P_D = 0.7$, independently across time. The results after $500$ Monte Carlo runs are shown in Figure 15, and the performance is clearly better than in the wake-scenario due to the fact that each target is never simulated by more than one detection at a time. This shows that the scattering effect in real sensors, due to the beamforming, makes the tracking problem considerably harder and is an important element in further research.

It is also interesting to see that even though the modified PDAF performs worse than the standard PDAF, the modified multitarget algorithms perform almost the same as the standard JPDAF. This indicates that applying the modified JPDAF or JPDACF on targets without wakes will not degrade the tracking performance. For tracking in environments with different kinds of targets, with and without wakes, this is a desirable property.

Another issue worth mentioning is the increasing trend of the position RMS error for Sensor 1, and the decreasing trend for Sensor 2. This is due to the fact that the estimated position error increases with the distance to the sensors, and the targets are starting close to Sensor 1, and moving towards Sensor 2. Notice how these trends in the single sensors are averaged out in the centralized tracking where the sensors' data are fused.

It is also shown that the use of multiple sensors is more effective in preventing lost tracks in this special case than in the previous cases where the targets had wakes. This gives an another justification of using multiple sensors when tracking targets in the presence of wakes, because a target could be mistaken for having a wake even when it does not have one.

[2] This would correspond to "closed breathing system" scuba divers or mechanical underwater vehicles.

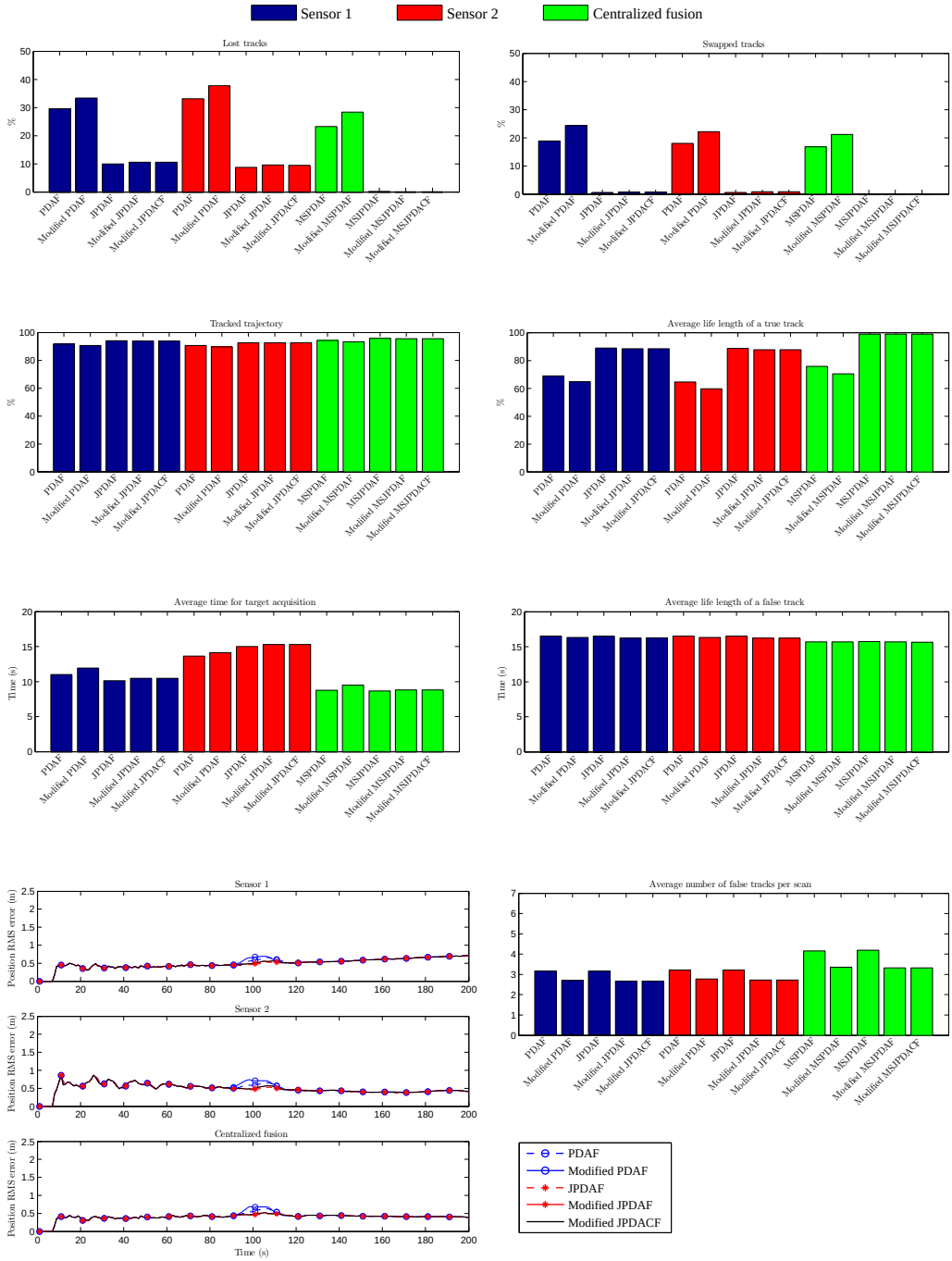


***Figure 15:*** *Simulation results from the crossing scenario where the probabilistic wake model is erroneous applied to targets without wakes. Each target is simulated as point detections with detection probability $P_D = 0.7$, independent across time. The different features discussed in Section 5.5 are shown.*

# 6 Conclusions

An important factor in a multitarget tracking system is to correctly associate each measurement received from a detector to its origin. The JPDAF has been a solution to this problem due to its effectiveness and low computational demand. In the JPDAF all false measurements are assumed due to i.i.d. uniformly spatially distributed noise or clutter. This assumption is not adequate for targets that generate wakes, because detections originating from the wake are not uniformly distributed and may result in a lost track if they are not properly modelled. The solution presented incorporates a model of the wakes behind the targets in a multitarget environment. The purpose of this wake model is to weight wake-originated measurements lower than in a regular JPDAF to avoid the tracks following these measurements and therefore be forced to turn into the wake. To achieve this, we presented a model formed by the sum of single models each linearly increasing behind their associated targets.

A systematic comparison of the standard data association filters (PDAF and JPDAF) and their corresponding modified versions are presented in a multitarget multisensor environment. Four different simulation scenarios are examined where two targets in the presence of wakes are crossing, moving in parallel to each other, one following after another, and finally meeting and then passing each other. It is shown that the wake model presented is a useful modification of the JPDAF in all four scenarios. The only stated drawback using the wake model is when a target is moving after another one, surrounded by the wake from the target in front. In that case, if the rear target is lost, it is harder to reacquire the track because the measurements are assumed originating from the wake and not the true target.

This paper also presents the coupled version of the JPDAF, called JPDACF, and a modified JPDACF (with a wake model) is developed and tested. The simulations show that the modified JPDACF is not improving the performance compared to the simpler modified JPDAF, indicating that there is no significant correlation between the targets' estimation errors.

The simulation scenarios consider two sensors, and the data association filters at the local sensors are compared with multisensor (MS) filters in a centralized tracking configuration. A sequential state updating scheme is used in the multisensor filters, and the results show that the data fusion provides significant improvement in the tracking performance.

This paper also examines the effect of applying the wake model on point-targets without wakes. The results show that the modified JPDAF and JPDACF perform almost the same as the standard JPDAF. This makes the modification practical for real systems where both targets with wakes and targets without wakes are operating in the same environment.

## Appendix A: Specification of the Joint Wake Model

In this appendix the joint wake model $p_W(z_k)$ introduced in Section 3 is presented, and an analytical expression for the probability $P_{GW}$ is derived. The joint wake model is the sum of all $N_T$ single wake models $p_W^t(z_k)$ behind each target $t$ under consideration

$$p_W(z_k) = \frac{1}{N_T} \sum_{t=1}^{N_T} p_W^t(z_k) \tag{53}$$

Next, consider the single wake model $p_W^t(z_k)$ of target $t$, and let $\bar{z}$ and $v$ be the predicted position and velocity of the target, respectively. Reference to Figure 16 may be helpful in the following.

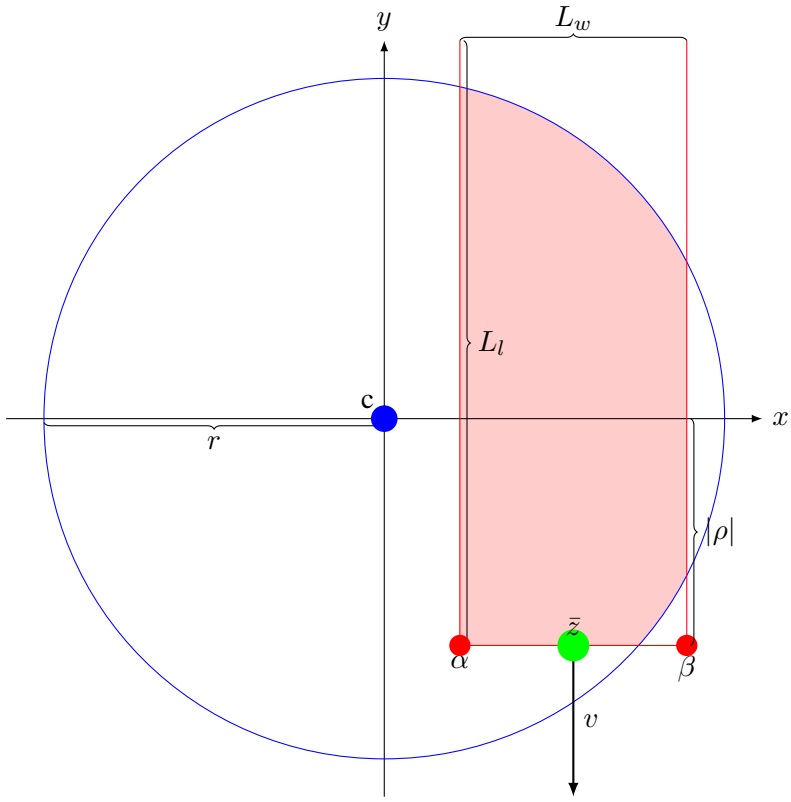


***Figure 16:*** *Specification of variables for integration of the wake model, with length $L_l$ and width $L_w$, inside the joint validation region with center $c$ and radius $r$. The wake has front corners $[\alpha\ \rho]$ and $[\beta\ \rho]$ and is oriented behind the target with position $\bar{z}$ and velocity $v$.*

The single wake model is assumed linearly increasing with length $L_l$ behind the predicted position of the target, i.e., in the direction opposite to $v$, and uniform with width $L_w$ in the direction perpendicular to the target's velocity $v$. This model can be expressed by defining the independent variables $l$ and $w$ as the respective distances behind and sideways (relative to $v$) to the target. From the above assumption, $l$ and $w$ have the following densities

$$p_l(l) = \frac{2l}{L_l^2} \;\; 0 \le l \le L_l \qquad p_w(w) = \frac{1}{L_w} \;\; 0 \le w \le \frac{L_w}{2} \tag{54}$$

which yields

$$p_W^t(z_k) = p_l(l)p_w(w) = \frac{2l}{L_l^2 L_w} \tag{55}$$

Notice that even though a current estimate of the velocity $v$ is available in the filter, a better way in practice is to use an average of the latest estimates since the wake will not change direction as rapidly as the current target velocity estimate. In the simulations an average of the latest 6 estimates is used.

The joint validation region containing all candidate measurements in the multitarget environment is defined as a circle with radius $r$ and center $c$. The center $c$ is calculated as the average between all the predicted target positions, and the radius $r$ is defined as the distance to the farthest validated measurement.

The probability $P_{GW}$ in (25), used to restrict the density of the joint wake model $p_W(z_k)$ to the joint validation region, has to be calculated for each scan by integration of $p_W(z_k)$ inside the region. Since $p_W(z_k)$ is the sum of all single wake models $p_W^t(z_k)$, $P_{GW}$ is obtained by calculating $P_{GW}^t$ for each target $t$ and then summing them up

$$P_{GW} = \sum_{t=1}^{N_T} P_{GW}^t \tag{56}$$

The calculation of $P_{GW}^t$ is derived next. Assume a Cartesian coordinate system with origin at position $c$ and $y$-axis parallel to $v$ but in the opposite direction, see Figure 16. Define the two front corners of the wake model with elements $\alpha$ and $\beta$ for the $x$-axis, and $\rho$ for the $y$-axis

$$\begin{aligned} \rho &= (c - \bar{z})^T v/|v| \\ \alpha &= \sqrt{|c - \bar{z}|^2 - \rho^2} - w/2 \\ \beta &= \sqrt{|c - \bar{z}|^2 - \rho^2} + w/2 \end{aligned} \tag{57}$$

The integration depends on if the front corners $[\alpha \;\rho]^T$ and $[\beta \;\rho]^T$ are inside or outside the joint validation region (circle), and will be broken into one, two or three parts. To do

this, define three binary variables $\delta_\rho$, $\delta_\alpha$ and $\delta_\beta$ as follows:

$$\delta_\rho = \begin{cases} 1 & \text{if} \quad \rho < 0 \\ 0 & \text{otherwise} \end{cases} \tag{58}$$

$$\delta_\alpha = \begin{cases} 1 & \text{if} \quad \sqrt{\alpha^2+\rho^2} > r \\ 0 & \text{otherwise} \end{cases} \tag{59}$$

$$\delta_\beta = \begin{cases} 1 & \text{if} \quad \sqrt{\beta^2+\rho^2} > r \\ 0 & \text{otherwise} \end{cases} \tag{60}$$

Then the integral can be written as

$$\begin{aligned} P_{GW}^t = & \frac{2}{L_l^2 L_w} \Bigg\{ \delta_\rho \delta_\alpha \int_{\max(\alpha,-r)}^{-\sqrt{r^2-\rho^2}} \int_{-\sqrt{r^2-x^2}}^{\sqrt{r^2-x^2}} (y-\rho)\mathrm{d}y\mathrm{d}x \\ & + \int_{\alpha(1-\delta_\alpha)-\delta_\alpha\sqrt{r^2-\rho^2}}^{\beta(1-\delta_\beta)+\delta_\beta\sqrt{r^2-\rho^2}} \int_{\rho}^{\sqrt{r^2-x^2}} (y-\rho)\mathrm{d}y\mathrm{d}x \\ & + \delta_\rho \delta_\beta \int_{\sqrt{r^2-\rho^2}}^{\min(\beta,r)} \int_{-\sqrt{r^2-x^2}}^{\sqrt{r^2-x^2}} (y-\rho)\mathrm{d}y\mathrm{d}x \Bigg\} \end{aligned} \tag{61}$$

For simplicity we substitute the limits of integration along the $x$-axis as follows:

$$\begin{aligned} a &= \max(\alpha, -r) \\ b &= -\sqrt{r^2-\rho^2} \\ c &= \alpha(1-\delta_\alpha) - \delta_\alpha\sqrt{r^2-\rho^2} \\ d &= \beta(1-\delta_\beta) + \delta_\beta\sqrt{r^2-\rho^2} \\ e &= \sqrt{r^2-\rho^2} \\ f &= \min(\beta, r) \end{aligned} \tag{62}$$

which yields

$$
\begin{aligned}
P_{GW}^{t} =& \frac{2}{L_l^2 L_w} \left\{ \delta_\rho \delta_\alpha \int_a^b \int_{-\sqrt{r^2-x^2}}^{\sqrt{r^2-x^2}} (y-\rho) \mathrm{d}y \mathrm{d}x \right. \\
&+ \int_c^d \int_\rho^{\sqrt{r^2-x^2}} (y-\rho) \mathrm{d}y \mathrm{d}x \\
&\left. + \delta_\rho \delta_\beta \int_e^f \int_{-\sqrt{r^2-x^2}}^{\sqrt{r^2-x^2}} (y-\rho) \mathrm{d}y \mathrm{d}x \right\} \qquad (63) \\
=& \frac{1}{L_l^2 L_w} \left\{ \rho r^2 \left( \arcsin \frac{c}{r} - \arcsin \frac{d}{r} \right) + \frac{c^3 - d^3}{3} \right. \\
&+ 2\rho \delta_\alpha \delta_\rho \left( a\sqrt{r^2-a^2} - b\sqrt{r^2-b^2} \right) - c(\rho^2 + r^2) \\
&+ 2\rho \delta_\beta \delta_\rho \left( e\sqrt{r^2-e^2} - f\sqrt{r^2-f^2} \right) + d(\rho^2 + r^2) \\
&+ 2\rho \delta_\alpha \delta_\rho r^2 \left( \arcsin \frac{a}{r} - \arcsin \frac{b}{r} \right) + \rho c \sqrt{r^2-c^2} \\
&\left. + 2\rho \delta_\beta \delta_\rho r^2 \left( \arcsin \frac{e}{r} - \arcsin \frac{f}{r} \right) - \rho d \sqrt{r^2-d^2} \right\}
\end{aligned}
$$

## Appendix B: Covariance Update in the Modified JPDACF

In this section the updated stacked covariance for the JPDACF in (46) is derived. The updated covariance $P_{k|k}^S$, conditioned on all measurements up to time $k$, $Z^k$, is

$$
P_{k|k}^S = E \left\{ \left[ x_k^S - \hat{x}_{k|k}^S \right] \left[ x_k^S - \hat{x}_{k|k}^S \right]^T \middle| Z^k \right\} \qquad (64)
$$

This can be expressed as a weighted sum of all joint association event conditioned estimation error covariances by using the total probability theorem

$$
\begin{aligned}
P_{k|k}^S =& \sum_{\Theta_k} P\{\Theta_k | Z^k\} \qquad (65) \\
&\times E \left\{ \left[ x_k^S - \hat{x}_{k|k}^S \right] \left[ x_k^S - \hat{x}_{k|k}^S \right]^T \middle| Z^k, \Theta_k \right\}
\end{aligned}
$$

Let $\hat{x}^S_{k|k}(\Theta)$ be the state estimate conditioned on the joint association event $\Theta_k$. By using this, (65) can be rewritten as

$$\begin{aligned}
P^S_{k|k} =& \sum_{\Theta_k} P\{\Theta_k|Z^k\} E\left\{ \left[ \left( x^S_k - \hat{x}^S_{k|k}(\Theta) + \hat{x}^S_{k|k}(\Theta) - \hat{x}^S_{k|k} \right) \right] \right. \\
& \left. \times \left[ \left( x^S_k - \hat{x}^S_{k|k}(\Theta) + \hat{x}^S_{k|k}(\Theta) - \hat{x}^S_{k|k} \right) \right]^T \middle| Z^k, \Theta_k \right\} \\
=& \sum_{\Theta_k} P\{\Theta_k|Z^k\} E\left\{ \left( x^S_k - \hat{x}^S_{k|k}(\Theta) \right) \left( x^S_k - \hat{x}^S_{k|k}(\Theta) \right)^T \right. \\
& + \left( x^S_k - \hat{x}^S_{k|k}(\Theta) \right) \left( \hat{x}^S_{k|k}(\Theta) - \hat{x}^S_{k|k} \right)^T + \left( \hat{x}^S_{k|k}(\Theta) - \hat{x}^S_{k|k} \right) \left( x^S_k - \hat{x}^S_{k|k}(\Theta) \right)^T \\
& \left. + \left( \hat{x}^S_{k|k}(\Theta) - \hat{x}^S_{k|k} \right) \left( \hat{x}^S_{k|k}(\Theta) - \hat{x}^S_{k|k} \right)^T \middle| Z^k, \Theta_k \right\} \\
=& \sum_{\Theta_k} P\{\Theta_k|Z^k\} E\left\{ \left( x^S_k - \hat{x}^S_{k|k}(\Theta) \right) \left( x^S_k - \hat{x}^S_{k|k}(\Theta) \right)^T \middle| Z^k, \Theta_k \right\} \\
& + \sum_{\Theta_k} P\{\Theta_k|Z^k\} \left( \hat{x}^S_{k|k}(\Theta) - \hat{x}^S_{k|k} \right) \left( \hat{x}^S_{k|k}(\Theta) - \hat{x}^S_{k|k} \right)^T \\
=& \sum_{\Theta_k} P\{\Theta_k|Z^k\} \underbrace{E\left\{ \left( x^S_k - \hat{x}^S_{k|k}(\Theta) \right) \left( x^S_k - \hat{x}^S_{k|k}(\Theta_k) \right)^T \middle| Z^k, \Theta_k \right\}}_{P_\Theta} \\
& + \underbrace{\sum_{\Theta_k} P\{\Theta_k|Z^k\} \hat{x}^S_{k|k}(\Theta) \hat{x}^S_{k|k}(\Theta)^T - \hat{x}^S_{k|k} \hat{x}^{S\ T}_{k|k}}_{\tilde{P}} \\
=& \sum_{\Theta_k} P\{\Theta_k|Z^k\} P_\Theta + \tilde{P}
\end{aligned} \tag{66}$$

where the identity

$$\sum_{\Theta_k} P\{\Theta_k|Z^k\} = 1 \tag{67}$$

is used together with the fact that

$$\hat{x}^S_{k|k}(\Theta) = E\left\{ x^S_k | Z^k, \Theta_k \right\} \tag{68}$$

$$\hat{x}^S_{k|k} = \sum_{\Theta_k} P\{\Theta_k|Z^k\} \hat{x}^S_{k|k}(\Theta) \tag{69}$$

Next, $P_\Theta$ in the first term of (66) will be derived

$$P_\Theta = E\left\{ \left( x^S_k - \hat{x}^S_{k|k}(\Theta) \right) \left( x^S_k - \hat{x}^S_{k|k}(\Theta) \right)^T \middle| Z^k, \Theta \right\} \tag{70}$$

where the conditioned estimation error is

$$\begin{aligned}\tilde{x}_k^S(\Theta) =& x_k^S - \hat{x}_{k|k}^S(\Theta) \\ =& F^S x_{k-1}^S + v_{k-1}^S - F^S \hat{x}_{k-1|k-1}^S - I_\Theta^x W_k^S I_\Theta^z \nu_k^S(\Theta)\end{aligned} \tag{71}$$

Substituting (under the assumption that all targets are observed)

$$\begin{aligned}\nu_k^S(\Theta) =& z_k^S(\Theta) - H^S F^S \hat{x}_{k-1|k-1}^S \\ =& H^S F^S x_{k-1}^S + H^S v_{k-1}^S + w_k^S - H^S F^S \hat{x}_{k-1|k-1}^S \\ =& H^S F^S \tilde{x}_{k-1}^S + H^S v_{k-1}^S + w_k^S\end{aligned} \tag{72}$$

in (71) yields

$$\begin{aligned}\tilde{x}_k^S(\Theta) = & \left(I - I_\Theta^x W_k^S I_\Theta^z H^S\right) F^S \tilde{x}_{k-1}^S \\ & + \left(I - I_\Theta^x W_k^S I_\Theta^z H^S\right) v_{k-1}^S - I_\Theta^x W_k^S I_\Theta^z w_k^S\end{aligned} \tag{73}$$

Using this in (70) gives

$$\begin{aligned}P_\Theta = & \left(I - I_\Theta^x W_k^S I_\Theta^z H^S\right) P_{k|k-1}^S \left(I - I_\Theta^x W_k^S I_\Theta^z H^S\right)^T \\ & + I_\Theta^x W_k^S I_\Theta^z R^S I_\Theta^z W_k^{S^T} I_\Theta^x\end{aligned} \tag{74}$$

where

$$P_{k|k-1}^S = F^S P_{k-1|k-1}^S F^{S^T} + Q^S \tag{75}$$

In (74) the assumptions in (2) are used together with the following independence assumptions between the estimation error and the two noises

$$E\left\{\tilde{x}_k^S v_k^{S^T} | Z^k, \Theta_k\right\} = 0 \tag{76}$$

$$E\left\{\tilde{x}_{k-1}^S w_k^{S^T} | Z^k, \Theta_k\right\} = 0 \tag{77}$$

The last term $\tilde{P}$ in (66) is

$$\begin{aligned}\tilde{P} =& \sum_{\Theta_k} P\{\Theta_k | Z^k\} \hat{x}_{k|k}^S(\Theta) \hat{x}_{k|k}^S(\Theta)^T - \hat{x}_{k|k}^S \hat{x}_{k|k}^{S^T} \\ =& \sum_{\Theta_k} P\{\Theta_k | Z^k\} \left(\hat{x}_{k|k-1}^S + I_\Theta^x W_k^S I_\Theta^z \nu_k^S(\Theta)\right) \\ & \times \left(\hat{x}_{k|k-1}^S + I_\Theta^x W_k^S I_\Theta^z \nu_k^S(\Theta)\right)^T \\ & - \left(\hat{x}_{k|k-1}^S + \sum_{\Theta_k} P\{\Theta_k | Z^k\} I_\Theta^x W_k^S I_\Theta^z \nu_k^S(\Theta)\right) \\ & \times \left(\hat{x}_{k|k-1}^S + \sum_{\Theta_k} P\{\Theta_k | Z^k\} I_\Theta^x W_k^S I_\Theta^z \nu_k^S(\Theta)\right)^T\end{aligned} \tag{78}$$

which after cancellations becomes the spread of innovations

$$\begin{aligned}\tilde{P} = &\sum_{\Theta_k} P\{\Theta_k|Z^k\} I_\Theta^x W_k^S I_\Theta^z \nu_k^S(\Theta) \nu_k^S(\Theta)^T I_\Theta^z W_k^{S^T} I_\Theta^x \\ &- \left( \sum_{\Theta_k} P\{\Theta_k|Z^k\} I_\Theta^x W_k^S I_\Theta^z \nu_k^S(\Theta) \right) \\ &\times \left( \sum_{\Theta_k} P\{\Theta_k|Z^k\} I_\Theta^x W_k^S I_\Theta^z \nu_k^S(\Theta) \right)^T \end{aligned} \tag{79}$$

Using (79) and (74) in (66) yields the updated stacked covariance

$$\begin{aligned}P_{k|k}^S = &\sum_{\Theta_k} P\{\Theta_k|Z^k\} \\ &\times \left\{ I_\Theta^x W_k^S I_\Theta^z \left( \nu_k^S(\Theta) \nu_k^S(\Theta)^T + R^S \right) I_\Theta^z W_k^{S^T} I_\Theta^x \right. \\ &\left. + \left( I - I_\Theta^x W_k^S I_\Theta^z H^S \right) P_{k|k-1}^S \left( I - I_\Theta^x W_k^S I_\Theta^z H^S \right)^T \right\} \\ &- \left( \sum_{\Theta_k} P\{\Theta_k|Z^k\} I_\Theta^x W_k^S I_\Theta^z \nu_k^S(\Theta) \right) \\ &\times \left( \sum_{\Theta_k} P\{\Theta_k|Z^k\} I_\Theta^x W_k^S I_\Theta^z \nu_k^S(\Theta) \right)^T \end{aligned} \tag{80}$$

## References

[1] M. Athans, R. H. Whiting, and M. Gruber, "A suboptimal estimation algorithm with probabilistic editing for false measurements with applications to target tracking with wake phenomena," *IEEE Transactions on Automatic Control*, vol. 22, no. 3, pp. 372–384, June 1977.

[2] Y. Bar-Shalom, "Tracking methods in a multitarget environment," *IEEE Transactions on Automatic Control*, vol. 23, no. 4, pp. 618–626, Aug. 1978.

[3] Y. Bar-Shalom, K. C. Chang, and H. A. P. Blom, "Tracking of splitting targets in clutter using an interacting multiple model joint probabilistic data association filter," in *Proceedings of the 30th IEEE Conference on Decision and Control*, Brighton, UK, Dec. 1991, pp. 2043–2048.

[4] Y. Bar-Shalom and X. R. Li, *Multitarget-Multisensor Tracking: Principles and Techniques*. Storrs, CT: YBS Publishing, 1995.

[5] Y. Bar-Shalom, X. R. Li, and T. Kirubarajan, *Estimation with Application to Tracking and Navigation.* New York: Wiley-Interscience, 2001.

[6] D. K. Barton, *Modern Radar System Analysis.* Norwood, MA: Artech House, 1988.

[7] S. Blake and S. Watts, "A multitarget track-while-scan filter," in *Proceedings of the IEE Radar 87 Conference*, London, UK, Oct. 1987.

[8] E. A. Bloem and H. A. P. Blom, "Joint probabilistic data association methods avoiding track coalescence," in *Proceedings of the 34th IEEE Conference on Decision and Control*, vol. 3, New Orleans, LA, Dec. 1995, pp. 2752–2757.

[9] H. A. P. Blom and E. A. Bloem, "Probabilistic data association avoiding track coalescence," *IEEE Transactions on Automatic Control*, vol. 45, no. 2, pp. 247–259, Feb. 2000.

[10] H. Chen, T. Kirubarajan, and Y. Bar-Shalom, "Comparison of centralized and distributed tracking algorithms using air-to-air scenarios," in *Proceedings of the SPIE Conference on Signal and Data Processing of Small Targets*, vol. 4048, July 2000, pp. 440–451.

[11] ——, "Performance limits of track-to-track fusion versus centralized estimation: Theory and application," *IEEE Transactions on Aerospace and Electronic Systems*, vol. 39, no. 2, pp. 386–400, Apr. 2003.

[12] H. Chen, K. Zhang, and X. R. Li, "Optimal data compression for multisensor target tracking with communication constraints," in *Proceedings of the 43rd IEEE Conference on Decision and Control*, vol. 3, Dec. 2004, pp. 2650–2655.

[13] R. J. Fitzgerald, "Development of practical PDA logic for multitarget tracking by microprocessor," in *Multitarget Multisensor Tracking: Advanced Applications*, Y. Bar-Shalom, Ed. Norwood, MA: Artech House, 1990, ch. 1, pp. 1–23.

[14] T. E. Fortmann, Y. Bar-Shalom, and M. Scheffe, "Sonar tracking of multiple targets using joint probabilistic data association," *IEEE Journal of Oceanic Engineering*, vol. 8, no. 3, pp. 173–184, July 1983.

[15] P. P. Gandhi and S. A. Kassam, "Analysis of CFAR processors in homogeneous background," *IEEE Transactions on Aerospace and Electronic Systems*, vol. 24, no. 4, pp. 427–445, July 1988.

[16] X. Lurton, *An Introduction to Underwater Acoustics: Principles and Applications.* New York: Springer, 2002.

[17] D. Musicki and R. Evans, "Joint integrated probabilistic data association: JIPDA," *IEEE Transactions on Aerospace and Electronic Systems*, vol. 40, no. 3, pp. 1093–1099, July 2004.

[18] D. Musicki, R. Evans, and S. Stankovic, "Integrated probabilistic data association," *IEEE Transactions on Automatic Control*, vol. 39, no. 6, pp. 1237–1241, June 1994.

[19] L. Y. Pao and C. W. Frei, "A comparison of parallel and sequential implementations of a multisensor multitarget tracking algorithm," in *Proceedings of the American Control Conference*, vol. 3, Seattle, WA, June 1995, pp. 1683–1687.

[20] A. Papoulis and S. U. Pillai, *Probability, Random Variables and Stochastic Processes*, 4th ed. New York: McGraw-Hill, 2002.

[21] A. Rødningsby and Y. Bar-Shalom, "Tracking of divers using a probabilistic data association filter with a bubble model," *IEEE Transactions on Aerospace and Electronic Systems*, vol. 45, no. 3, July 2009.

[22] A. Rødningsby, Y. Bar-Shalom, O. Hallingstad, and J. Glattetre, "Multitarget tracking in the presence of wakes," in *Proceedings of the 11th International Conference on Information Fusion*, Cologne, Germany, July 2008, pp. 1536–1543.

[23] J. P. Serra, *Image Analysis and Mathematical Morphology*. London, UK: Academic Press, 1982.

[24] W. J. Smith, *Modern Optical Engineering: The Design of Optical Systems*, 2nd ed. New York: McGraw-Hill, 1990.

[25] S. M. Tonissen and Y. Bar-Shalom, "Maximum likelihood track-before-detect with fluctuating target amplitude," *IEEE Transactions on Aerospace and Electronic Systems*, vol. 34, no. 3, pp. 796–808, July 1998.

[26] R. J. Urick, *Principles of Underwater Sound*, 3rd ed. New York: McGraw-Hill, 1983.